Non-Linear Finite Element Analysis of Jointed Plain Concrete Pavement Due to Wheel Load

MOHAMMAD NEAZ MURSHED

Department of Civil Engineering

BANGLADESH UNIVERSITY OF ENGINEERING AND TECHNOLOGY

DHAKA

July, 2011

NON-LINEAR FINITE ELEMENT ANALYSIS OF JOINTED PLAIN CONCRETE PAVEMENT DUE TO WHEEL LOAD

by

Mohammad Neaz Murshed

A thesis

Submitted to the

Department of Civil Engineering

in partial fulfillment of the requirement for the degree

of

MASTER OF SCIENCE IN CIVIL ENGINEERING (TRANSPORTATION)

BANGLADESH UNIVERSITY OF ENGINEERING AND TECHNOLOGY

DHAKA

July, 2011

A thesis titled **"Non-Linear Finite Element Analysis of Jointed Plain Concrete Pavement Due to Wheel Load"** submitted by Mohammad Neaz Murshed, Roll no. 100604415 (P), Session October 2006, has been accepted as satisfactory in partial fulfillment of the requirement for the degree of Master of Science in Civil Engineering (Transportation) on 6th July, 2011.

BOARD OF EXAMINERS

1. _____
   Dr. Md. Mizanur Rahman
   Associate Professor
   Department of Civil Engineering,
   Bangladesh University of Engineering and Technology,
   Dhaka-1000.
   — Chairman (Supervisor)

2. _____
   Dr. Md. Zoynul Abedin
   Professor and Head
   Department of Civil Engineering,
   Bangladesh University of Engineering and Technology,
   Dhaka-1000.
   — Member (Ex-Officio)

3. _____
   Dr. Tanweer Hasan
   Professor
   Department of Civil Engineering,
   Bangladesh University of Engineering and Technology,
   Dhaka-1000.
   — Member

4. _____
   Mr. Md. Abdullah Al Mamun, M.Sc.
   Project Manager (EE)
   Dapdapia Bridge Construction Project
   Sarak Bhaban, Dhaka, Bangladesh.
   — Member

DEDICATED

To

My Parents

DECLARATION

It is hereby declared that except for the contents where specific references have been made to the works, manuals and papers of other authors, the studies contained in this thesis are the result of investigation carried out by the author under the supervision of Dr. Md. Mizanur Rahman, Associate Professor, Department of Civil Engineering, Bangladesh University of Engineering and Technology.

No part of this thesis has been submitted to any other university or other educational establishments for a degree, diploma or other qualifications.

(Mohammad Neaz Murshed)

ACKNOWLEDGEMENT

All praise for Allah, the most gracious and the most merciful.

The author expresses his heartiest gratitude and sincere indebtedness to his supervisor Dr. Md. Mizanur Rahman, Associate Professor, Department of Civil Engineering, BUET for his continuous guidance, relentless discussions, helpful suggestions, affectionate encouragement and generous help at every stage of this study.

The author expresses his profound gratitude to Professor Md. Joynul Abedin, Professor and Head of the Department of Civil Engineering, BUET for his continuous encouragement, inspiration, and relentless support at all stages of the study.

The author is thankful to Mr. Shameem Ahmed, Assistant Professor, Department of Civil Engineering, BUET, and appreciates his encouragements, advice, and helpful suggestions throughout this study.

The author is also thankful to his family members for their continual inspiration and support.

ABSTRACT

The behavior of a jointed plain concrete pavement (JPCP) has been investigated under single wheel load for interior loading using finite element technique to predict the critical pavement responses for nonlinear geomaterial characterization. Pavement foundation geomaterials, i.e., fine grained subgrade soils and unbound aggregates used in untreated base/subbase layers, exhibit nonlinear behavior. The idealized pavement system is analyzed using both 3D and axisymmetric (2D) finite element analysis. The developed 3D and axisymmetric models were analyzed for four combinations of material characterizations- (1) linear base and subgrade material, (2) nonlinear base and linear subgrade, (3) linear base and nonlinear subgrade, and (4) nonlinear base and nonlinear subgrade. Effects of slab thickness, base course material thickness, base course material strength, and subgrade type on the critical pavement responses were also studied.

For the finite element analysis an axisymmetric and 3-D finite element model of jointed plain concrete pavement was developed using the general purpose finite element software ABAQUS. Granular base course and subgrade soil was modeled with solid elements considering its nonlinear material behaviors, and concrete slab was modeled with linear elastic material using solid elements. Eight nodded isoparametric brick element was used for 3D modeling and 4 noded linear quadrilateral element was used in axisymmetric modeling. The developed 3D FE model was successfully verified with available numerical results.

3D finite element analysis results for nonlinear material characterization predicts 12.4% higher surface deflection than linear elastic characterization. But the maximum tensile stress and vertical compressive stress on top of subgrade for both nonlinear and linear analysis were found to be negligible. 2D axisymmetric FE analysis was carried out and the results were compared with those predicted by 3D FE analysis. The axisymmetric finite element analysis results conforms closely with the 3D FE analysis results for vertical surface deflection and compressive stress on subgrade with a variation of 1.3% and 2.4% respectively. But the maximum tensile stress predicted by axisymmetric FE analysis at the bottom of the concrete slab is about 14% grater than the 3D FE analysis result. Nonlinear characterization of the base course material has no significant effect on the pavement responses as the stresses developed in the base course material layer is within the elastic limit. Nonlinear characterization of subgrade soil has considerable effect on the deflection of the top surface. The parametric study shows that for a jointed plain concrete pavement, the maximum values of pavement deflection, tensile stress and subgrade pressure are reduced significantly up to a thickness of 225 mm (9 inch) above which the influence of slab thickness on pavement responses reduces. The effects of base course material thickness and strength properties on the maximum values of pavement deflection,

tensile stress and subgrade pressure are less significant compared to effects of slab thickness. The subgrade type has similar but significant effects on the pavement responses due to wheel load.

Table of Contents

Chapter 1

INTRODUCTION

1.1 GENERAL

Rigid pavements are one of the principal kinds of pavement widely in use throughout the world for both roadways and runways. But the design procedures available today are mostly based on empirical equations dependent pavement analysis results. With the advent of computer and the versatile finite element method, numerical analysis is gaining popularity day by day over empirical methods of pavement analysis to determine the critical pavement responses. Research works has been carried out through the globe to predict the critical pavement responses using versatile finite element analysis software widely available today. Initially, the finite element analyses of pavement systems were limited in extent to linear elastic material characterizations. But previous laboratory studies have shown that the resilient response of both the coarse-grained unbound granular materials used in untreated base/subbase courses and fine grained subgrade follow nonlinear, stress-dependent behavior. With the availability of powerful computers and robust finite element software, it is now possible to consider material nonlinearity for the prediction of pavement responses with greater efficiency and accuracy. Pavement analysis forms the basis of any pavement design process. Most of the pavement design procedures available today are produced in the developed countries are based on the native material properties of the organization or region developing the design procedure. Finite element analysis method can be the basis of the development of appropriate pavement design procedures for developing countries considering the native environment and material properties common to that area.

1.2 BACKGROUND OF RESEARCH

The design of pavements has evolved greatly but still empiricism plays a very important part in the analysis of pavements. The formulas Westergaard (1926) developed originally considered only a single wheel load with a circular, semicircular, elliptical, or semi-elliptical contact area. Whereas, the influence charts developed by Pickett and Ray (1951)

can be applied to multiple-wheel loads of any configuration. Both the formulas and the influence charts are applicable only to a large slab on a liquid foundation. The assumption behind liquid foundation is that the subgrade is composed of a set of independent springs. This implies that deflection at any given point is proportional to the force at that point and independent of the forces at all other points. This assumption is totally unrealistic and does not properly represent soil behaviors. Westergaard used this assumption due to its simplicity. Eventually, with the availability of hi-speed and large capacity personal computers it is no longer necessary to make such fictitious assumptions. The more realistic solid or layer foundations can be used. With the development of the robust finite element method, a break through has been made in the analysis of rigid pavements. Multiple slabs with loading on a solid, liquid, or layer foundation with load transfer across joints can now be analyzed with greater accuracy and efficiency with greater speed.

Finite element methods for analyzing slabs on elastic foundations of both liquid and solid types were developed by Cheung and Zienkiewicz (1965). These methods were applied to jointed slabs on liquid foundation by Huang and Wang (1973, 1974) and on solid foundations by Huang (1974). In Collaboration with Huang, Chou (1981) developed finite element computer programs named WESLIQID and WESLAYER for the analysis of liquid and layered foundations, respectively. Other available finite element computer programs include ILLI-SLAB developed by the University of Illinois, JSLAB developed by the Portland Cement Association (PCA) and RISC developed by Resource International, Inc. ILLISLAB was originally developed in 1977 for the structural analysis of one or two layers of slabs with or without mechanical load transfer system at joints and cracks. Heinrichs et al. (1989) compared several available computer models for rigid pavements and concluded that both ILLI-SLAB and JSLAB, which is a similar finite element program, developed by PCA, were efficient to use and could structurally model many key design factors of importance. They also indicated that the ILLISLAB had extensive checking, revisions, and verification by many researchers and was free of errors than any other available program. The KENSLABS computer program developed by Huang (1985) is based on finite element method, in which the slab is divided into

rectangular finite elements with large number of nodes. Both wheel loads and subgrade reactions are applied to the slab as vertical concentrated forces at the nodes. The program was designed to analyze slabs on liquid, solid or layer foundations. All these three foundation types considered subgrade, subbase and base to be linearly elastic. Shaikh (2005) also carried out a behavioral study of rigid pavement section using general purpose finite element software ANSYS. The model was generated directly using ANSYS CAD modeler. The surface layer is simulated through a two-dimensional plane surface while the subbase and subgrade are considered as elastic, homogeneous and linear springs supporting the top surface and are been modeled through one individual spring using effective or composite stiffness. He concluded that non linear properties of both concrete and foundation material can be used in order to better simulate the real field condition.

As the demand for applied wheel loads and number of load applications increases, it becomes very important to properly characterize the behavior of subgrade soils and unbound aggregate layers as the foundations of the layered pavement structure. Unfortunately, most commonly used elastic layered programs assume linear elastic material behavior for the unbound aggregate base/subbase and subgrade soil layers. Previous laboratory studies have shown that the resilient responses of both coarse-grained unbound granular materials used in untreated base/subbase courses and fine-grained subgrade follow nonlinear, stress-dependent behavior under repeated traffic loading by Thompson and Robnett (1979); Brown and Pappin (1981); Uzan (1985); Tutumluer (1995); Rowshanzamir (1995). Unbound granular materials exhibit stress hardening, whereas, fine-grained soils show stress-softening type behavior.

Although, consideration of non-linearity in unbound layers is necessary for accurate modeling of a flexible pavement structure, the necessity of non-linear consideration in rigid pavements has not been studied as closely. Assumption of unbound layers to be linearly elastic raises many problems. For example, granular layers may have a lower modulus than the subgrade, and measured vertical strain at the top of the subgrade may be twice the theoretical value. Nazarian and Stokoe(1995) have shown that non-linear

behavior occurs in Falling Weight Deflection (FWD) testing. An increase in the load magnitude of the FWD results in an increase in deflection that is greater than one to one. Nazarian, et. al. also showed the effect of non-linearity with depth in a farm to- market test road.

Several procedures have been developed to consider the non-linearity of unbound layers in pavement structures. Some analyses attempt to model the non-linearity by considering the plastic behavior of subgrade soils. Others approximate non-linear effects through iterative linear elastic procedures. Most recently, finite element code has been utilized in modeling the stress state dependency of granular base layers, and the strain level dependence of subgrade materials. Kou and Huang (2006) compared nonlinear analysis and linear analysis for subgrade materials and concluded that the determination of the resilient modulus for the linear models is critical to interpret the behaviors of nonlinear materials.

As stresses and strains are used more and more to determine the relative condition of layers in a pavement structure, the need for consideration of non-linear material behavior becomes increasingly important. Linear elastic approximations of unbound material behavior are no longer acceptable in pavement analysis. Errors from such approximations have been noted and documented. The stress state dependency of granular materials, and strain based subgrade soil models must be considered for an accurate estimation of true pavement response. A finite element type analysis needs to be employed to model such nonlinear resilient behavior and more realistically predict pavement responses for a mechanistic pavement analysis.

1.3 OBJECTIVE OF THE STUDY

Critical pavement responses of jointed plain concrete pavement due to single wheel interior loading are examined using both 3-D and axisymmetric finite element analysis. Finite element analysis technique is carried out with the following specific objectives:

i. To investigate jointed plain concrete pavement responses due to wheel loadng in 3-D linear and nonlinear finite element analysis.

ii. To investigate jointed plain concrete pavement responses due to wheel loading in axisymmetric linear and nonlinear finite element analysis.

iii. To compare the pavement responses obtained from axisymmetric with 3-D finite element analysis due to loading.

iv. To investigate the effects of pavement geometries (thickness of concrete slab, base) and material properties on pavement responses under wheel loading with a general purpose finite element software.

1.4 SCOPE AND METHODOLOGY OF THE STUDY

The proposed methodology consists of following steps:

i. In the present study, a jointed plain concrete pavement section resting on a base and a subgrade of variable thickness has been used to develop models for 3-D and axisymmetric finite element analysis with a general purpose finite element program.

ii. The devloped 3-D and axisymmetric models has been subjected to single wheel loads to investigate the pavement responses (stress, strain and deflection) due to interior loading.

iii. Pavement responses has been predicted from the 3-D analysis using linear elastic concrete behavior and the following pavement layer charecterizations -

   (a) linear elastic base and subgrade;
   (b) nonlinear base and linear subgrade;
   (c) linear base and nonlinear subgrade;
   (d) nonlinear base and nonlinear subgrade;

iv. Pavement responses has also been predicted from the axisymmetric analysis considering linear elastic behavior of concrete and the following pavement layer charecterizations -

   (a) linear elastic base and subgrade;
   (b) nonlinear base and linear subgrade;
   (c) linear base and nonlinear subgrade;
   (d) nonlinear base and nonlinear subgrade;

v. Effects of varous parameters (pavement geometries-thickness of slab, base) and pavement material properties on pavement responses under wheel loading has been analysed using the developed 3D reference model.

vi. Analysis has been carried out for different slab thickness keeping other parameters of the pavment sytem unchnged to the nvestigate its effect on pavement response..

vii. Analysis has also been performed for different base thickness keeping the slab thickness unchanged to investigate the effect of base thickness on pavement response.

viii. The effect of base course material strength properties on pavemnt responses has also been performed and compared.

1.5 ORGANIZATION OF THE THESIS

The thesis is organized in a systematic way from the development of finite element models- 3D and axisymmetric for a jointed plain concrete pavement (JPCP) system to the performance of finite element analysis on the developed models in order to investigate the pavement responses for different material characterization of the pavement layers. Chapter 1 introduces a general statement of the problem and the objectives of this research. Chapter 2 reviews the available literature discussing various analytical or computational studies conducted on observing the responses of pavement systems. Chapter 3 describes the development of the 3-D and axisymmetric finite element model of the jointed plain concrete pavement system. The performances of the developed model are verified with the available analytical results in this chapter. Chapter 4 discuses the predicted responses of jointed plain concrete pavement and also covers the effect of different parameters on the pavement responses. Finally, Chapter 5 draws conclusion of the current work and discusses recommendations for future work in the area of concrete pavement response analysis.

Chapter 2
LITERATURE REVIEW

2.1 INTRODUCTION

Pavements are intricate physical systems involving complex soil-structure interactions. From the beginning of the 20th century, extensive research in this field is being carried out resulting in the emergence of various classical solutions of pavement problems based on various simplifying assumptions. Availability of hi-speed and large capacity personal computers, fortified by the development of the robust finite element method, more realistic solutions of complicated pavement problems can be achieved with greater accuracy, efficiency, and speed.

Rigid pavements are constructed of Portland cement concrete. The development of design methods for rigid pavements is not as dramatic as that of flexible pavements because the flexural stress in concrete has long been considered as a major, or even the only, design factor. The allowable number of load repetitions to cause fatigue cracking depends on the stress ratio between flexural tensile stress and concrete modulus of rupture. Of late, pumping is identified as an important failure criterion. Pumping is the ejection of soil slurry through the joints and cracks of cement concrete pavement, caused during the downward movement of slab under the heavy wheel loads. Other major types of distress in rigid pavements include faulting, spalling, and deterioration. Analytical solutions ranging from simple closed form formulas to complex derivations are available for determining the stresses and deflections in concrete pavements.

The intent of this literature survey is to provide a brief outline of rigid pavement types, available solution techniques and the various analytical and numerical studies and field tests that have been performed to date in the area of rigid pavement analysis.

2.2 DIFFERENT COMPONENTS OF RIGID PAVEMENTS

Rigid pavements are placed either directly on the prepared subgrade or on a single layer of granular or stabilized material. Because there is only one layer of material under the concrete and above the subgrade, some call it a base course, others a subbase. Sometimes an additional subbase course may be used if needed. Figure 2.1 shows a typical cross section of a typical rigid pavement.

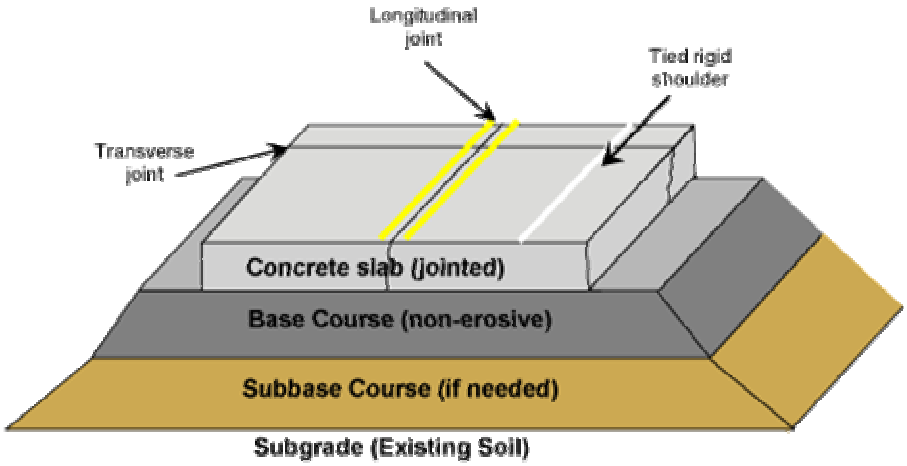

Figure 2.1: Typical Cross Section of a Rigid Pavement

The subgrade is the native roadbed soil at the site and the engineer must generally work with what is available. If necessary, better materials may be brought in or the subgrade may be stabilized, but this represents an additional cost. Subgrades may need to be stabilized to improve low-strength soil, reduce potential for swelling due to moisture, or to improve construction conditions. If the project is on a tight schedule, stabilization reduces the risk of construction delays due to wet weather. Subgrades may be stabilized with lime or cement. Lime stabilization is most suitable for clayey soils with high moisture content. Cement stabilization is used for coarse-grained soils or soils with high silt content.

The AASHTO Guide for Design of Pavement Structures (AASHTO 1993: I-21) defines a subbase as "one or more compacted layers of granular or stabilized material" between the subgrade and concrete pavement slab. The Guide cites the following reasons for using subbases:

- To provide uniform, stable, and permanent support,

- To increase the modulus of subgrade reaction k,
- To minimize the damaging effects of frost action,
- To prevent pumping of fine-grained soils at joints, cracks, and edges of the rigid slab, and
- To provide a working platform for construction equipment.

The Guide further states that a subbase is not necessary if the traffic is relatively light (less than one million ESALs) and the roadbed soil quality is equal to that of a subbase. Use of a subbase solely to increase the k is not economical, in the absence of the other reasons (PCA 1984: 6). As a practical matter, the last reason cited in the previous list may be the strongest, because it helps avoid construction delays due to wet weather and helps the contractor build a smoother pavement. A key consideration is whether the subbase is expected to also function as sub-drainage.

The basic materials in the pavement slab are Portland cement concrete, reinforcing steel, load transfer devices, and joint sealing materials. The steel reinforcements in the form of wire mesh or deformed bars do not increase the structural capacity of the pavements but allow the use of longer joint spacing. Dowels or aggregate interlock are used for load transfer across the joints.

2.3 TYPES OF RIGID PAVEMENTS

There are a number of different types of concrete pavements that have been built. However, for the most part, they have two features in common. First, they resist traffic loads through flexure of the concrete. If reinforcement is used, it is used for crack control and not to carry load. The second element is that concrete pavements contract due to drying shrinkage of the concrete, and expand and contract due to thermal effects, and these movements must be dealt with. Different types of pavements use joints, reinforcing steel, or both.

Concrete pavements can be classified into four types: jointed plain concrete pavement (JPCP), jointed reinforced concrete pavement (JRCP), continuous reinforced concrete pavement (CRCP), and prestressed concrete pavement (PCP). Except for PCP with lateral pre-stressing, a longitudinal joint should be installed between two traffic lanes to prevent longitudinal cracking. The term “conventional

concrete pavements" is generally taken to mean either jointed plain, jointed reinforced or continuously reinforced concrete pavements.

2.3.1 Jointed Plain Concrete Pavement

Jointed plain concrete pavement, or JPCP, consists of un-reinforced concrete slabs 3.6–6.0 meter (12–20 ft) in length with transverse contraction joints between the slabs. The joints are spaced closely enough together so that cracks should not form in the slabs until late in the life of the pavement. Therefore, for JPCP, the pavement expansions and contractions are addressed through joints. JPCP is illustrated in Figure 2.2.

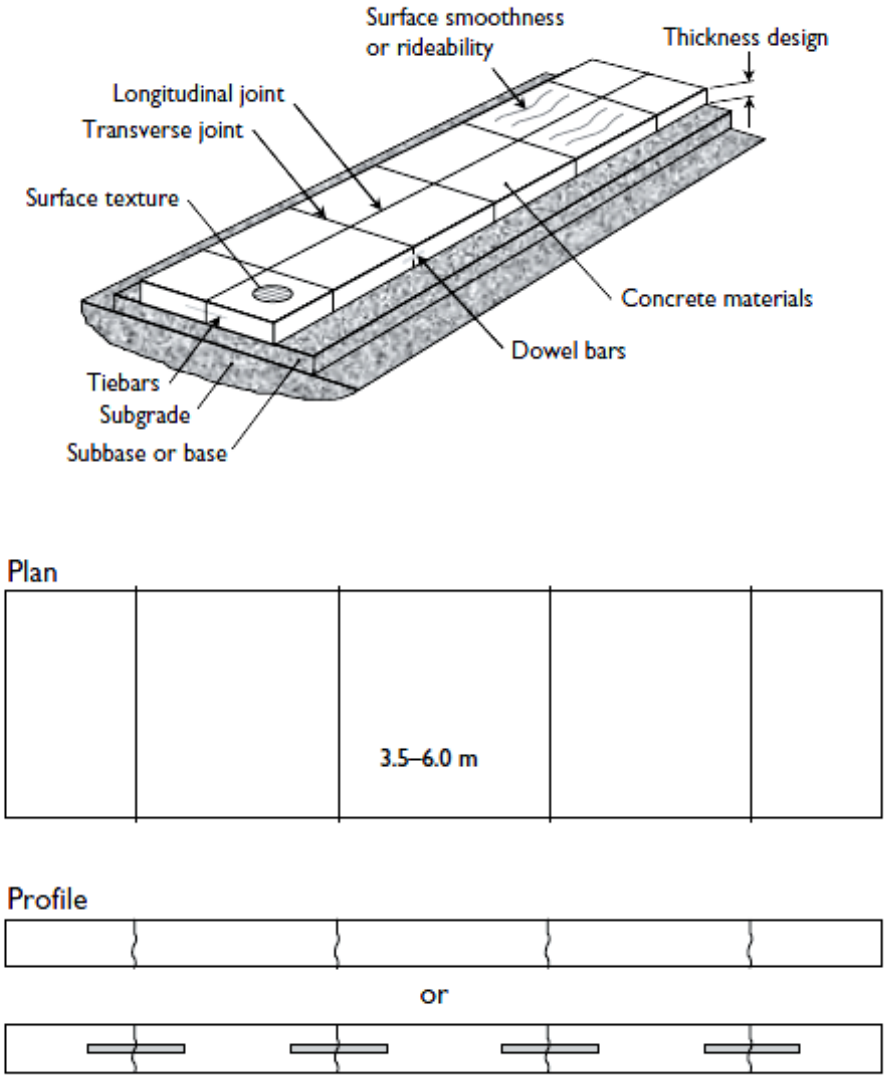

Figure 2.2 Jointed Plain Concrete Pavement (JPCP).

One important performance issue with JPCP is load transfer across the joints. If joints become faulted, then drivers encounter bumps at the joints and experience a rough ride. Two methods are used to provide load transfer across JPCP joints – aggregate interlock and dowels.

Aggregate interlock joints are formed during construction by sawing 1/4−1/3 of the way through the pavement to create a plane of weakness. A crack then propagates through the remaining thickness of the pavement as the concrete contracts. This crack has a rough surface because it propagates around the aggregates through the green cement paste, and as long as it remains narrow the joint can transfer load from one slab to another through bearing stress of the aggregate particles against each other across the crack. Load transfer is compromised if the joint opens too widely or if the aggregates wear away. The quality and erosion resistance of the material supporting the slab at the joint also affect load transfer. When the pavement carries heavy vehicle traffic, particularly at high speeds, aggregate interlock will break down over time and will not prevent faulting over the life of the pavement. In this case, dowels are provided across the joint for load transfer. Dowels are smooth rods, generally plain or epoxy-coated steel, which are usually greased or oiled on side to allow the joints to open and close without resistance.

JPCP is the most commonly used type of concrete pavement because it is usually the cheapest to construct. It is economical because there is no need to pay for any reinforcing steel in the slabs or for labor to place the steel. JPC pavements, like other conventional concrete pavements, often use tie bars to connect adjacent traffic lanes. Tie bars are deformed reinforcing steel and, unlike dowels, are not intended to allow the joints to open and close. Tie bars are used to separate lanes for highway pavements.

2.3.2 Jointed Reinforced Concrete Pavement

Jointed reinforced concrete pavement, or JRCP, is distinguished from JPCP by longer slabs and light reinforcement in the slabs. This light reinforcement is often termed temperature steel. JRCP slab lengths typically range from 7.5 to 9 meter (25–30 ft), although slab lengths up to 30 meter (100 ft) have been used. With these slab lengths, the joints must be doweled. The slab steel content is typically in the range of 0.10–

0.25 percent of the cross-sectional area, in the longitudinal direction, with less steel in the transverse direction. Either individual reinforcing bars or wire fabrics and meshes may be used. Because the steel is placed at the neutral axis or midpoint of the slab, it has no effect on the flexural performance of the concrete and serves only to keep cracks together. JRCP is illustrated in Figure 2.3.

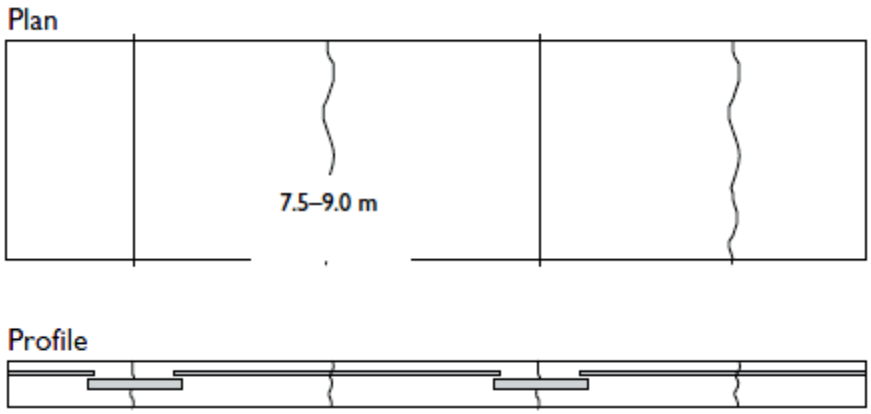

Figure 2.3Jointed Reinforced Concrete Pavement (JRCP)

Although JRCP was widely used in the past, it is less common today. The only advantage that JRCP has over JPCP is fewer joints, and this is outweighed by the cost of the steel and the poor performance of the joints and the cracks. Because the joints are spaced further apart than JPCP, they open and close more, and load transfer suffers as joints open wider. JRCP joints always use dowels. Furthermore, even though the slabs are longer, the cracks still form at the same interval as JPCP, and therefore JRCP slabs generally have one or two interior cracks each. The light steel reinforcement across these cracks is generally not enough to maintain load transfer, and therefore the cracks fault as well as the joints. As a result, the latest proposed AASHTO M-EPDG procedure does not have provisions for JRCP.

2.3.3 Continuously Reinforced Concrete Pavement

Continuously reinforced concrete pavement, or CRCP, is characterized by heavy steel reinforcement and an absence of joints. Much more steel is used for CRCP than for JRCP, typically on the order of 0.4–0.8 percent by volume in the longitudinal direction. Steel in the transverse direction is provided in a lower percentage as temperature steel. CRCP is illustrated in Figure 2.4.

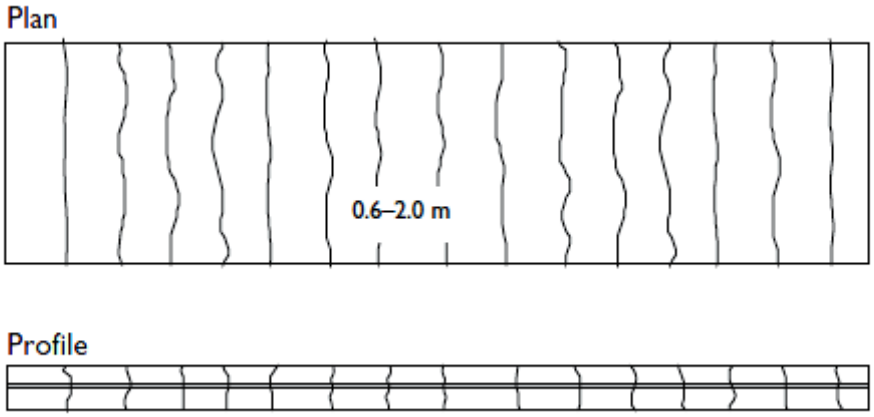

Figure 2.4 Continuously Reinforced Concrete Pavement (CRCP)

Cracks form in CRCP approximately 0.6–2 meter (2–6 ft) apart. The reinforcement holds the cracks tightly together and provides for aggregate interlock and shear transfer. CRC pavements require anchors at the beginning and end of the pavement to keep the ends from contracting due to shrinkage, and to help the desired crack pattern develop.

Because of the steel reinforcement, CRCP costs more than JRCP, and is thus used less frequently in most regions. However, it provides a smoother ride and a longer life than any other type of pavement.

2.3.4 Prestressed and Precast Concrete Pavement

All conventional concrete pavements rely on the flexural strength of the concrete to resist traffic loads over time. By using prestressing tendons to induce a net compressive force in the pavement section it is possible to considerably decrease the thickness of the pavement, because the traffic loads must overcome the compressive stress before inducing a net tensile stress and flexural fatigue into the pavement.

In addition to prestressed pavements for original construction or overlays, precast concrete sections with either conventional or prestressed reinforcement have been used as full depth patches. Precast sections may be left in place as a permanent

pavement, or may be temporary to allow traffic until a permanent full depth patch is placed.

Prestressed concrete was introduced in the late 1940s and was used first in airport pavements. About 1959, two-way prestressed slabs were used at Biggs military airfield in Texas. The 24-in (610-mm) plain pavement was replaced with 9-in (230-mm) post-tensioned slabs. Unfortunately, the fear of the unknown, the need to use more skilled labor, and the reluctance of mile-a-day slipform contractors to embrace this unproven technology have held this concrete-saving technology back. About a dozen highways with prestressed concrete pavements of various designs were built in the United States between 1970 and 1990. Prestressed pavement's potential advantages include more efficient use of construction materials (due to reduced pavement thickness) and fewer joints and cracks, with reduced maintenance and longer pavement life. Much longer slabs may be used than conventional pavements – generally on the order of 122 meter (400 ft) although slabs as long as 300 meter (1,000 ft) have been built in Europe. Prestressed pavement thickness is on the order of 40–50 percent of conventional concrete pavement thickness, or about 100–150 mm (4–6 in) for highways. Prestressed concrete pavements have been used in airport applications in Europe and to a limited extent in the United States.

Precast concrete panels have been used in two ways for concrete pavement rehabilitation. These are: temporary replacement for removed panels until concrete can be placed during the next scheduled closure; and permanent pavement (selective panel replacement). Potential advantages of precast concrete panels include higher quality concrete, better curing, less risk of weather disruption, and reduced delay before opening to traffic. Important issues include leveling the panels to avoid bumps at panel edges, and load transfer between precast panels or between precast panels and existing pavement. Precast panels are generally reinforced with mild steel, primarily to prevent damage during transportation and handling.

2.4 SOLUTION TECHNIQUES

There are two general solution techniques available for the determination of stresses and deflections in concrete pavements- analytical solutions and numerical solutions. With the availability of computers and their ever increasing computational capacity,

the numerical solution techniques especially the finite element methods are gaining more and more popularity as they provide better flexibility for incorporation of realistic material properties and boundary conditions.

2.4.1 Analytical Solutions

Analytical solutions ranging from simple closed form formulas to complex derivations are available for determining the stresses and deflections in concrete pavements. Three methods can be used to determine the stresses and deflections in concrete pavements: closed-form formulas, influence charts, and finite-element computer programs. The formulas originally developed by Westergaard can be applied only to a single-wheel load with a circular, semicircular, elliptical, or semielliptical contact area. The influence charts developed by Pickett and Ray (1951) can be applied to multiple-wheel loads of any configuration. Both methods are applicable only to a large slab on a liquid foundation. If the loads are applied to multiple slabs on a liquid, solid, or layer foundation with load transfer across the joints, the finite-element method should be used. The liquid foundation assumes the subgrade to be a set of independent springs. Deflection at any given point is proportional to the force at that point and independent of the forces at all other points. This assumption is unrealistic and does not represent soil behaviors. Due to its simplicity, it was used in Westergaard's analysis. However, with the ever-increasing speed and storage of personal computers, it is no longer necessary to assume the foundation to be a liquid with a fictitious k value. The more realistic solid or layer foundation can be used.

Goldbeck's Formula:

Goldbeck (1919) developed a simple equation for the design of rigid pavements by assuming the pavement as a cantilever beam with a concentrated load at the corner of the pavement as shown in figure2.5. The same equation was applied by Older (1942) in the Bates Road Test. The Goldbeck (1919) and Older (1924) formula is the earliest one for use in concrete pavement design.

$$\sigma_c = \frac{Px}{\frac{1}{6}(2x)h^2} = \frac{3P}{h^2} \qquad (2.1)$$

Where, σ_c is the stress due to corner loading, P is the concentrated load, and h is the thickness of the slab.

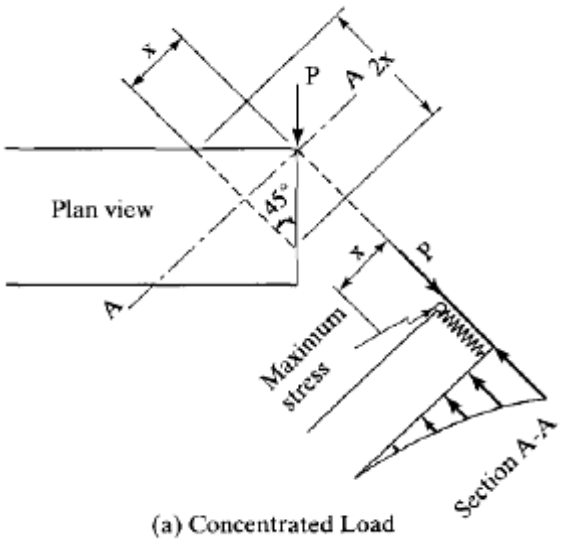

Figure 2.5: A Slab Subjected to Corner Load

Westergaard's Analysis Based on Liquid Foundations:

Westergaard carried out the most extensive theoretical studies on the stresses and deflections in concrete pavements. He developed equations due to temperature curling as well as three cases of loading: load applied near the corner of a large slab, load applied near the edge of a large slab but at a considerable distance from any corner, and load applied at the interior of a large slab at a considerable distance from any edge. Figure 2.6 displays the three critical load positions on rigid pavements.

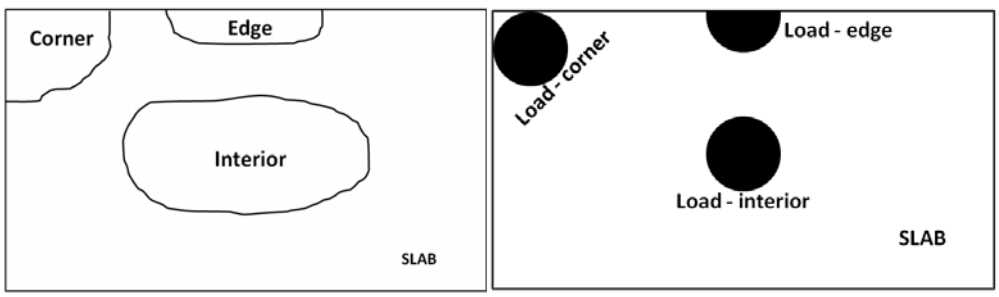

Figure 2.6: Critical Load Positions

The simplifying assumption that formed the basis for the analysis was that the eactive pressure between the slab and the subgrade at any given point is proportional to the deflection at that point, independent of the deflections at any other points. This type of foundation is typically known as a liquid or Winkler foundation. Westergaard also assumed that the slab and subgrade were in full contact.

Westergaard (1926b) applied a method of successive approximations and obtained the formulas for corner loading:

$$\sigma_c = \frac{3P}{h^2}\left[1-\left(\frac{a\sqrt{2}}{l}\right)^{0.6}\right] \tag{2.2}$$

$$\Delta_c = \frac{P}{kl^2}\left[1.1-0.88\left(\frac{a\sqrt{2}}{l}\right)\right] \tag{2.3}$$

in which Δ_c is the corner deflection, l is the radius of relative stiffness, a is the contact radius, and k is the modulus of subgrade reaction . He also found that the maximum moment occurs at a distance of $2.38\sqrt{al}$ from the corner. For a concentrated load with $a = 0$, Equations 2.2 and 2.1 are identical.

The earliest formula developed by Westergaard for the stress in the interior of a slab under a circular loaded area of radius ***a*** is

$$\sigma_i = \frac{3(1+\nu)P}{2\pi h^2}\left(\ln\frac{l}{b}+0.6159\right) \tag{2.4}$$

in which l is the radius of relative stiffness and

b = a when $a \geq 1.724h$ (2.5 a)

$b = \sqrt{1.6a^2+h^2}-0.675h$ when, a < 1 .724h (2.5 b)

For a Poisson ratio of 0.15 and in terms of base-10 logarithms, Equation 2.4 can be written as

$$\sigma_i = \frac{0.316P}{h^2}\left(4\log\left(\frac{l}{b}\right)+1.069\right) \tag{2.6}$$

The deflection equation due to interior loading (Westergaard, 1939) is

$$\Delta_i = \frac{P}{8kl^2}\left\{1+\frac{1}{2\pi}\left[\ln\left(\frac{a}{2l}\right)-0.673\right]\left(\frac{a}{l}\right)^2\right\} \tag{2.7}$$

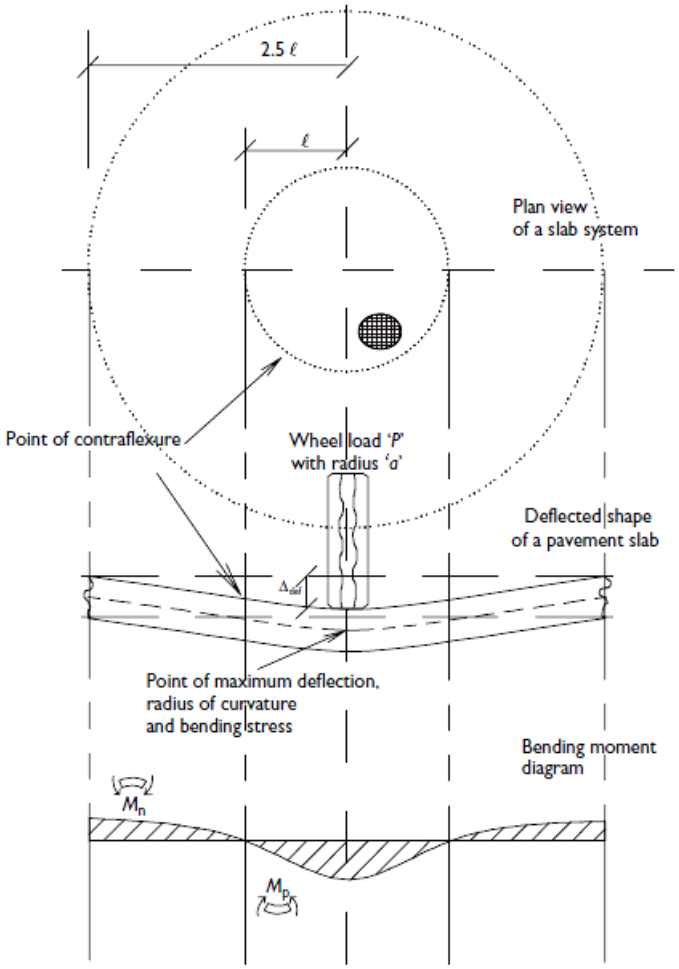

Figure 2.7: Deflected Shape of an Internally Loaded Slab

The stress due to edge loading was presented by Westergaard (1926b, 1933, 1948) in several different papers. In his 1948 paper, he presented generalized solutions for maximum stress and deflection produced by elliptical and semi-elliptical areas placed at the slab edge. Setting the length of both major and minor semiaxes of the ellipse to the contact radius *a,* leads to the corresponding solutions for a circular or semicircular loaded area. In the case of a semicircle, its straight edge is in line with the edge of the slab. The results obtained from these new formulas differ significantly from those of

the previous formulas. According to Ioannides et al. (1985), the following equations are the correct ones to use:

$$\underset{(Circle)}{\sigma_e} = \frac{3(1+\upsilon)P}{\pi(3+\upsilon)h^2}\left[\ln\left(\frac{Eh^3}{100ka^4}\right)+1.84-\frac{4\upsilon}{3}+\frac{1-\upsilon}{2}+\frac{1.18(1+2\upsilon)a}{l}\right] \quad (2.8)$$

$$\underset{(Semicircle)}{\sigma_e} = \frac{3(1+\upsilon)P}{\pi(3+\upsilon)h^2}\left[\ln\left(\frac{Eh^3}{100ka^4}\right)+3.84-\frac{4\upsilon}{3}+\frac{(1+2\upsilon)a}{2l}\right] \quad (2.9)$$

$$\underset{(Circle)}{\Delta_e} = \frac{\sqrt{2+1.2\upsilon P}}{\sqrt{Eh^3k}}\left[1-\frac{(0.76+0.4\upsilon)a}{l}\right] \quad (2.10)$$

$$\underset{(Semicircle)}{\Delta_e} = \frac{\sqrt{2+1.2\upsilon P}}{\sqrt{Eh^3k}}\left[1-\frac{(0.323+0.17\upsilon)a}{l}\right] \quad (2.11)$$

Pickett's Analysis Based on solid Foundations:

Pickett et al. (1951) developed theoretical solutions for concrete slabs on an elastic half space in view of the fact that the actual subgrade behaved more like an elastic solid than a dense liquid. Instead of its merits, the refined method has not received the attention it deserves due to the complexities of the mathematics involved. However, Pickett and Badaruddin (1956) developed a simple influence chart for determining eht edge stress based on solid foundations.

Figure 2.8 shows the applications of influence charts for determining the moment at the interior of slab. The moment is at point *O* in the *n* direction. To use the chart, it is necessary to determine the radius of relative stiffness l according to the following equation:

$$l = \left[\frac{Eh^3}{12(1-\upsilon^2)k}\right]^{0.25} \quad (2.12)$$

By counting the number of blocks N covered by the tire imprints, the moment in the n direction M can be determined from

$$M = \frac{ql^2 N}{10{,}000} \tag{2.13}$$

in which q is the contact pressure. The stress is determined by dividing the moment by the section modulus:

$$\sigma_i = \frac{6M}{h^2} \tag{2.14}$$

For the tire imprints shown in Figure 2.6, the moment is under the center of the lower left tire in the lateral direction. If the moment in the longitudinal direction is desired, the tire assembly must rotate 90° clockwise so that two of the tires lie in the zone of negative blocks, and the moment becomes much smaller.

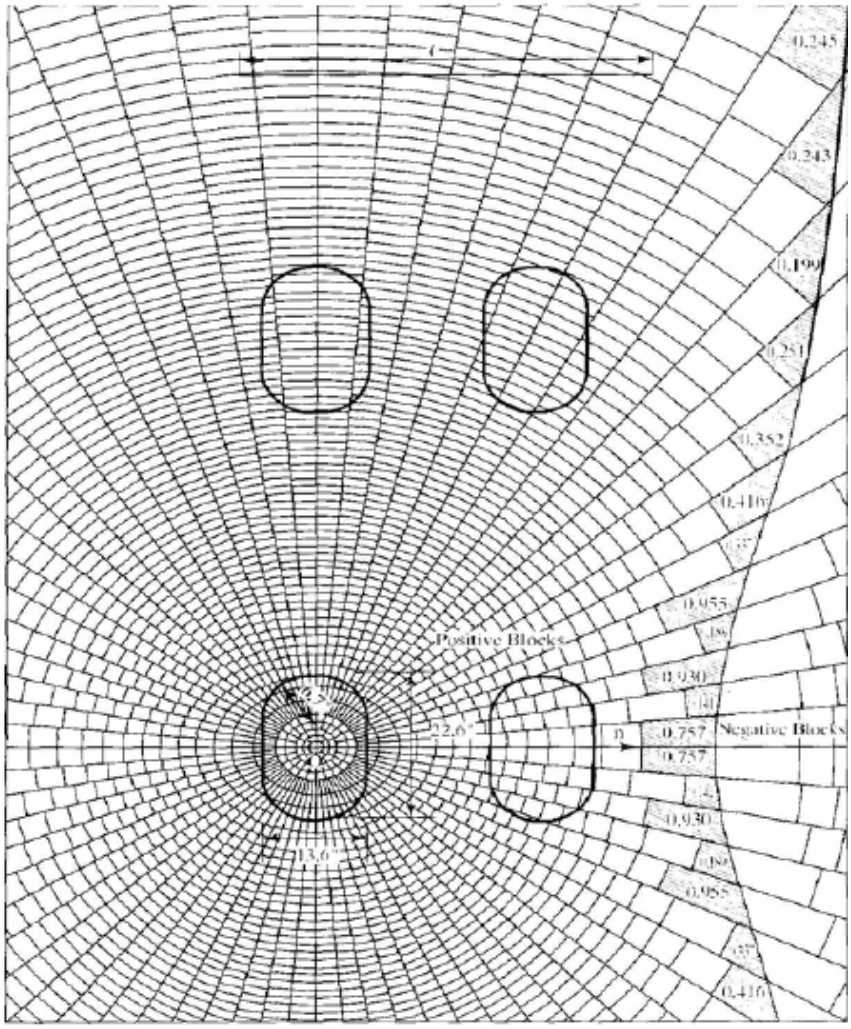

Figure 2.8: Application of Influence Chart for Determining Moment

2.4.2 Numerical Solutions

All the analytical solutions mentioned above were based on the assumption that the slab and the subgrade are in full contact. It is well known that, due to pumping, temperature curling, and moisture warping, the slab and subgrade are usually not in contact. With the advent of computers and numerical methods, some analyses based on partial contact were developed.

Discrete Element Methods:

Hudson and Matlock (1966) applied the discrete element method assuming the subgrade to be a dense liquid. The discrete element method is more or less similar to the finite difference method in that the slab is seen as an assemblage of elastic joints, rigid bars, and torsional bars. Saxena (1973) extended the method for analyzing slabs on an elastic solid foundation.

Finite Element Methods:

Development of powerful finite element (FE) method resulted in a breakthrough in the analysis of rigid pavements. The FE method has been used extensively to analyze multilayered pavement systems with the advantage of including advanced pavement material models in the solutions as opposed to the use of linear elastic layered programs. Most of the general purpose FE programs such as ABAQUS, ADINA, and ANSYS have readily built in material models. These programs also offer an interface to implement new material models through a user-defined material subroutine (UMAT), in case one needs to develop a particular material model for specific engineering behavior not provided in the FE program's material library.

2.5 TRENDS IN RIGID PAVEMENT ANALYSIS:

Finite element methods for analyzing slabs on elastic foundations of both liquid and solid types were developed by Cheung and Zeinkiewicz (1965).The methods were applied on liquid foundations by Huang and Wang (1973) and on solid foundations by Huang (1974). Chou (1981) developed finite element computer programs named WESLIQUID and WESLAYER in collaboration with Huang for the analysis of liquid and layered foundations. The consideration of foundation as a layered system is more realistic when layers of base and subbase exist above the subgrade. Other finite

element computer programs available include ILLI-SLAB developed at the University of Illinois, JSLAB developed by Portland Cement Association, and RISC developed by Resource International, Inc.

The KENSLABS computer program (Huang, 1985) is based on the finite-element method, in which the slab is divided into rectangular finite elements with a large number of nodes. Both wheel loads and subgrade reactions are applied to the slab as vertical concentrated forces at the nodes. KENSLABS can have two layers of slab, either bonded or unbonded. The two layers can be an HMA on top of a PCC or a PCC over a cement-treated base. In the latter case, the cement-treated base can be considered as the second layer of slab or the first layer of the foundation. When it is considered to be the foundation, it is assumed that there is no bond between the concrete slab and the foundation. KENSLABS, together with its input program SLABSINP and graphic programs SGRAPH and CONTOUR, is part of a computer package called KENPAVE. In its present dimensions, it can be applied to a maximum of 6 slabs, 7 joints, and 420 nodes. Each slab can have a maximum of 15 nodes in the x-direction and 15 nodes in the y-direction. Damage analysis can be made by dividing each year into a maximum of 1 2 periods, each with a maximum of 12 load groups. ILLI-SLAB was originally developed in 1977 for the structural analysis of one or two layers of slabs with or without mechanical load transfer systems at joints and cracks (Tabatabaie, 1977). It has since been continuously revised and expanded through several research studies to improve its accuracy and ease of application. Its capabilities are similar to KENSLABS, which was originally developed in 1973 and has been continuously updated and improved for classroom use.

Heinrichs et al. (1989) compared several available computer models for rigid pavements and concluded that both ILLI-SLAB and JSLAB, which is a similar finite - element program developed by the PCA, were efficient to use and could structurally model many key design factors of importance. They also indicated that ILLI-SLAB had had extensive checking, revisions, and verification by many researchers and was more nearly free of errors than any other available program. They presented the results of several cases by different models, with which KENSLABS can be compared. ILLI-SLAB was later extended (and renamed ILLISLAB94) to overcome the typical limitations of 2-D programs (Khazanovich, 1994; Khazanovich and Yu,

1996). Features that distinguish ILLISLAB94 from other programs include a wide selection of subgrade models and the ability to analyze the effects of separation between pavement layers, linear and nonlinear temperature distribution, and partial depth cracks in the concrete layer. ILLISLAB94 was further improved by ERES (Khazanovich et al., 2000) and renamed ISLAB2000, with many additional features, including analysis of mismatched joints and cracks, improved void-analysis model, convenient graphical input and output processors, automated mesh generator and load placement, batch processing of factorial runs, convenient handling of exceptions, and visualization of analysis results.

Hossain (1992) investigated the behaviour of a conventional concrete pavement of uniform thickness and a thickened edge box type pavement with holes for utility services using Finite Element software ANSYS. The materials used in the study were linearly elastic. The study carried out the effects of thickness, width and length of a conventional pavement, thickness of subbase and the subgrade CBR on the pavement deflection, tensile stress and subgrade pressure. The study showed that for a conventional pavement, the maximum values of pavement deflection, tensile stress and subgrade pressure are reduced with an increase in slab thickness. The presence of a subbase further reduces the above values among which the most significant reduction takes place in the subgrade contact pressure value. An increase in pavement width and length of slab also reduces the tensile stress and deflection. When a better quality subbase is used, the deflection and tensile stress are reduced. Similar effects are noticed for a better quality subgrade.

Shaikh (2005) also carried out a behavioral study of rigid pavement section using general purpose finite element software ANSYS. The model was generated directly using ANSYS CAD modeler. The surface layer is simulated through a two-dimensional plane surface while the subbase and subgrade are considered as elastic, homogeneous and linear springs supporting the top surface and are been modeled through one individual spring using effective or composite stiffness. He concluded that non linear properties of both concrete and foundation material can be used in order to better simulate the real field condition.

As the demand for applied wheel loads and number of load applications increases, it becomes very important to properly characterize the behaviour of subgrade soils and unbound aggregate layers as the foundations of the layered pavement structure. Unfortunately, most commonly used elastic layered programs assume linear elastic material behavior for the unbound aggregate base/subbase and subgrade soil layers. Previous laboratory studies have shown that the resilient responses of both coarse-grained unbound granular materials used in untreated base/subbase courses and fine-grained subgrade follow nonlinear, stress-dependent behaviour under repeated traffic loading by Thompson and Robnett (1979); Brown and Pappin (1981); Uzan (1985); Tutumluer (1995); Rowshanzamir (1995). Unbound granular materials exhibit stress hardening, whereas, fine-grained soils show stress-softening type behaviour.

Although, consideration of non-linearity in unbound layers is necessary for accurate modeling of a flexible pavement structure, the necessity of non-linear consideration in rigid pavements has not been studied as closely. Assumption of unbound layers to be linearly elastic raises many problems. For example, granular layers may have a lower modulus than the subgrade, and measured vertical strain at the top of the subgrade may be twice the theoretical value. Nazarian and Stokoe have shown that non-linear behavior occurs in Falling Weight Deflection (FWD) testing. An increase in the load magnitude of the FWD results in an increase in deflection that is greater than one to one. Nazarian, et. al. also showed the effect of non-linearity with depth in a farm to-market test road.

Several procedures have been developed to consider the non-linearity of unbound layers in pavement structures. Some analyses attempt to model the non-linearity by considering the plastic behavior of subgrade soils. Others approximate non-linear effects through iterative linear elastic procedures. Most recently, finite element code has been utilized in modeling the stress state dependency of granular base layers, and the strain level dependence of subgrade materials. Kou and Huang compared nonlinear analysis and linear analysis for subgrade materials and concluded that the determination of the resilient modulus for the linear models is critical to interpret the behaviors of nonlinear materials.

2.6 SUMMARY

This chapter provides a brief account of the analytical and numerical research work that has been carried out for studying the responses of rigid pavements due to traffic loads. It appears that the earlier numerical or analytical research in this area has been confined to linear elastic material characterization. As stresses and strains are used more and more to determine the relative condition of layers in a pavement structure, the need for consideration of non-linear material behavior becomes increasingly important. Linear elastic approximations of unbound material behavior are no longer acceptable in pavement analysis. Errors from such approximations have been noted and documented. The stress state dependency of granular materials, and strain based subgrade soil models must be considered for an accurate estimation of true pavement response. A finite element type analysis needs to be employed to model such nonlinear resilient behavior and more realistically predict pavement responses for a mechanistic pavement analysis. Hence, it is obvious that there is scope of potential study in this area with more realistic non-linear soil models.

Chapter 3
DEVELOPMENT OF FINITE ELEMENT MODEL

3.1 INTRODUCTION

This chapter describes the three-dimensional finite element modeling of jointed plain concrete pavement on a base course material above a subgrade. The finite element model consists of three components – the concrete surface, the granular base course material and the subgrade soil. Choice of element types for modeling the concrete surface, the granular base, the subgrade soil and the interface is also described.

3.2 SELECTION OF FINITE ELEMENT SOFTWARE

A significant number of general purpose finite element analysis computer tools or software packages are available today that can be used for civil engineering purpose. ABAQUS, DIANA, ANSYS, STRAND, ADINA, FEMSKI, and STAAD etc are some of the most widely used and accepted finite element analysis tools. These packages vary in their degree of complexity, utility and versatility. Some of these programs are intended for a specific type of structure. Considering the detailed documentation, flexibility and versatility of capabilities the package ABAQUS has been proved to be relatively better for the current study. Moreover different feature of soil and soil-structure interaction can be easily simulated by ABAQUS. The version of ABAQUS that has been used for this study is ABAQUS 6.8.

3.3 DEVELOPMENT OF THE 3D FINITE ELEMENT MODEL

For the successful development of a finite element model for a jointed plain concrete pavement, clear understanding of the different components of the pavement system and their interaction with one another is vitally important. The surface course of a jointed plain concrete pavement is made of Portland cement concrete without any reinforcements. The concrete slab may be laid directly on top of the subgrade soil or a base course layer of granular material may be used to facilitate good drainage. Load transfer across the joints is facilitated either by aggregate interlock or by dowel bars when incorporated into the pavement structure.

The finite element modeling of this study consists of three components – the jointed plain concrete pavement surface, the granular base course material, and the subgrade soil. It also encompasses the interfaces between any two of these three components of the pavement system. In Fig. 3.1, a schematic diagram of a jointed plain concrete pavement system has been shown.

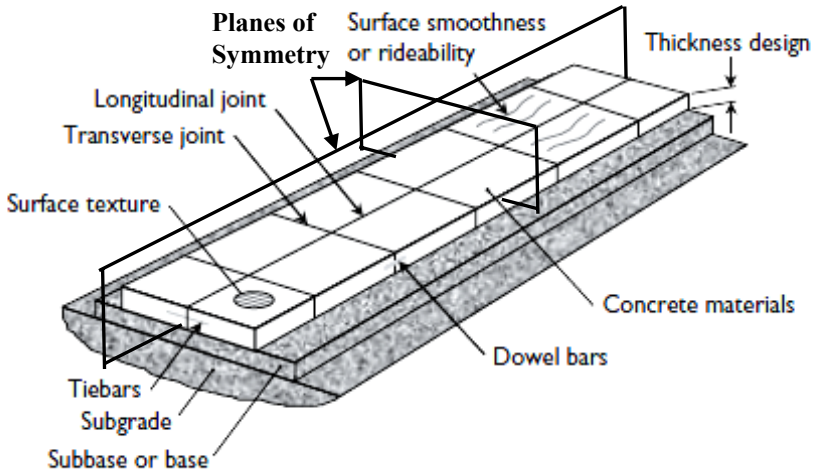

Fig. 3.1 Schematic Diagram of a Jointed Plain Concrete Pavement

The pavement system has two vertical planes of symmetry as shown in Fig.3.1, one along the center line of pavement and another across the center line of the pavement. These planes of symmetry provide an inherent benefit in the finite element modeling and analysis of the pavement system. Because of these symmetries, only one quarter of the pavement is sufficient for finite element modeling, which requires less computing capacity with a consequent save in analysis time. Fig. 3.2 shows a schematic diagram of a one quarter of the jointed plain concrete pavement (JPCP) that will be used for developing the present 3D FE model. The concrete slab is considered to be laid on a granular base course material instead of being placed directly on the natural subgrade soil. Soil is considered to extend horizontally across the pavement beyond the base course material and concrete slab edge. In the Fig 3.2, X direction corresponds to the width of the pavement and Z direction corresponds to the length of

the pavement in the direction of traffic movement and Y direction corresponds to the depth of the pavement.

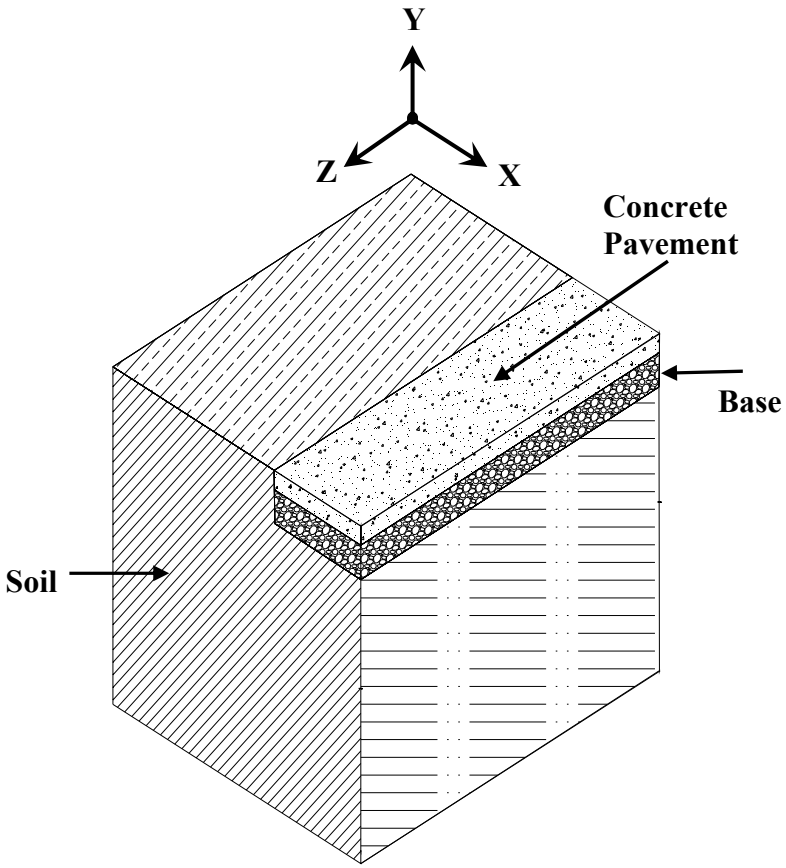

Fig. 3.2 Schematic View of Quarter of the Jointed Plain Concrete Pavement System

3.3.1 Modeling of Soil

Characterization of soil is a complex phenomenon because of its nonlinearity and several other factors such as its interaction with structures and time dependent effects-creep, temperature and load history. Due to the orthotropic nature of soil, selection of proper element and material property inputs are very important to simulate the actual condition.

3.3.1.1 Element

The soil can be modeled using C3D8 and C3D6 elements. C3D8 is 8-node linear brick used for the three-dimensional modeling of solid structures. The element is defined by eight nodes. Each node of the element has three degrees of freedom at each

node: translations in the nodal x, y, and z directions. C3D6 is 6-node linear brick. Like C3D8 each node of the element has three degrees of freedom. Soil of different soil layers can be modeled by same elements but with different material properties. The C3D8 and C3D6 are shown in Fig. 3.3. In this study, C3D8 is used for modeling soil.

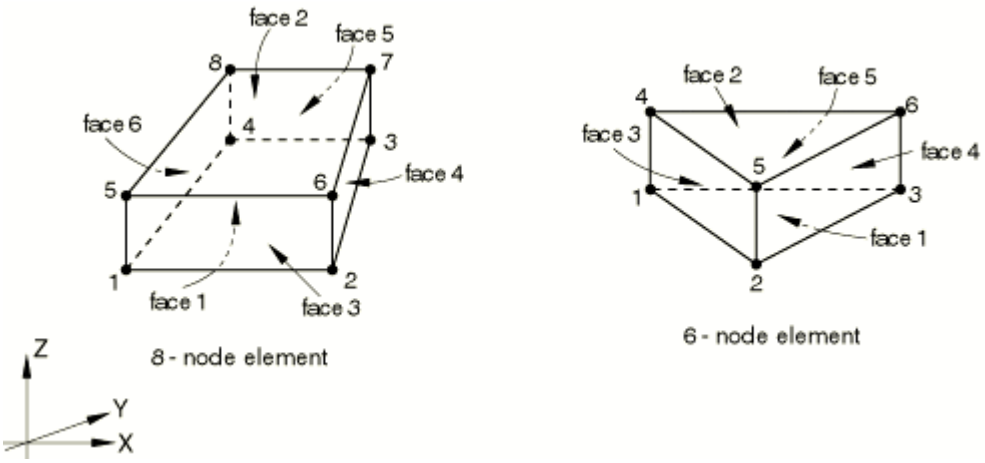

Fig. 3.3 C3D8 and C3D6 Elements

3.3.1.2 Material

Soil is modeled as an elastoplastic isotropic material. So elastic property and plastic property have to be defined. Elastic property is defined as a linear elasticity based on elastic modulus (E) and Poisson's ratio (v). But defining plastic property of a soil is rather complex. ABAQUS has the following four different plastic martial models for soil:

- Extended Drucker-Prager models
- Modified Drucker-Prager/ Cap model
- Mohr-Coulomb plasticity
- Critical state (clay) plasticity model

In this study Modified Drucker-Prager / Cap model is selected for soil plasticity as which has following features:

- It is intended to model cohesive geological materials that exhibit pressure-dependent yield, such as soils and rocks;

- It is based on the addition of a cap yield surface to the Drucker-Prager plasticity model, which provides an inelastic hardening mechanism to account for plastic compaction and helps to control volume dilatancy when the material yields in shear;
- It can be used in Abaqus/ Standard to simulate creep in materials exhibiting long-term inelastic deformation through a cohesion creep mechanism in the shear failure region and a consolidation creep mechanism in the cap region;
- It can be used in conjunction with either the elastic material model or, in Abaqus/ Standard if creep is not defined, the porous elastic material model; and
- It provides a reasonable response to large stress reversals in the cap region; however, in the failure surface region the response is reasonable only for essentially monotonic loading.

The addition of the cap yield surface to the Drucker-Prager model serves two main purposes: it bounds the yield surface in hydrostatic compression, thus providing an inelastic hardening mechanism to represent plastic compaction; and it helps to control volume dilatancy when the material yields in shear by providing softening as a function of the inelastic volume increase created as the material yields on the Drucker-Prager shear failure surface.

The yield surface has two principal segments: a pressure-dependent Drucker-Prager shear failure segment and a compression cap segment, as shown in Fig. 3.4. The Drucker-Prager failure segment is a perfectly plastic yield surface (no hardening). Plastic flow on this segment produces inelastic volume increase (dilation) that causes the cap to soften. On the cap surface plastic flow causes the material to compact.

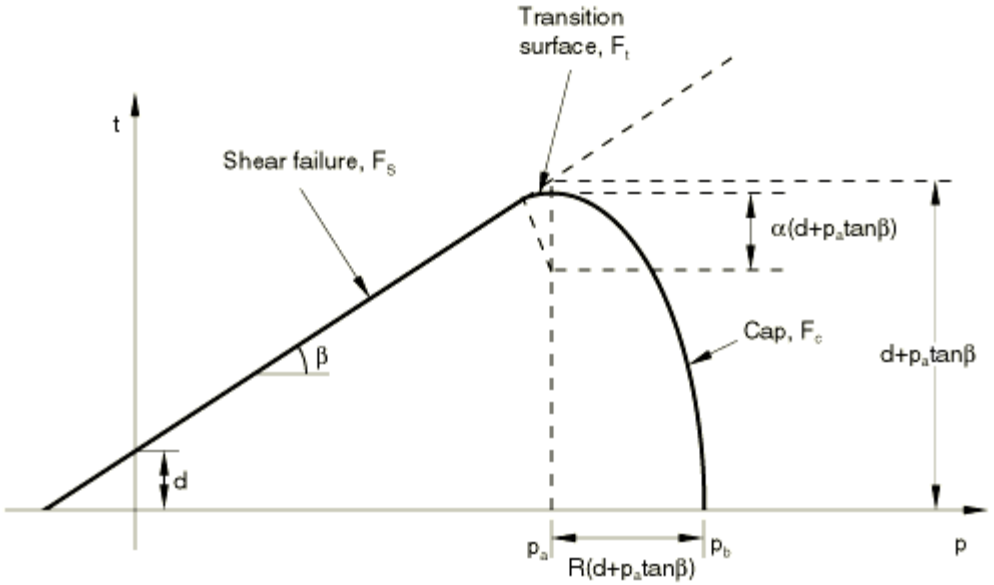

Fig. 3.4 Modified Drucker-Prager/Cap Model: Yield Surfaces in the p–t Plane.

The elastic behavior can be modeled as linear elastic or by using the porous elasticity model including tensile strength. If creep has been defined, the elastic behavior must be modeled as linear. The Drucker-Prager failure surface is written as

$$F_S = t - p\tan\beta - d = 0; \tag{3.1}$$

Where $\beta(\theta, f_i)$ and $d(\theta, f_i)$ represent the angle of friction of the material and its cohesion, respectively, and can depend on temperature, θ and other predefined fields, $f_i, i = 1, 2, 3\ldots$. The deviatoric stress measure t is defined as

$$t = \frac{1}{2}q\left[1 + \frac{1}{K} - \left(1 - \frac{1}{K}\right)\left(\frac{r}{q}\right)^3\right]; \text{and} \tag{3.2}$$

$p = -\frac{1}{3}trace(\sigma)$: is the equivalent pressure stress, $q = \sqrt{\frac{3}{2}S:S}$: is the Mises equivalent stress, $r = (\frac{9}{2}S:S\cdot S)^{\frac{1}{3}}$: is the third stress invariant, and $S = \sigma + pI$: is the deviatoric stress. $K(\theta, f_i)$: is a material parameter that controls the dependence of the yield surface on the value of the intermediate principal stress, as shown in Fig. 3.5.

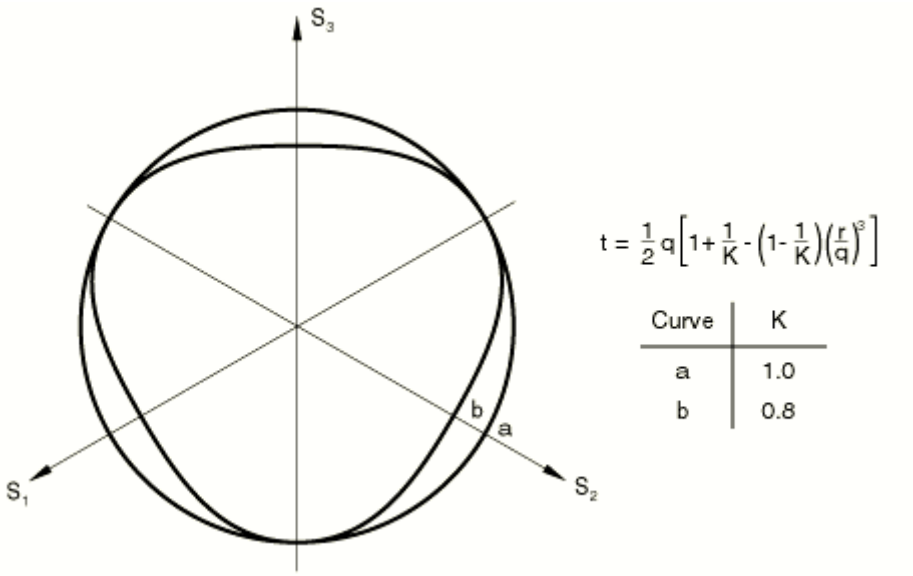

Fig. 3.5 Typical Yield/Flow Surfaces in the Deviatoric Plane.

The yield surface is defined so that K is the ratio of the yield stress in triaxial tension to the yield stress in triaxial compression. $K = 1$ implies that the yield surface is the Von Mises circle in the deviatoric principal stress plane (the Π-plane), so that the yield stresses in triaxial tension and compression are the same; this is the default behavior in Abaqus/Standard and the only behavior available in Abaqus/Explicit. To ensure that the yield surface remains convex requires, $0.778 \le K \le 1.0$

The cap yield surface has an elliptical shape with constant eccentricity in the meridional (p–t) plane (Fig. 3.4) and also includes dependence on the third stress invariant in the deviatoric plane (Fig. 3.5). The cap surface hardens or softens as a function of the volumetric inelastic strain: volumetric plastic and/or creep compaction causes hardening, while volumetric plastic and/or creep dilation causes softening. The cap yield surface is

$$F_C = \sqrt{\left[p - p_a\right]^2 + \left[\frac{Rt}{\left(1 + \alpha - \alpha / \cos\beta\right)}\right]^2} - R\left(d + p_a \tan\beta\right) = 0; \qquad (3.3)$$

Where $R(\theta, f_i)$ is a material parameter that controls the shape of the cap, $\alpha(\theta, f_i)$ is a small number that we discuss later, and $p_a(\varepsilon_{vol}^{pl} + \varepsilon_{vol}^{cr})$ is an evolution parameter that represents the volumetric inelastic strain driven hardening/softening. The

hardening/softening law is a user-defined piecewise linear function relating the hydrostatic compression yield stress, p_b and volumetric inelastic strain (Fig. 3.6):

$$p_b = p_b(\varepsilon_{vol}^{in}|o + \varepsilon_{vol}^{pl} + \varepsilon_{vol}^{cr}) \tag{3.4}$$

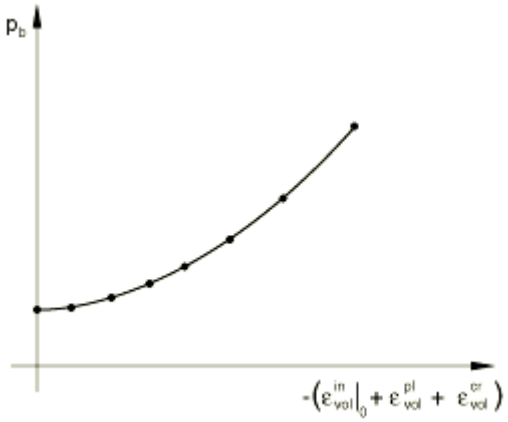

Fig. 3.6 Typical Cap Hardening.

The volumetric inelastic strain axis in Fig.3.6 has an arbitrary origin: $\varepsilon_{vol}^{in}|o(=\varepsilon_{vol}^{pl}|o + \varepsilon_{vol}^{cr}|o)$ is the position on this axis corresponding to the initial state of the material when the analysis begins, thus defining the position of the cap (p_b), in Fig 3.4, at the start of the analysis. The evolution parameter p_a is given as

$$p_a = \frac{p_b - Rd}{(1 + Rtna\beta)} \tag{3.5}$$

The parameter α is a small number (typically 0.01 to 0.05) used to define a transition yield surface,

$$F_t = \sqrt{(p - p_a)^2 + \left[t - \left(1 - \frac{\alpha}{cas\beta}\right)(d + p_a \tan\beta)\right]^2} - \alpha(d + p_a \tan\beta) = 0; \tag{3.6}$$

so that the model provides a smooth intersection between the cap and failure surfaces. Plastic flow is defined by a flow potential that is associated on the cap and nonassociated on the failure yield surface and transition yield surfaces. The

nonassociated nature of these surfaces stems from the shape of the flow potential in the meridional plane. The flow potential surface in the meridional plane is shown in Fig. 3.7.

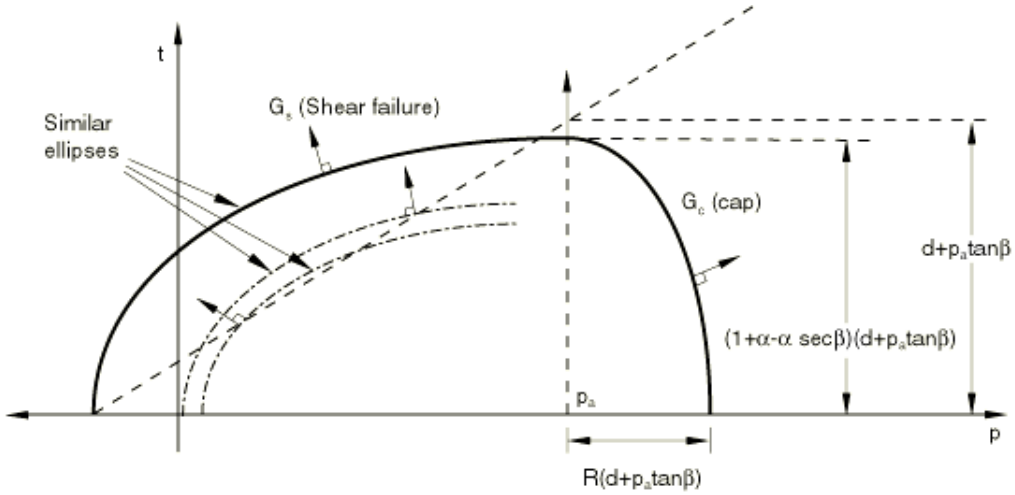

Fig 3.7 Modified Drucker-Prager/Cap Model: Flow Potential in the p–t Plane.

It is made up of an elliptical portion in the cap region that is identical to the cap yield surface:

$$G_C = \sqrt{[p - p_a]^2 + \left[\frac{Rt}{(1 + \alpha - \alpha / \cos\beta)}\right]^2} \tag{3.7}$$

and another elliptical portion in the failure and transition regions that provides the nonassociated flow component in the model:

$$G_S = \sqrt{[(p_a - p)\tan\beta]^2 + \left[\frac{t}{(1 + \alpha - \alpha / \cos\beta)}\right]^2} \tag{3.8}$$

The two elliptical portions, G_c and G_s, form a continuous and smooth potential surface. Nonassociated flow implies that the material stiffness matrix is not symmetric, so the unsymmetric solver should be invoked by the user. However, if the region of the model in which nonassociated inelastic deformation is occurring is confined, it is possible that a symmetric approximation to the material stiffness matrix

will give an acceptable convergence rate: in such cases the unsymmetric solver may not be needed.

3.3.2 Modeling of Granular Base

Granular material characterization is also a complex phenomenon because of its nonlinear stress dependent behavior and several other factors. The cross-anisotropic, or laterally isotropic, behavior is a response that is particular to unbound granular materials. Selection of proper element and material property inputs are very important to simulate the actual condition.

3.3.2.1 Element

The granular base can be modeled using C3D8 and C3D6 elements. C3D8 is 8-node linear brick used for the three-dimensional modeling of solid structures. The element is defined by eight nodes. Each node of the element has three degrees of freedom at each node: translations in the nodal x, y, and z directions. C3D6 is 6-node linear brick. Like C3D8 each node of the element has three degrees of freedom. The C3D8 and C3D6 are shown in Fig. 3.3. In this study, C3D8 is used to model granular base.

3.3.2.2 Material

In this study Extended Drucker-Prager model is selected for granular base plasticity as it has following features.

- To be used to model frictional materials, which are typically granular-like soils and rock, and exhibit pressure-dependent yield (the material becomes stronger as the pressure increases);
- To be used to model materials in which the compressive yield strength is greater than the tensile yield strength;
- Allow a material to harden and/or soften isotropically;
- Generally allow for volume change with inelastic behavior: the flow rule, defining the inelastic straining, allows simultaneous inelastic dilation (volume increase) and inelastic shearing;
- Can include creep if the material exhibits long-term inelastic deformations;
- Can be defined to be sensitive to the rate of straining;
- Can be used in conjunction with either the elastic material model like Linear elastic behavior;

- Can be used in conjunction with the models of progressive damage and failure to specify different damage initiation criteria and damage evolution laws that allow for the progressive degradation of the material stiffness and the removal of elements from the mesh and;
- To be intended to simulate material response under essentially monotonic loading.

The yield criteria for this class of models are based on the shape of the yield surface in the meridional plane. The yield surface can have a linear form, a hyperbolic form, or a general exponent form.

For this analysis hyperbolic yield surface is selected. This surface is illustrated in Fig. 3.8 and 3.9. Basic parameter of this model is the inclined angle of yield surface in the meridional plane (β), cohesion of the material (d') and the dilation angle (ψ). Angle to yield surface (β) can be easily relate to the angle internal frictional angle (φ) of aggregate by the equation 3.9

$$\tan \beta = \frac{6 \sin \varphi}{3 - \sin \varphi} \tag{3.9}$$

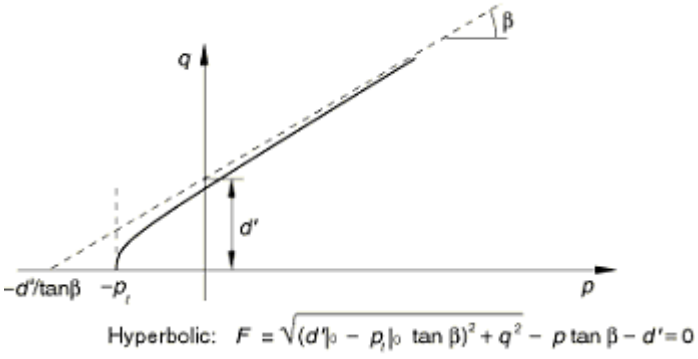

Here,

P_t = initial hydrostatic tension strength of the material

d' = cohesion of the material

β = slope of the yield surface in the p–q stress plane

Fig. 3.8: Yield Surface in the Meridional Plane.

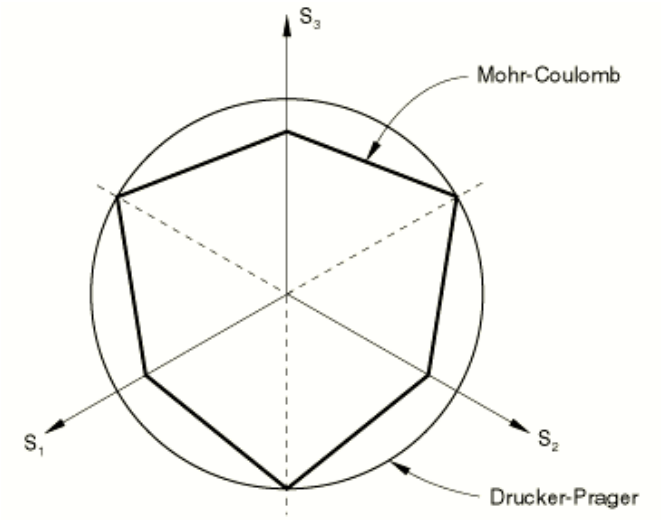

Fig. 3.9: Yield Surface in the Deviatoric Plane.

Granular base is assumed cohesionless, so d' should be 0. But to avoid singularity problem a very small value like 10 Pa is defined as d'.

Extended Drucker-Prager model is capable of hardening and softening. Fig. 3.10 shows yield surface and hardening in the p–q plane and flow rule of hyperbolic model. Fig. 3.11 shows a typical hardening curve used as a hardening parameter.

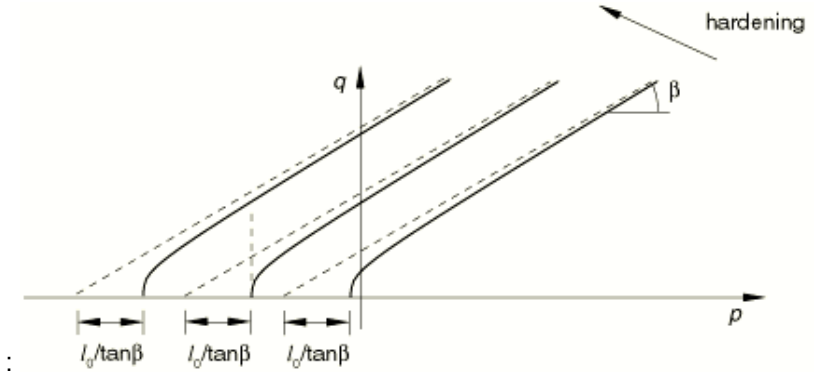

:

Fig. 3.10: Yield Surface and Hardening in the p–q Plane and Flow Rule of Hyperbolic Model

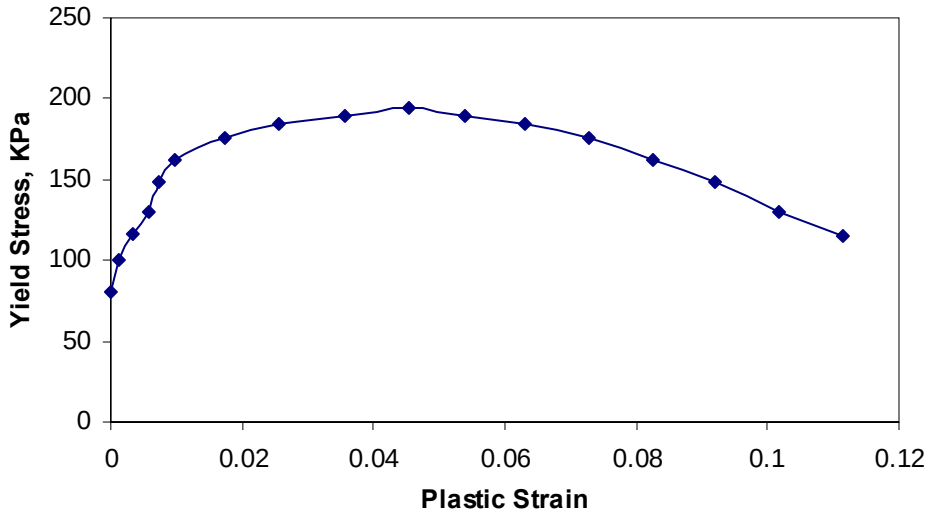

Fig. 3.11: Typical Hardening Curve

3.3.3 Modeling of Concrete Slab

3.3.3.1 Element

The concrete slab can be modeled using C3D8 and C3D6 elements. C3D8 is 8-node linear brick used for the three-dimensional modeling of solid structures. The element is defined by eight nodes. Each node of the element has three degrees of freedom at each node: translations in the nodal x, y, and z directions. C3D6 is 6-node linear brick. Like C3D8 each node of the element has three degrees of freedom. The C3D8 and C3D6 are shown in Fig. 3.3. In this study, C3D8 is used to model concrete slab.

3.3.3.2 Material

For this study, concrete is considered to be homogenous and linearly elastic following Hooke's law. The input parameters are modulus of Elasticity, $\boldsymbol{E}$ and Poisson's ration $\boldsymbol{\upsilon}$.

3.3.4 Interface between Different Pavement Components

In the model, the subgrade soil, granular base and concrete slab are in close contact with one another. In this study, classical isotropic Coulomb's friction algorithm is used to simulate the interaction. To define contact pair following issues were considered.

- Surface –to-surface contact discretization;
- Finite sliding tracking approach; and
- Concrete slab is chosen as master surface and granular base is chosen as slave surface for slab-base interaction. Similarly, granular base is chosen as master surface and subgrade soil is chosen as slave surface for base-subgrade interaction.

3.3.5 Co-ordinate System

The Cartesian coordinate system has been considered as the global co-ordinate system. X-axis has been considered as the direction across the pavement, Y-axis as the vertical upward direction and Z-axis as the direction along the pavement in the direction of traffic movement. The transverse section or the cross-section of the pavement is on the X-Y plane. Directions of the axis are shown in Fig. 3.2 and 3.12.

3.3.6 Boundary Conditions

For the developed model, the following boundary conditions are imposed as shows in Fig. 3.12:

- Translation in the vertical direction (Y- axis) is restrained for the bottom of the subgrade soil. (Uy = 0);

- Translation in the horizontal direction (X-axis) is restrained for the Y-Z planes constituting the boundaries of the model. (Ux = 0);

- Translation in the horizontal direction (Z-axis) is restrained for the X-Y planes constituting the boundaries of the model. (Uz = 0);

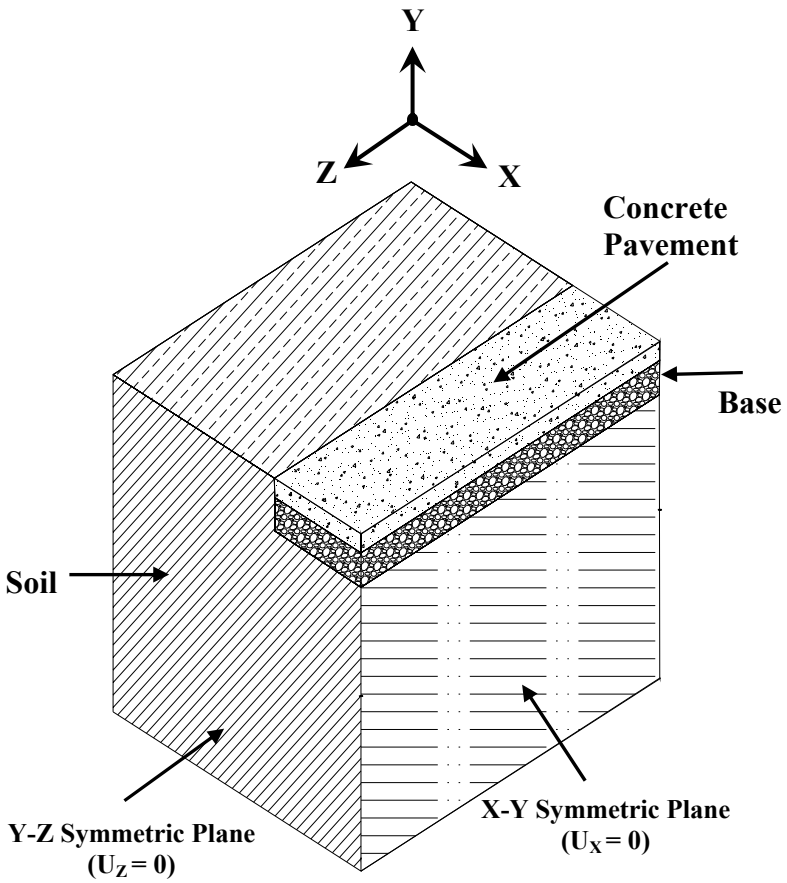

Fig. 3.12: Boundary Condition of the Developed Model

3.3.7 Load

For the analysis of the developed pavement model, two stages of loadings were considered. In the first stage, gravity load was applied on the whole pavement system. In the next stage, wheel load was applied on the concrete slab surface as a uniform pressure over a fixed area based on the considerations of axle load, wheel configuration and tire pressure.

3.4 DEVELOPMENT OF THE 2D AXISYMMETRIC FINITE ELEMENT MODEL

For axisymmetric analysis CAX3, CAX4, CAX6 and CAX8 can be used.CAX3 is a 3 node linear element, CAX4 is a 4-noded bilinear, axisymmetric solid (continuum) element, CAX6 is a six node quadratic element and CAX8 is an eight node biquadratic element. Each node of the element has two degrees of freedom in the

nodal r and z direction. The elements are shown in fig. 3.13. In this study, CAX4 element was used.

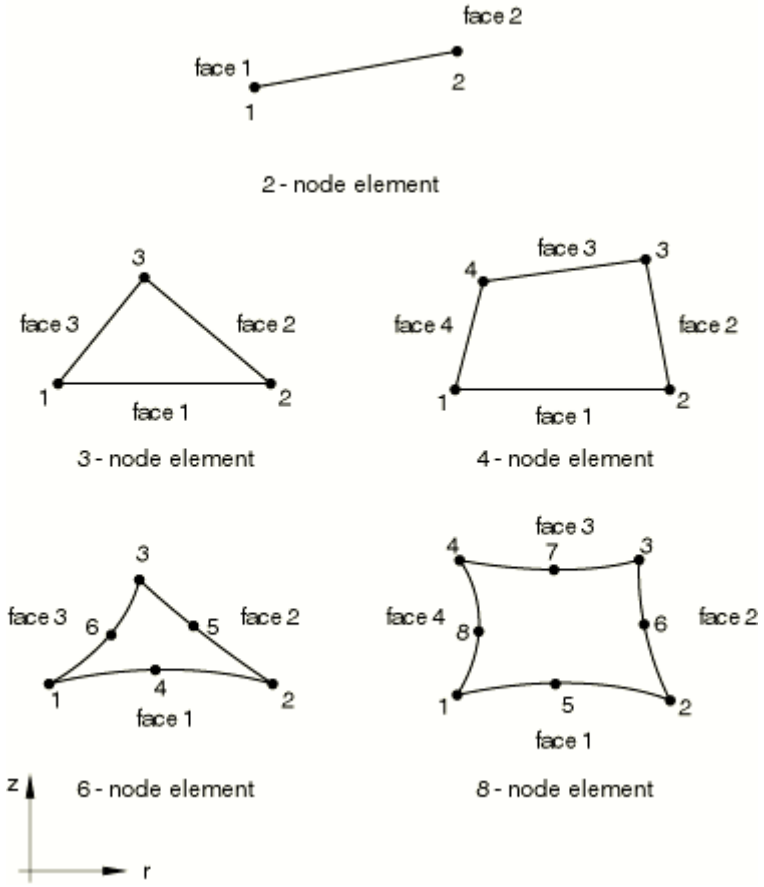

Fig. 3.13 CAX3, CAX4, CAX6, and CAX8 Elements

3.5 IDEALIZATION OF THE PAVEMENT SYSTEM

For analyzing the pavement system it is required to idealize the physical system. The following section describes the simplification of different properties of actual structure to be used in the finite element model.

3.5.1 Structural Idealization

A typical two-lane jointed plain concrete pavement slab with lane width of 3.5 meter (12 feet) each was selected and one lane was considered for developing the model for analysis. A joint spacing of 3.5 meter (12feet) was selected for transverse joints for this study. For the purpose of simplicity, one quarter of the pavement system was

analyzed as it has two axis of symmetry, one along the pavement and another across the pavement as shown in Fig.3.1 and Fig. 3.2. Depth of the subgrade soil and its extension in the horizontal direction was found out through sensitivity analysis discussed later in this chapter. No shoulder, either concrete or flexible, was considered in this study. Natural subgrade was considered beyond the boundary of concrete slab and granular base in the horizontal direction. Smooth boundary conditions were applied along the bottom and the side faces of the boundary of the model which is described in the preceding paragraphs. The objective of using smooth boundary conditions is to make the system as flexible as possible. Here, the bottom surface as well as all other vertical sides was considered to be on rollers so that no rigid body motion takes place. Relative displacements were allowed at the interfaces of concrete with granular base and soil but no relative displacement was allowed between granular base and soil interfaces. Interaction with adjacent slabs (i.e. transfer of load and deflection along pavement slab joints) was not considered in this analysis.

3.5.2 Properties of Material

Any highway slab-soil system involves a wide variety of subgrade soil. Extreme variability in properties such as soil strength, gradation and permeability always pose a great difficulty in the task of highway design. To consider all the varieties of material properties is beyond the scope of the present study.

The jointed plain concrete pavement is composed of three different material type- concrete slab, base or subbase aggregate (if used) and subgrade soil. For the present study, concrete is assumed to be linearly elastic, homogenous and isotropic. The base course aggregate and the subgrade soil are considered to exhibit stress dependent nonlinear behavior. The material properties used in this study are described in the following sections.

3.5.2.1 Concrete

The properties of concrete required for analysis of the pavement system are Modulus of Elasticity (E_c), density and Poisson's ratio (v). For modeling different components of the concrete slab, modulus of elasticity of concrete E_c, density, and Poisson's ratio v are taken to be 25 GPa , 2400 kg/m^{3}and 0.2 respectively.

3.5.2.2 Granular Base

Availability of strength and deformation characteristic data for aggregate layer materials is a great concern for proper modeling of these materials. Lack of testing facilities and high cost of performing the necessary tests to determine their characteristic properties are responsible for this dearth. For the present study, test data from the Minnesota Road Research Project (Mn/ROAD) were used. The Minnesota Department of Transportation in cooperation with the Federal Highway Administration and the Local Roads Research Board of Minnesota constructed the project. Aggregate layer materials have been tested both in the laboratory and in the field. These tests have been conducted by the Minnesota Department of Transportation and the University of Illinois. Table 3.1 shows the classes of aggregates used in the mentioned project and Table 3.2 lists the results of rapid shear test results for them and the results are shown in Fig. 3.14.

Table: 3.1. Characteristics of Mn/ ROAD Base Aggregates

Aggregate Class	Function	Maximum size, mm	Percent Finer than 0.075 mm	Fractured Particles	Plasticity	
					LL	PI
3 Sp	Base	12.5	12	----	≤35	≤12
4 Sp	Base	37.5	8	----	≤35	≤12
5 Sp	Base	25.0	6	Min	≤25	≤6
6 Sp	Base	25.0	3	Max	≤25	≤6

Table: 3.2. Results from UIUC Rapid Shear Tests

Material	m.c., %	Opt. m.c., %	ρ_{dry}, Kg/m^3	Φ, degrees	c, KPa	Peak σ_d, KPa (σ_3 = 103 KPa)
cl 3 Sp	6.8	8.0	2034	44	48	648
cl 4 Sp	9.4	9.4	2115	31	117	614
cl 5 Sp	6.8	7.7	2195	43	76	793
cl 6 Sp	6.3	6.8	2147	47	124	1220

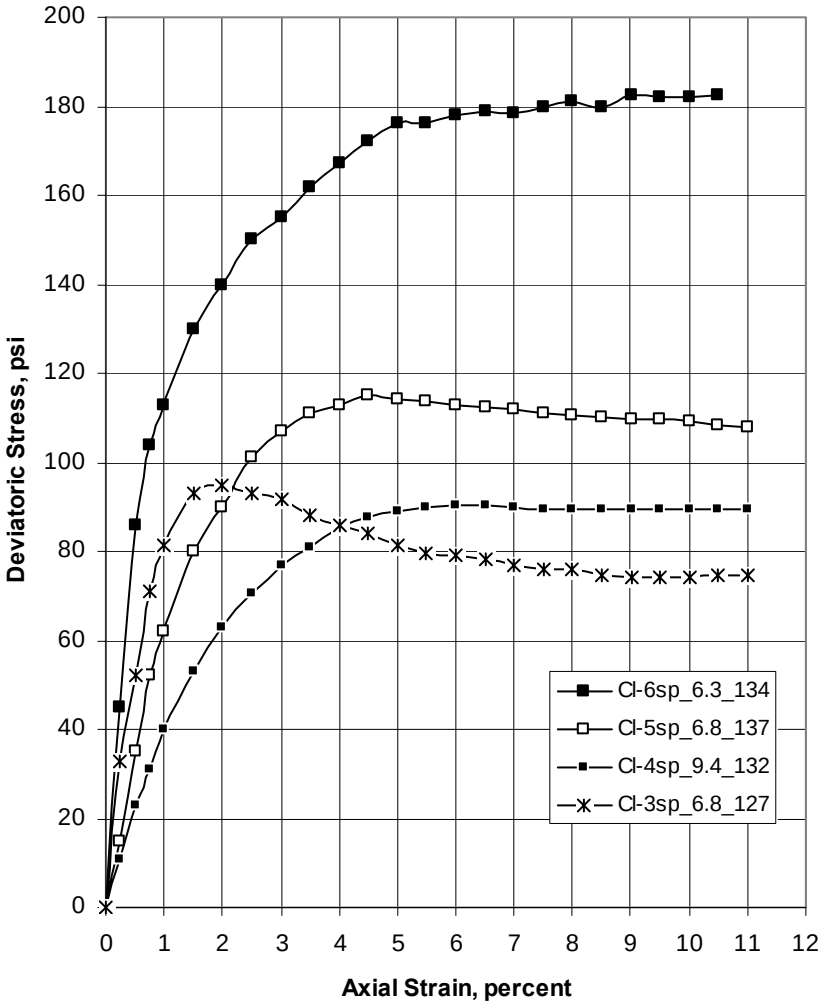

Fig. 3.14 UIUC Rapid Shear Test Results

3.5.2.3 Soil

Subsurface exploration should be carried out to determine the presence and influence of geologic and environmental conditions that may affect the performance of the pavement system. Subsoil investigation should be conducted to evaluate the capacity of foundation materials to resist the applied loads and to determine the soil properties vital for a representative finite element analysis. The type, compacted density and strength properties of the soil envelope adjacent to the structure should be established.

The modulus of elasticity of the soil estimated using the SPT values from RPT-Nedeco-BCL (May, 1987) and equations suggested by J.E. Bowles (1988) and the standard values of Poisson's ratio suggested by J.E. Bowles (1988) are shown in Table 3.3 and table 3.4. Unit weights, Effective Angles of Internal Friction and Coefficeint of Friction with concrete are tabulated in Table 3.5. The characteristic properties used for the surrounding soil in the FE model are listed in Table 3.6.

The data used for determining the soil properties were collected from the detailed results of geotechnical investigation section of the final report on the Paisarhat Bridge Over Pisa River at Barisal, Bangladesh (May, 2000). The investigation was conducted by the Civil Engineering Department under Bureau of Research Testing and Consultancy (BRTC) of Bangladesh University of Engineering and Consultancy.

Table: 3.3. Soil Modulus of Elasticity (E_s)

Soil type	E_s (MPa)
Very soft Clay	2-15
Soft Clay	5-25
Medium Clay	15-50
Hard Clay	50-100
Sandy Clay	25-250
Loose sand	
Silty	5-20
Loose	10-25
Dense	50-81
Sand and gravel	
Loose	50-150
Dense	100-200

Table: 3.4. Values of Poisson's Ratio (v)

Soil Type	***N***
Clay, Saturated	0.4-0.5
Clay, unsaturated	0.1-0.3
Sandy Clay	0.2-0.3
Silt	0.3-0.35
Sand (Dense) Coarse (voids ratio= 0.4-0.7) Fine-grained (voids ratio= 0.4-0.7)	 0.15 0.25

Table: 3.5. Unit Weights, Effective Angles of Internal Friction and Coefficients of Friction with Concrete (Nilson et al (1986))

Soil	**Unit weights pcf (Kg/m^3)**	***Φ*** **Degrees**	***μ***
1.Sand or gravel without fine particles , highly permeable	110 – 120 (1760-1920)	33 – 40	0.5 – 0.6
2.Sand or gravel with silt mixture, low permeability	120 – 130 (1920-2080)	25 – 35	0.4 – 0.5
3.Silty sand, sand arid gravel with high clay content .	110 – 120 (1760-120)	23 – 30	0.3 – 0.4
4. Medium or stiff clay	100 – 120 (1600-1920)	25 – 35	0.2 – 0.4
5. Soft clay. Silt	90 – 110 (1440-1760)	20 – 35	0.2 – 0.3

Table: 3.6. Properties of Soil used in the FE Model

Soil Property	Value
Modulus of Elasticity. E_s	28 MPa
Poisson's Ratio	0.3
Angle of Internal Friction, Φ	22.4^o
Cohesion Intercept, c	89 KPa
Compression Index, C_c	0.27
Swell Index, C_s	0.03
Initial Void Ration, e_o	1.05
Preconsolidation Pressure, P_o'	130 KPa

3.5.3 Loading

As the effect of the load value, configuration and shape are not considered in this study; only a single wheel load of 40 KN (9,000 lb) of an equivalent 80KN (18,000 lb) single axle load is adopted. The stiffening effect of the tire wall is neglected, hence, the contact pressure on the road is assumed to be equal to the tire pressure. Furthermore, the contact pressure distribution is assumed uniform and is taken as 550 KPa (80 psi) which was applied over a circular area of 152 mm (6inch) at the center of the concrete slab this present study.

3.6 SENSITIVITY ANALYSIS

For sensitivity analysis a reference model is chosen on which sensitivity of different parameters are analyzed. Fig. 3.15 respectively shows a cross sectional view and a plan view of the pavement section used for this study. For the reference model, the thickness of the concrete slab and granular base was taken to be 225 mm (9 inch) and 300 mm (12 inch) respectively. No shoulder was considered for the present study. Instead, soil was considered to extend horizontally across the pavement beyond the concrete slab.

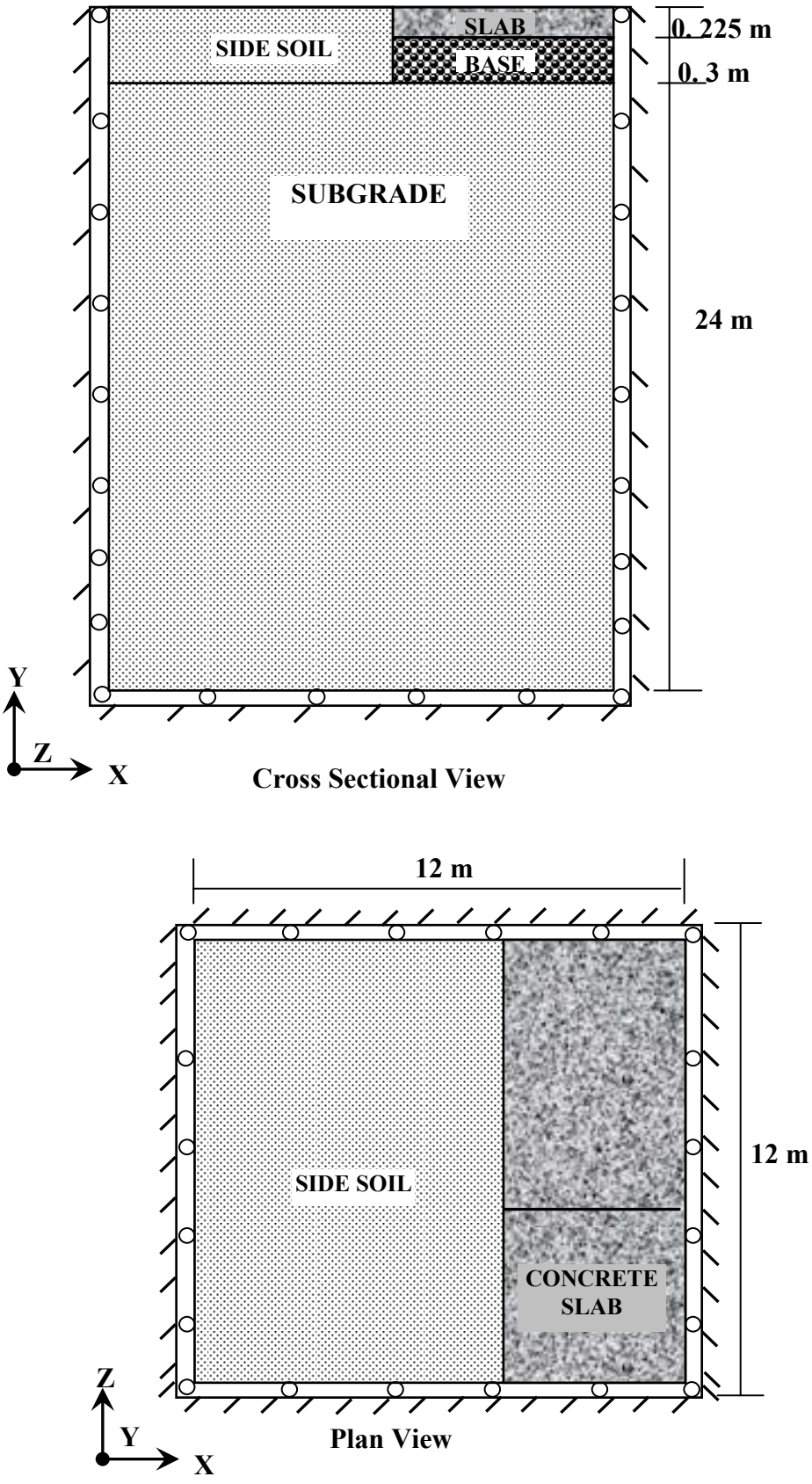

Fig. 3.15: Cross-Sectional and Plan View of the Reference Model

3.6.1 Optimum Mesh Size

In finite element analysis, an engineering structure is divided into small elements. These elements coincide with the geometry of the structure and represent the geometry and the mechanical properties in the regions. Up to a certain limit if finer elements are used, the accuracy of the analysis increases. This is called optimum element size. After optimum size if finer elements are used, accuracy does not improve but computational effort increases. So, the elements size should be kept small enough to yield good results and yet large enough to reduce computational time. Smaller elements are desirable where stress gradient is high due to change in geometry, sharp corners etc. Large elements can be used where stress gradient is low. During mesh generation of a structural model, the aspect ratio of the elements should be kept in consideration. If the aspect ratio of any element in the developed model is abnormally high, solution may not converge.

As the loading on the pavement surface is localized, the finest mesh is required near the loaded area to capture the steep stress and strain gradient in these areas. The subdivision is carried out so that the element aspect ration remains close to one where the stress and strain gradients are high to achieve faster convergence.

The aim of optimization for any specific problem is to determine the rational values of design variables in order to minimize or maximize an objective function with given constraints. It is very significant to determine, "what should be the exact number of elements for a structure for which the FEA mesh is optimum?" There is no exact answer to this question. However, if the mesh becomes continuously finer until the variation in the result is less than a specified value or percentage, the optimum mesh density will be reached.

Main objective of this study is to examine the concrete pavement response i.e. deflection (δ_c) and tensile stress (σ_i) at the bottom of the concrete slab at the center point of loading. So deflection of the top surface of the concrete slab and tensile stress at the bottom of the slab at the center of the loaded area are considered as the prime variable for mesh sensitivity analysis. Fig. 3.16 and 3.17 show the variation of

deflection of top surface at the center point of circular loading and maximum tensile stress at the bottom of the concrete slab with different element sizes and found that a total number of 53855 elements were good enough to get optimum result considering the tradeoff between computational time and accuracy. In Fig.3.18, a schematic view of the generated mesh is shown for the rigid pavement model.

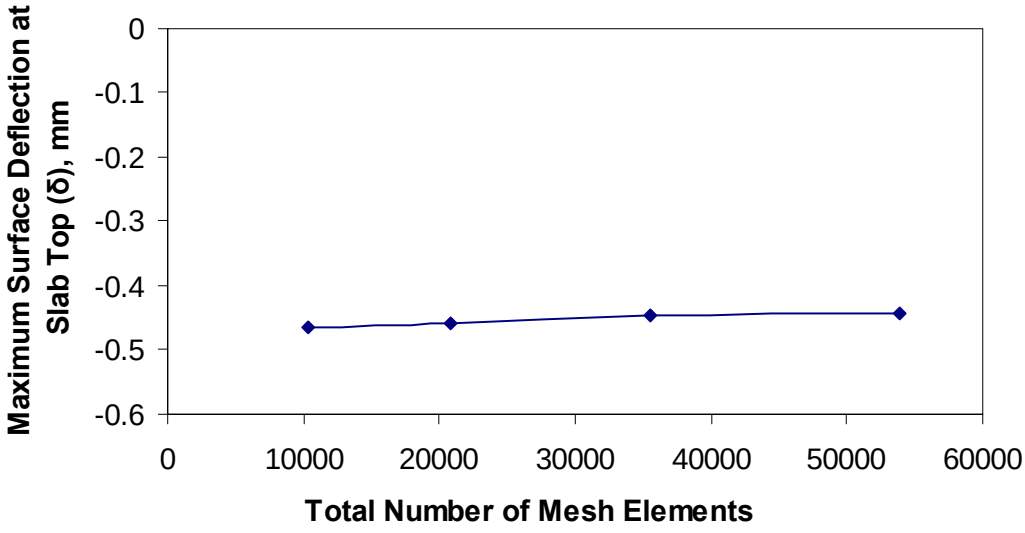

Fig. 3.16: Maximum Surface Deflection at the Bottom of Slab vs. Total Number of Mesh Elements

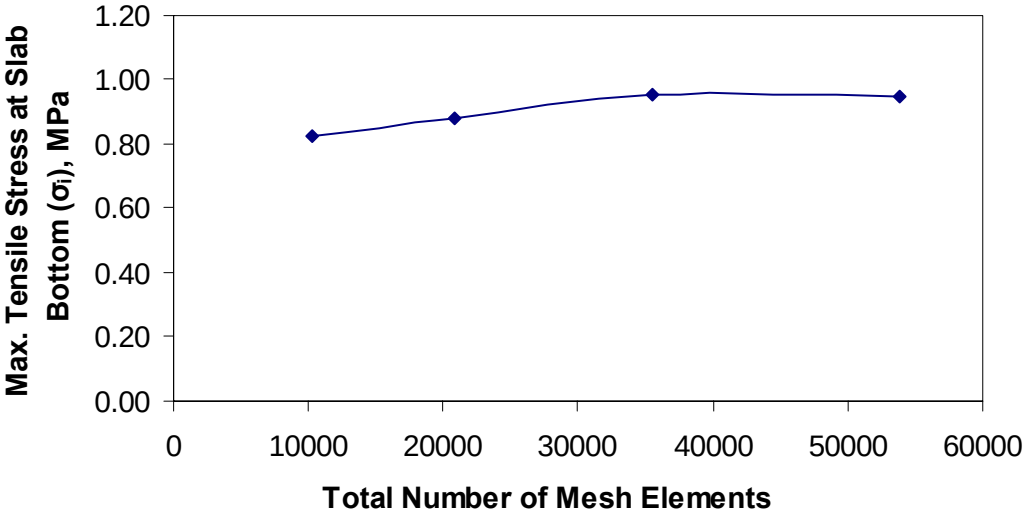

Fig. 3.17: Maximum Tensile Stress at Slab Bottom vs. Total Number of Mesh Elements

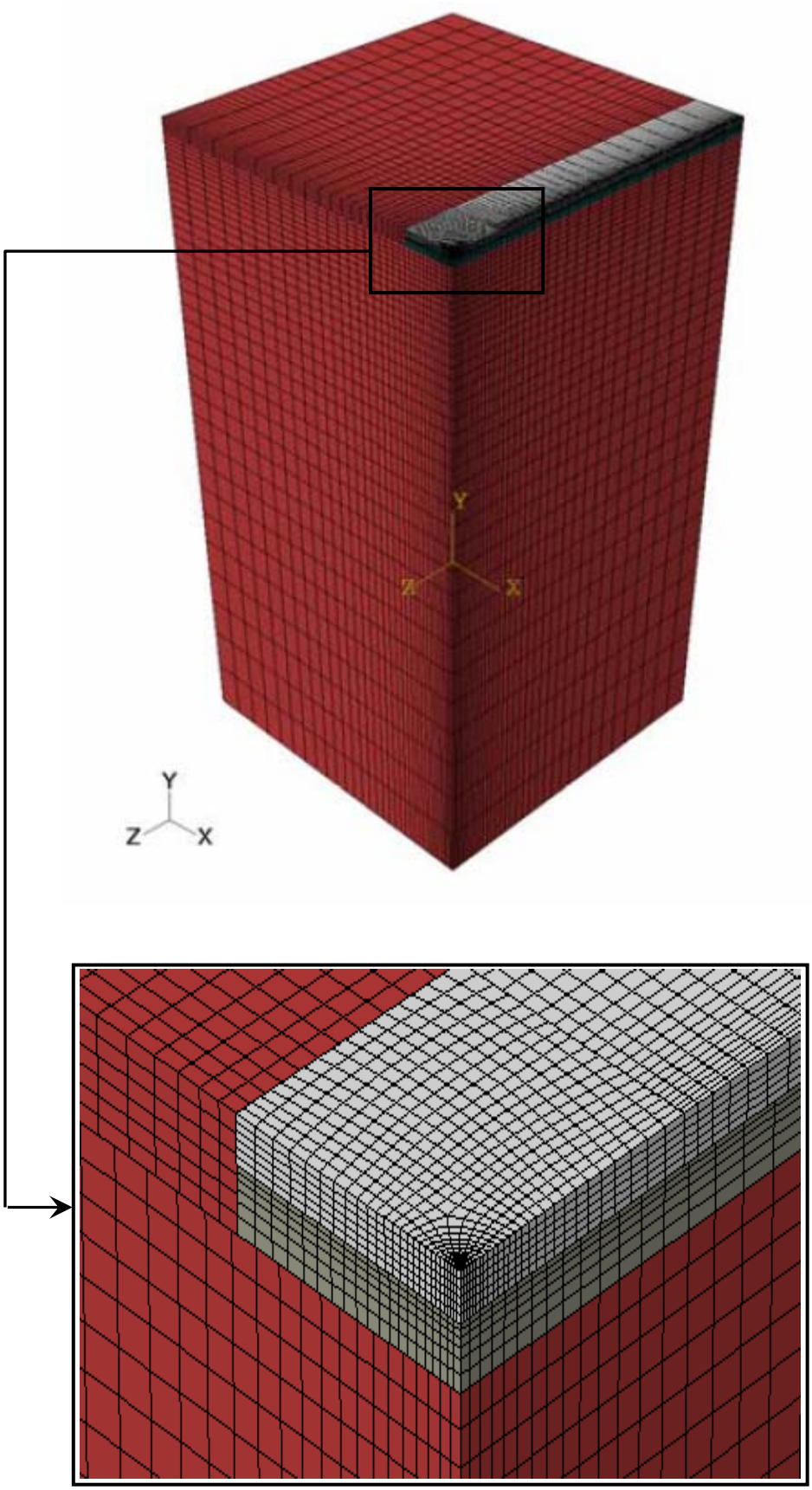

Fig. 3.18: Schematic View of the Generated Mesh

3.6.2 Effect of Soil Extension

Generally any soil problem can be idealized as a semi infinite problem. The native soil is extended both horizontally (X and Z direction) and vertically (Y-direction) to a large extent. However, FE models can not extend to infinity. So, for an effective modeling of a soil structure system, it is of utmost importance to determine the optimum extent of that soil beyond which the effect of soil becomes nominal.

A significant number of finite element analyses were performed changing the depth of the native soil layer i.e. subgrade. For the purpose of simplicity, horizontal extent of subgrade soil was also changed based on the approximation of stress distribution in the ration of (1 H: 1 V) i.e. the horizontal extent was considered to be half of the corresponding vertical extent of the subgrade soil for the one quarter of the pavement. Fig. 3.19 and 3.20 show the effect of site soil extent on the maximum deflection (δ_c) of the top of the concrete slab at the center of the circular loaded area and the maximum tensile stress (σ_i) at the bottom of the concrete slab respectively. From these figures it is evident that the values of the parameters do not show any significant change beyond a depth of 24 meter (80 feet). Therefore, a subgrade depth of 24 meter was considered to be sufficient for further analysis.

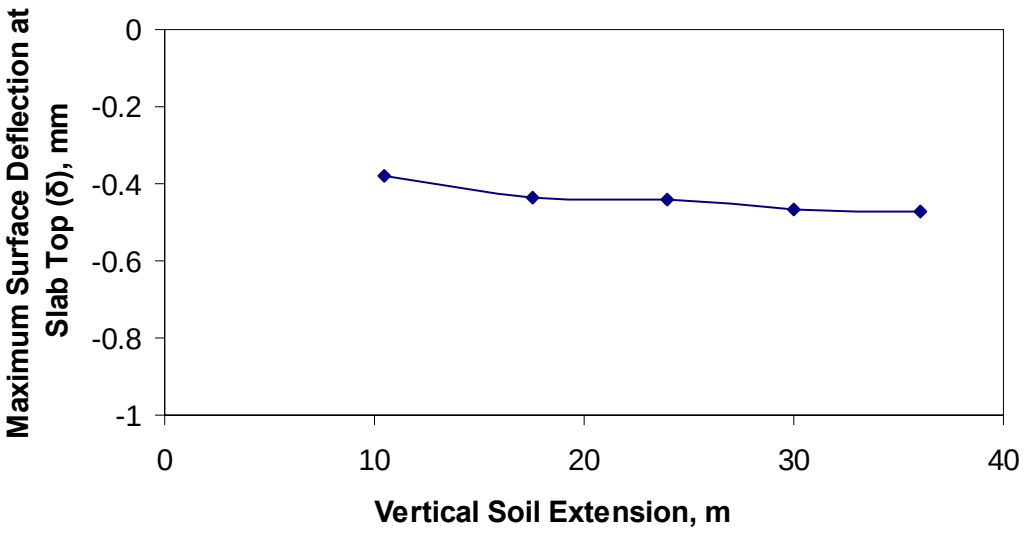

Fig. 3.19: Variation of Maximum Surface Deflection at the Bottom of Concrete Slab with Soil Extension in the Vertical Direction

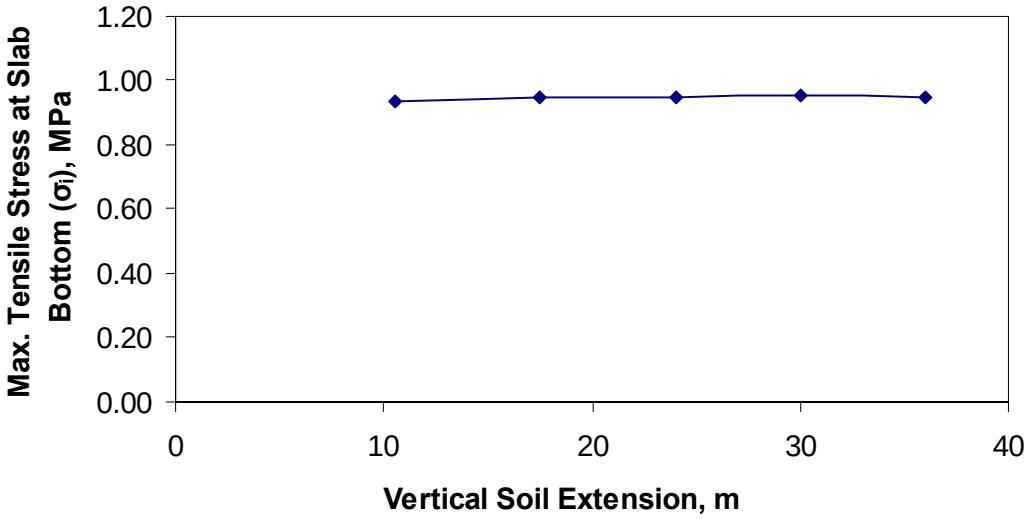

Fig. 3.20: Variation of Maximum Tensile Stress at Slab Bottom with Soil Extension in the Vertical Direction.

3.7 VERIFICATION OF FE MODEL

In the following few sections, an attempt has been made for the verification of the numerical modeling of the pavement system with the available numerical analysis results for both 3D and axisymmetric conditions.

Kim, *et al.* (2009) carried out a linear elastic analysis of flexible pavement for both 3D and axisymmetric modeling using the finite element software ABAQUS. He matched the results with the results provided by Huang (2004) obtained by the linear elastic layered program, KENLAYER.

3.6.1 Verification of 3D FE Modeling

The 3D model developed by Kim, *et al.* (2009), had 15,168 20-noded hexahedron element and 67,265 nodes. All the vertical boundary nodes had roller supports with fixed boundary nodes used at the bottom. The wheel load was applied as a uniform pressure of 551 KPa (80 psi) over a circular area of 152 mm (6 inch) radius. Table 3.7 lists the three-layered conventional flexible pavement geometries and the material properties used in the 3D linear elastic FE analyses.

Table: 3.7. Pavement Geometry and Material Properties for Finite Element Modeling verification

Layer	Thickness (mm)	E or M_R (MPa)	μ
Asphalt concrete	76	2759	0.35
Base	305	207	0.40
Subgrade	20955	41.4	0.45

For the verification of the 3D modeling of this study, the flexible pavement analyzed by Kim, *et al.*, was reconstructed in the ABAQUS environment using the same pavement geometries and material properties. Instead of 20-node hexahedron elements, 8-noded brick element was chosen which was used to develop the jointed plain concrete pavement for the present study. The reason behind the choice of 8-noded brick element instead of 20-noded hexahedron element is that, 20-noded hexahedron element choice results in grater computing capacity and time than the 8-noded brick element. Predicted pavement surface deflection ($\delta_{surface}$) and certain critical pavement responses, i.e., vertical stress and strain on top of subgrade (σ_v and ε_v) and horizontal stress at the bottom of the asphalt concrete layer (σ_h), are compared in Table 3.8 with the linear elastic KENLAYER closed-form solutions and results predicted by Kim. The results show in general a very good agreement with the KENLAYER result and results obtained by Kim, *et al.*

Table: 3.8. Comparison of Predicted Responses for 3D Model with Results from Kim., *et al.* Study

Pavement Response (tension is positive)	KENLAYER	ABAQUS with 20-node hexahedron elements (Kim., et al.)	ABAQUS with eight-node brick elements	Difference (%)
$\delta_{surface}$ (mm)	-0.927	-0.909	-0.913	+ 0.44
$\sigma_{h\ bottom\ of\ AC}$ (MPa)	0.777	0.777	0.821	+ 5.6
$\sigma_{v\ top\ of\ subgrade}$ (MPa)	-0.041	-0.040	-0.0365	- 10
$\varepsilon_{v\ top\ of\ subgrade}$ ($\mu\varepsilon$)	-936	-930	-845	-9.1

3.6.2 Verification of Axisymmetric Modeling

The axisymmetric model developed by Kim, *et al.* (2009), had 300 quadratic elements and 981 nodes. All the vertical boundary nodes had roller supports with fixed boundary nodes used at the bottom. The wheel load was applied as a uniform pressure of 551 KPa (80 psi) over a circular area of 152 mm (6 inch) radius. Table 3.7 lists the three-layered conventional flexible pavement geometries and the material properties used in the axisymmetric linear elastic FE analyses.

For the verification of the axisymmetric modeling of the present study, the flexible pavement analyzed by Kim, *et al.*, was reconstructed in the ABAQUS environment using the same pavement geometries and material properties. Instead of quadratic elements, 4 node bilinear axisymmetric element was used which was used to develop the jointed plain concrete pavement for the present study. The reason behind the choice of bilinear element instead of quadratic element is that, quadratic element choice results in grater computing capacity and time than the bilinear element. Predicted pavement surface deflection ($\delta_{surface}$) and certain critical pavement responses, i.e., vertical stress and strain on top of subgrade (σ_v and ε_v) and horizontal

stress at the bottom of the asphalt concrete layer (σ_h), are compared in Table 3.9 with the linear elastic KENLAYER closed-form solutions and results predicted by Kim. The results show in general a very good agreement with the KENLAYER result and results obtained by Kim, *et al.*

Table: 3.9. Comparison of Predicted Responses with Results from Kim., *et al.* Study

Pavement Response (tension is positive)	KENLAYER	ABAQUS with eight-node quadrilateral elements (Kim., et al.)	ABAQUS with four-node quadrilateral elements	Difference (%)
$\delta_{surface}$ (mm)	-0.927	-0.930	-0.925714	- 0.41
$\sigma_{h\ bottom\ of\ AC}$ (MPa)	0.777	0.777	0.813	+ 4.6
$\sigma_{v\ top\ of\ subgrade}$ (MPa)	-0.041	-0.041	-0.0348	- 15.1
$\varepsilon_{v\ top\ of\ subgrade}$ ($\mu\varepsilon$)	-936	-933	-807	-13.5

3.7 SUMMARY

This chapter summarizes the development of the 3-D and axisymmetric finite element model of the jointed plain concrete pavement taking into account of the soil-structure interaction. From this chapter, it is observed that the developed model can successfully simulate the experimental results and the adopted FE analysis methodology predicts the stresses to an acceptable degree of accuracy. Hence, it can be concluded that the developed model may be utilized for the purpose of the parametric study.

Chapter 4
PAVEMENT RESPONSES TO WHEEL LOAD

4.1 INTRODUCTION

The development of the 3-D and axisymmetric finite element model of jointed plain concrete pavement and verification of the finite element modeling has been outlined in the previous chapter. In this chapter, a detailed study of jointed plain concrete pavement responses i.e. stresses and deformation under static wheel load at the interior of the slab has been presented. Parametric study for the significant parameters has been performed and presented to understand their influence on the typical pavement responses. For this purpose, significant pavement geometry parameters such as - thickness of concrete slab and granular base, and different types of pavement material parameters such as- base and subgrade soil has been considered. A significant quantity of analyses is performed to observe the responses of jointed plain concrete pavement for each of the parameters. These responses have been represented both in tabular form and graphically for better perception. Probable reasons for the observed responses have also been presented.

4.2 SELECTION OF PARAMETERS AND DIMENSIONS OF THE REFERANCE MODEL

In order to study in detail the behaviour of jointed plain concrete pavement to find out the critical pavement responses the reference model has been chosen and analysed. The pavement geometries and elastic material properties for the reference model are provided in Table 4.1. For reference model the thickness of the concrete slab was chosen as 225 mm (9 inch) and the thickness of the granular base as 300 mm (12 inch). The vertical and horizontal extension of the subgrade soil was taken as 24 meter and 12 meter respectively as determined to be well enough from the sensitivity analysis for soil extension performed in the previous chapter. Fig. 4.1 shows a cross sectional view of the reference model.

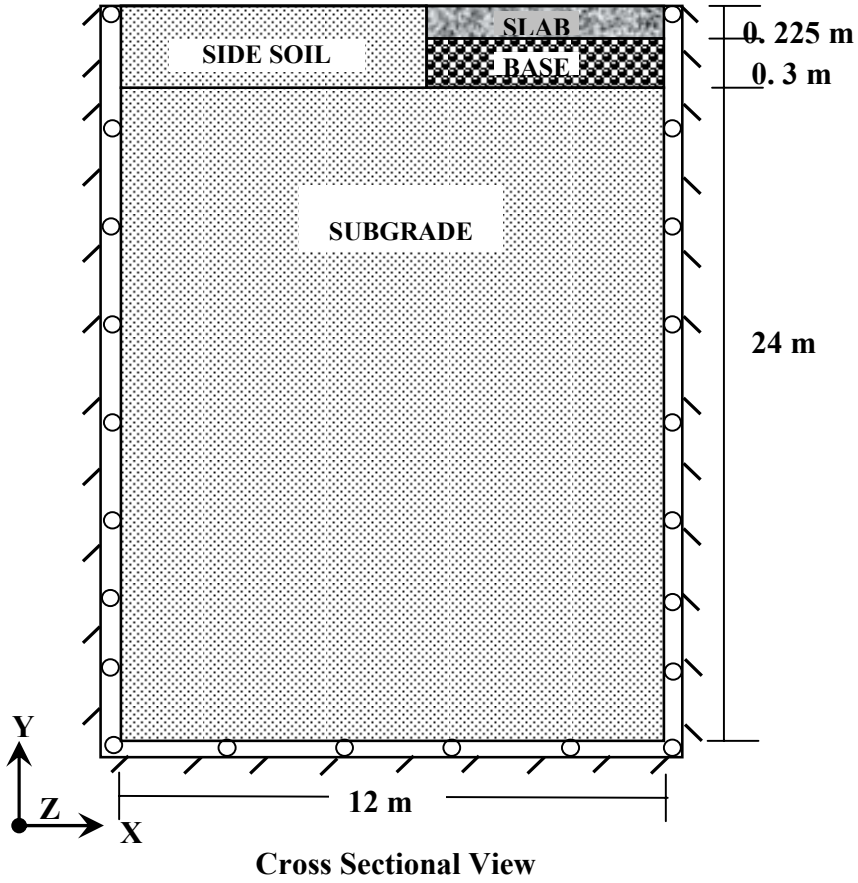

Fig. 4.1: Cross Section view of the Reference Model

Table: 4.1. Pavement Geometry and Material Properties

Layer	**Thickness / Depth (m)**	**Modulus of Elasticity , *Es* (MPa)**	**Poisson's Ratio, υ**	**Unit Weight, Kg/m^3**
Concrete Surface	0.225	25,000	0.2	2400
Granular Base	0.30	120	0.3	2147
Subgrade Soil	24	28	0.3	1920

Co-efficient of friction between concrete and granular base is considered to be 1.5. Plastic properties of granular base as Drucker-Prager Model parameters are listed in Table 4.2 and those of subgrade soil for Cap Model are listed in Table 4.3.

Table: 4.2. Plastic Properties of Granular Base for Drucker Prager Model

Material Property	**Specific Values**
Angle of Internal Friction of Soil (Coulomb),**Φ**	47°
Angle to Yield Surface (Drucker Prager), **β**	62°
Material cohesion (Drucker Prager), ***d***	10 Pa
Dilation Angle of Soil, **ψ**	20°

Table: 4.3. Plastic Properties of Subgrade Soil for Cap Model

Material Property	**Specific Values**
Material Cohesion, ***d***	552 KPa
Angle to Yield Surface, **β**	41°
Shape Parameter, ***R***	0.2
Position of Initial Yield surface	0
Transition surface Parameter, ***α***	0.05
Stress Ration, ***K***	1

4.3 PAVEMENT RESPONSES TO WHEEL LOAD

4.3.1 Comparisons of 3D Linear and Nonlinear Finite Element Analysis

Differences between the pavement responses for linear elastic and nonlinear material characterization for 3D finite element analysis were determined using the reference 3D finite element model developed in the previous chapter. Four different combinations of material characterizations were used all using linear elastic concrete material properties and the following pavement layer characterizations: (1) linear elastic; (2) nonlinear base and linear subgrade; (3) linear base and nonlinear subgrade; and finally, (4) nonlinear base and nonlinear subgrade. Table 4.4 gives detailed comparisons of the predicted critical pavement responses.

Table: 4.4. Predicted Pavement Responses for 3D Analysis

Pavement Responses	**Linear Elastic**	**Nonlinear base and linear subgrade**	**Linear base and nonlinear subgrade**	**Nonlinear base and nonlinear subgrade**
Maximum Surface Deflection at Slab Top, $\delta_{surface}$ (mm)	-0.394	-0.394	-0.443	-0.443
Maximim Tensile Stress at Slab Bottom, σ_i (MPa)	0.95001	0.95001	0.95001	0.95001
Vertical Compressive Stress on top of Subgrade, σ_v (Kpa)	-4.994	-4.994	-4.994	-4.994

The results of the 3D finite element analysis for the jointed plain concrete pavement due to applied wheel load are plotted in Fig. 4.2, 4.3, and 4.4 for the four combinations of pavement material characterization.

In Fig. 4.2, variation of vertical surface deflection of the top surface of the concrete slab is plotted with respect to distance from the centreline of the circular loaded area along the longitudinal direction of the pavement. The maximum vertical surface deflection of the concrete slab at the center of the circular wheel load is 0.394 mm for linear elastic analysis and 0.443 mm for nonlinear finite element analysis and decreases towards the edge of the concrete slab along the pavement direction. The maximum deflection predicted for nonlinear analysis is 12.4% greater than that predicted for linear elastic analysis. Consideration of nonlinearity of base course material has significantly no effect on the pavement surface deflection as shown in Fig. 4.5 .This is due to the fact that the base course material behaves as a linearly elastic material under the present loading condition. On the contrary, the subgrade soil settles more when material nonlinearity is considered.

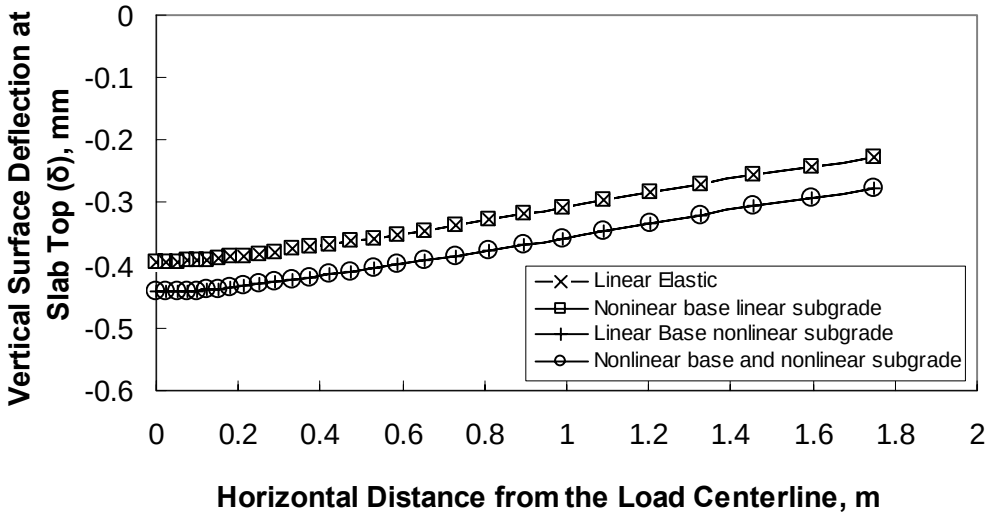

Fig. 4.2: Vertical Surface Deflection along Longitudinal Direction of Pavement for the Four Combinations of Material Characterization (3D FE Analysis)

.

Variation of the tensile stress developed at the bottom surface of the concrete slab along the longitudinal direction of the pavement is shown in Fig. 4.3. The maximum tensile stress developed at the bottom of the concrete slab predicted for the linear elastic and nonlinear elastic finite element analysis have the same value of 0.95 MPa (138 psi). The value of the tensile stress at the bottom of the concrete slab is maximum below the center of the circular wheel load and it decreases towards the edge of the pavement. Although the deflection predicted for nonlinearity of subgrade soil is grater than linear elastic condition the tensile stress at the bottom surface of slab has no difference. This phenomenon can be explained by the fact that the relative deflection of the center of the slab with respect to its corner is same resulting in the same bottom surface tensile stress.

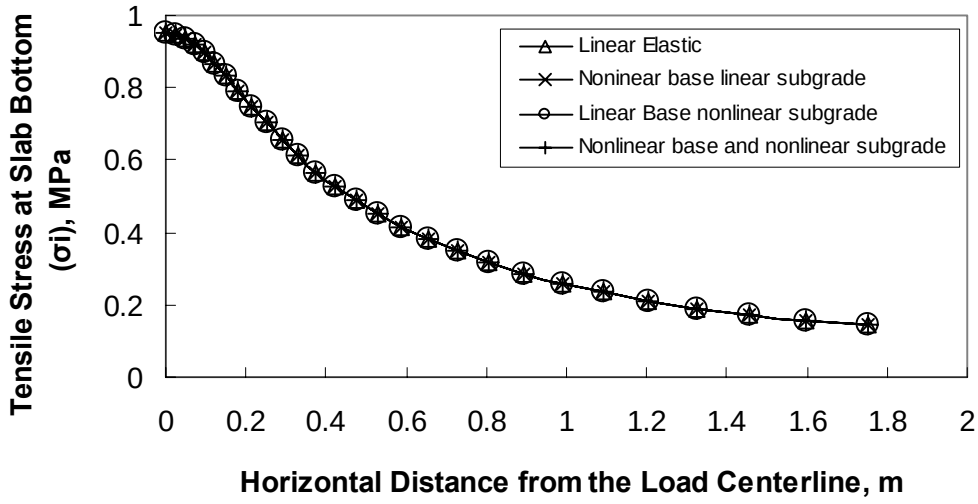

Fig. 4.3: Tensile Stress at Slab Bottom along Longitudinal Direction of Pavement for the Four Combinations of Material Characterization (3D FE Analysis)

The variation of vertical compressive stress on the subgrade surface along the longitudinal direction of the pavement is plotted in Fig. 4.4 for the four material characterization combinations. The maximum values of the vertical compressive stress on the top surface of the subgrade soil predicted by both linear elastic and nonlinear finite element analysis have been found to be 4.994 KPa. The compressive stress on subgrade soil surface is maximum below the center of circular wheel load and decreases towards the edge of concrete slab. The concrete slab acts as a rigid plate under the applied wheel load and distributes the load over a greater surface area of the underlying base and subgrade area thus minimising the effect of stress concentration and localized large deflection.

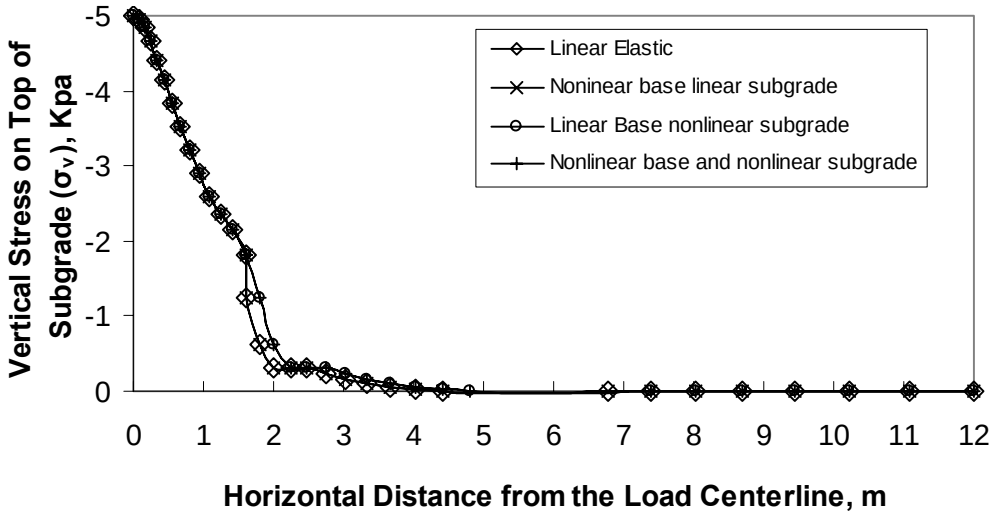

Fig. 4.4: Vertical Stress on Slab Top along Longitudinal Direction of Pavement for the Four Combinations of Material Characterization (3D FE Analysis)

Contours of the predicted pavement responses from the 3D analysis are shown in fig. 4.5, 4.6, and 4.7. In figure 4.5, vertical deflection of the pavement system is displayed.

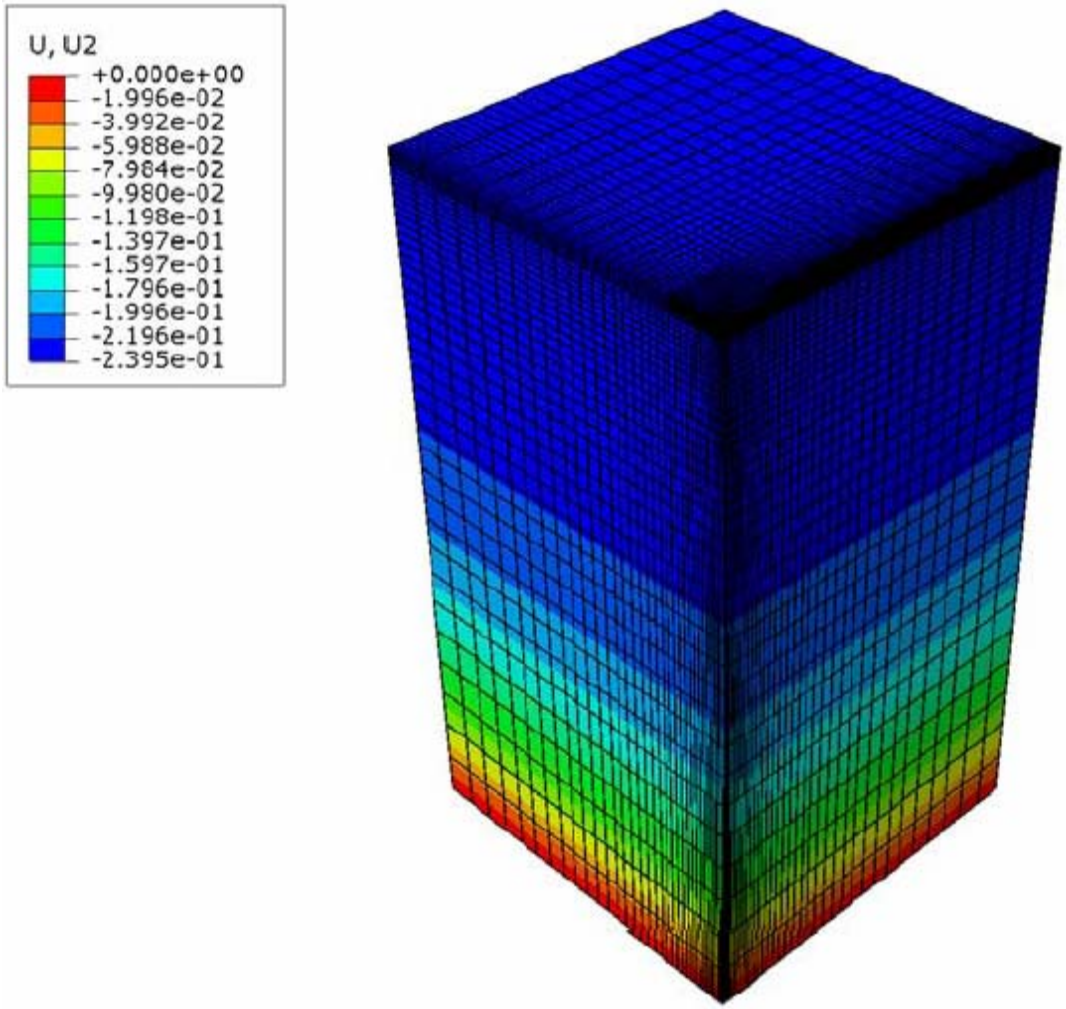

Fig. 4.5: Contours of Vertical Deflection of the Reference Model for 3D FE Analysis

Fig. 4.6 shows the maximum principal stress in the pavement system due to wheel load. Vertical compressive stress is shown in Fig 4.7 for wheel load application.

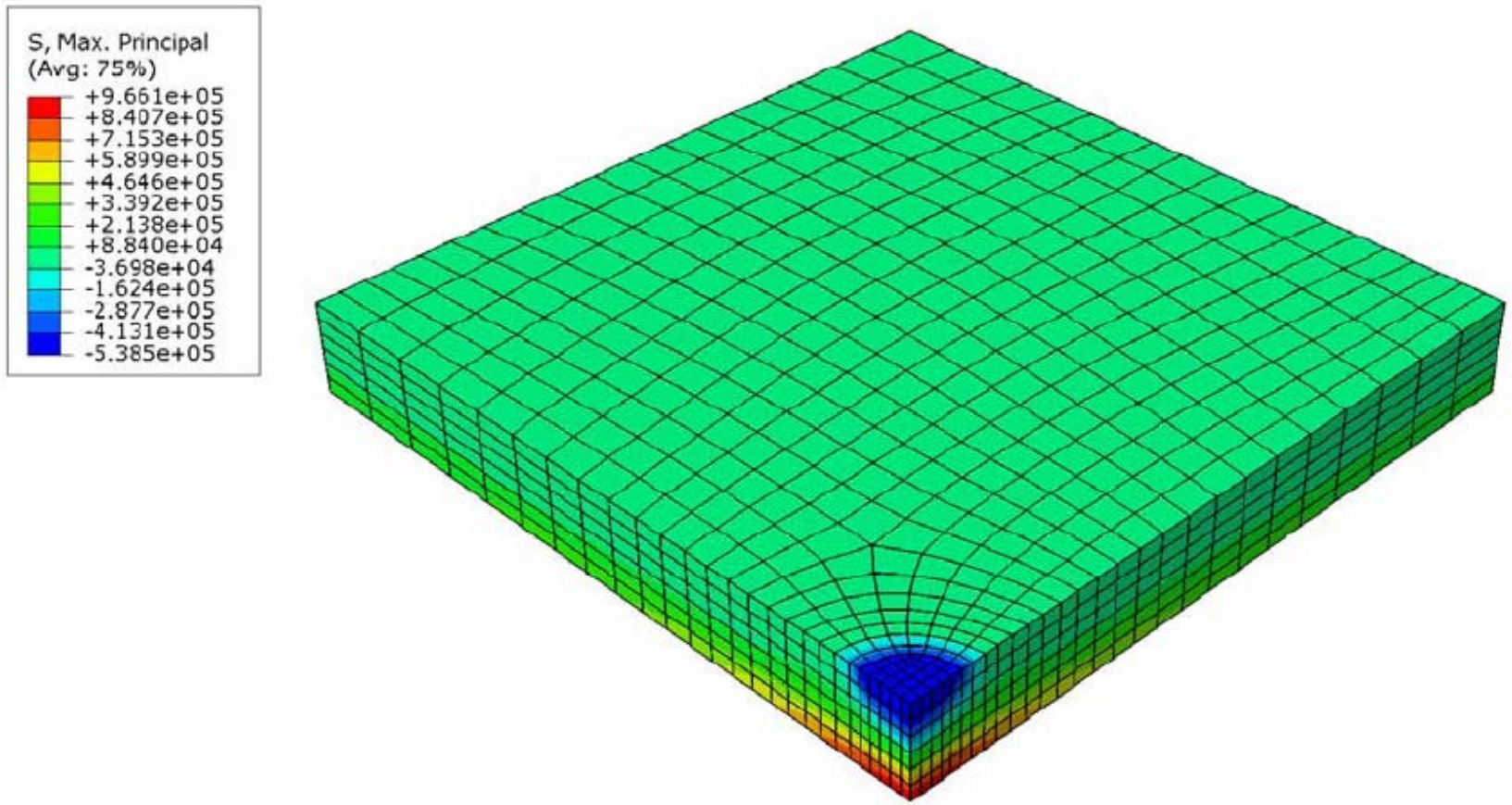

Fig. 4.3: Contours of Maximum Principal Stress of the Reference Model for 3D FE Analysis

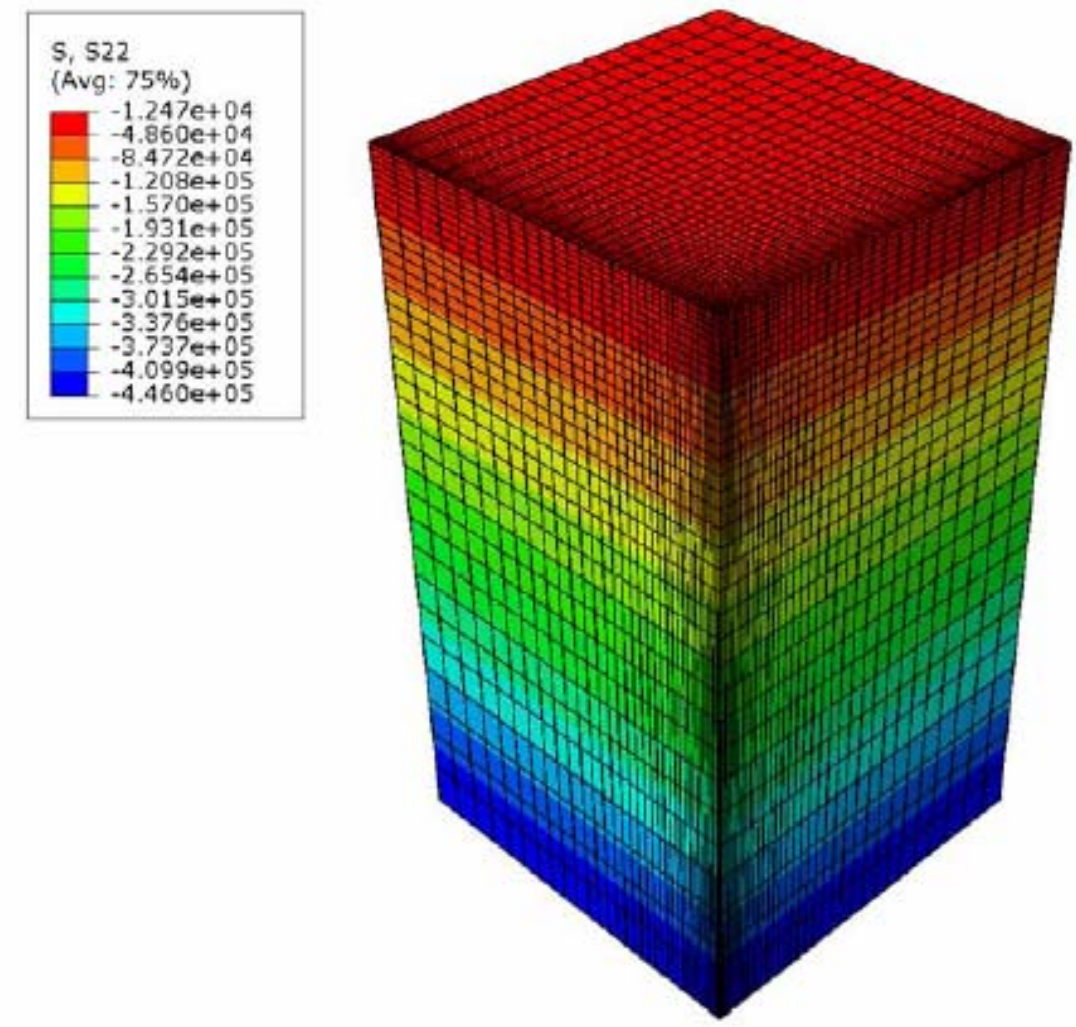

Fig. 4.4: Contours of Vertical Compressive Stress of the Reference Model for 3D FE Analysis

4.3.2 Comparisons of Axisymmetric FE Analysis with 3D FE Analysis

In order to carry out the comparison between the pavement responses predicted by axisymmetric finite element analysis with those of 3D finite element analysis, the results of the critical pavement responses i.e. vertical surface deflection of the concrete slab at the center of the circular loaded area, maximum tensile stress ate the bottom of the concrete slab, and the vertical compressive stress on top of subgrade directly under the center of the circular loaded area are listed in the Table 4.5 and 4.6.

Table: 4.5. Comparison of Predicted Pavement Responses for Axisymmetric FE Analysis with 3D FE Analysis (Linear Elastic)

Pavement Responses	Axisymmetric FE Analysis	3D FE Analysis
Maximum Surface Deflection at Slab Top, $\delta_{surface}$ (mm)	-0.385	-0.394
Maximim Tensile Stress at Slab Bottom, σ_i (MPa)	1.10579	0.95001
Vertical Compressive Stress on top of Subgrade, σ_v (Kpa)	-5.1195	-4.994

Table: 4.6. Comparison of Predicted Pavement Responses for Axisymmetric and 3D finite element analysis (Nonlinear)

Pavement Responses	Axisymmetric FE Analysis	3D FE Analysis
Maximum Surface Deflection at Slab Top, $\delta_{surface}$ (mm)	-0.449	-0.443
Maximim Tensile Stress at Slab Bottom, σ_i ($x10^3$ Kpa)	1.10584	0.95001
Vertical Compressive Stress on top of Subgrade, σ_v (Kpa)	-5.120	-4.994

In order to produce better contrast between the pavement responses predicted by axisymmetric FE analysis and 3D finite element analysis, the analysis results for nonlinear material characterization are plotted in Fig. 4.8, 4.9, and 4.10.

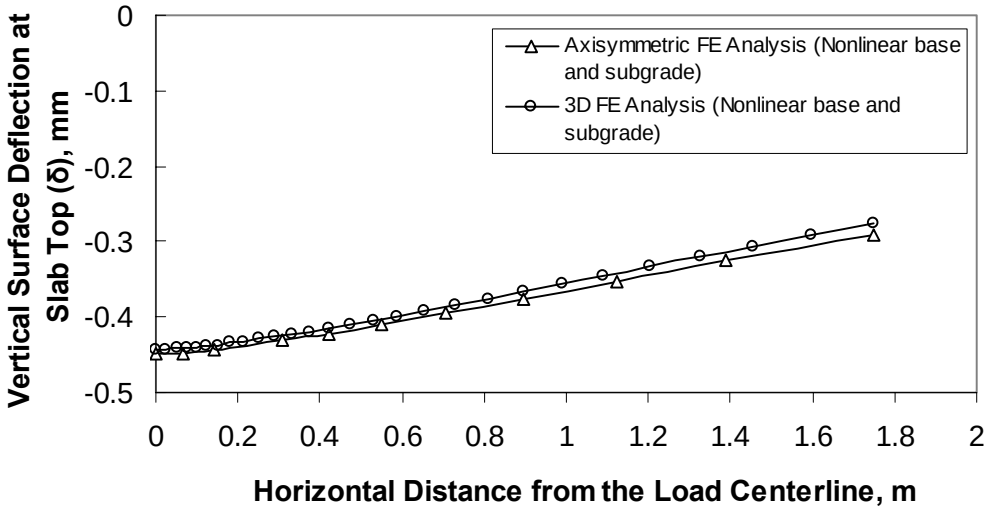

Fig. 4.8: Vertical Surface Deflection at Top of Slab vs. Horizontal Distance from Load Centreline for Axisymmetric and 3D FE (Nonlinear) Analysis

Fig. 4.8 shows the variation of vertical surface deflection at top of slab with distance from the centreline of the circular loaded area for nonlinear base and subgrade material characterization. The vertical deflection of the top surface of the slab predicted by axisymmetric nonlinear analysis is 0.449 mm which is slightly higher (1.3%) than the deflection of 0.443 mm predicted by 3D finite element analysis. In case of elastic analysis, the deflection of the top surface of the concrete slab in axisymmetric analysis is 0.385 mm which is lower (2.3%) than the deflection of 0.394 mm predicted by 3D FE analysis. The relative deflection of the center of the concrete slab with respect to the corner is greater for axisymmetric analysis than for 3D FE analysis.

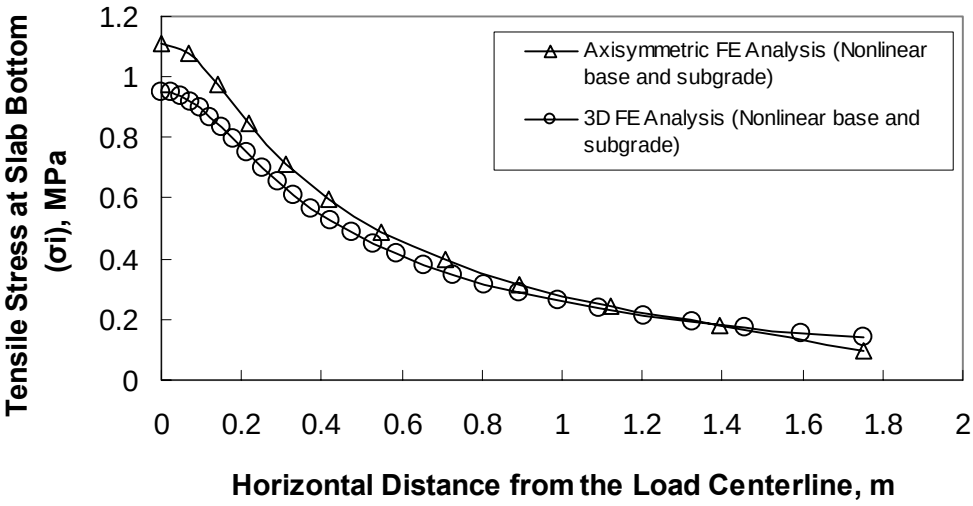

Fig. 4.9: Tensile stress at Slab Top vs. Horizontal Distance from Load centreline for Axisymmetric and 3D FE Analysis

In Fig. 4.9, variation of the tensile stress at the bottom of the concrete slab in the horizontal direction along the pavement is displayed. From the Fig.4.9, it is evident that the tensile stress at the bottom of the concrete slab below the center of the circular wheel load predicted by the axisymmetric FE analysis is 1.105 MPa (160 psi) which is quite greater (14%) than the predicted value of 0.95 MPa (138 psi) by 3D FE analysis for nonlinear analysis. Also for linear elastic material characterization, axisymmetric FE

analysis predicts greater (14%) tensile stress at the bottom of the concrete slab than 3D FE analysis. This increase in stress prediction can be ascribed to the fact that the relative deflection predicted by axisymmetric FE analysis is greater than the 3D analysis.

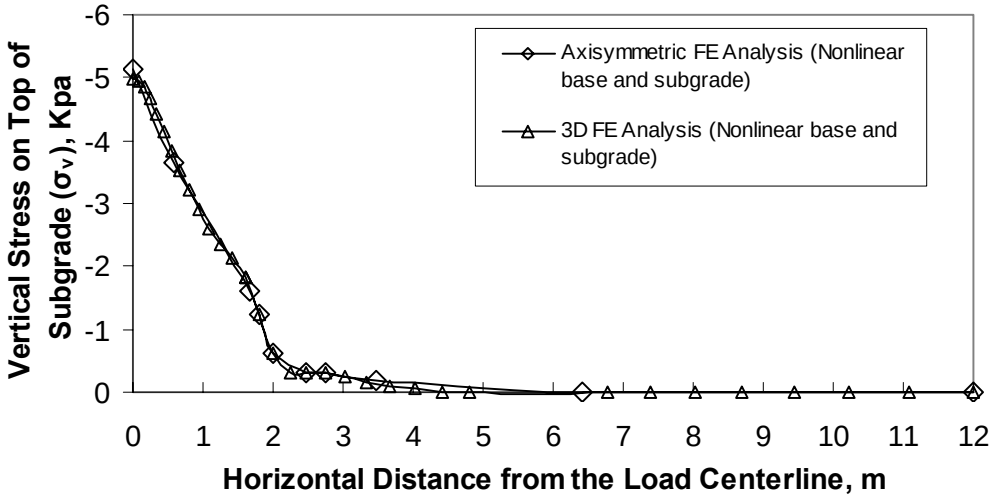

Fig. 4.10: Vertical stress on top of Subgrade vs. Horizontal Distance from Load centreline for Axisymmetric and 3D FE Analysis

The vertical stress on the top surface of the subgrade in the horizontal direction along the pavement direction is shown in Fig 4.10 for both axisymmetric and 3D FE analysis. The vertical compressive stress on top surface of subgrade below the center of the circular wheel load predicted by nonlinear axisymmetric finite element analysis is 5.12 KPa which is about 2.4 % greater than the vertical compressive stress value of 4.994 KPa predicted by 3D nonlinear FE analysis. The vertical compressive stress on top of subgrade predicted by axisymmetric FE analysis for linear elastic material characterization is about 2.4 % greater than 3D FE analysis.

4.3.3 Comparisons of Axisymmetric Linear and Nonlinear Finite Element Analysis

Similar to the 3D finite element analysis, the developed axisymmetric model was used to predict pavement responses using linear elastic concrete material properties and the following pavement layer characterizations: (1) linear elastic; (2) nonlinear base and linear subgrade; (3) linear base and nonlinear subgrade; and finally, (4) nonlinear base and nonlinear subgrade. Table 4.7gives detailed comparisons of the predicted critical pavement responses from axisymmetric finite element analysis.

Table: 4.7. Predicted Pavement Responses for Axisymmetric Analysis

Pavement Responses	**Linear Elastic**	**Nonlinear base and linear subgrade**	**linear base and nonlinear subgrade**	**Nonlinear base and nonlinear subgrade**
Maximum Surface Deflection at Slab Top, $\delta_{surface}$ (mm)	-0.385	-0.385	-0.449	-0.449
Maximim Tensile Stress at Slab Bottom, σ_i ($x10^3$ Kpa)	1.10579	1.106	1.10584	1.10584
Vertical Compressive Stress on top of Subgrade, σ_v (Kpa)	-5.1195	-5.1195	-5.120	-5.120

Similar to 3D finite element analysis, variation of the critical pavement responses of the jointed plain concrete pavement due to applied wheel load under the four combination of pavement material characterization are plotted in Fig. 4.11, 4.12, and 4.13 for the four combinations. In Fig. 4.11, variation of vertical surface deflection of the top surface of the concrete slab is plotted with respect to distance from the centreline of the circular loaded area along the longitudinal direction of the pavement. Fig. 4.15 displays the variation of the tensile stress developed at the bottom surface of the concrete slab along

the longitudinal direction of the pavement. The variation of vertical compressive stress on the subgrade surface along the longitudinal direction of the pavement is plotted in Fig. 4.16.

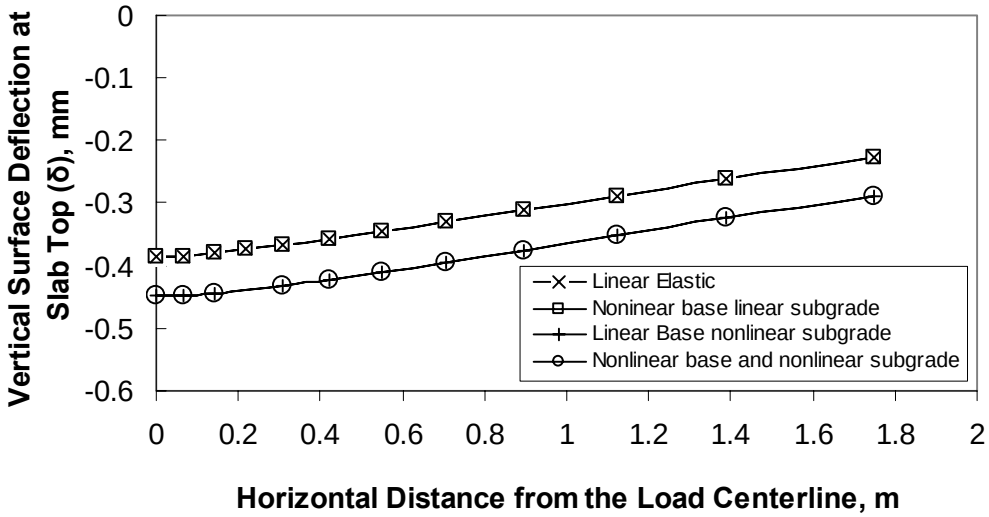

Fig. 4.14: Vertical Surface Deflection along Longitudinal Direction of Pavement for the Four Combinations of Material Characterization (Axisymmetric FE Analysis)

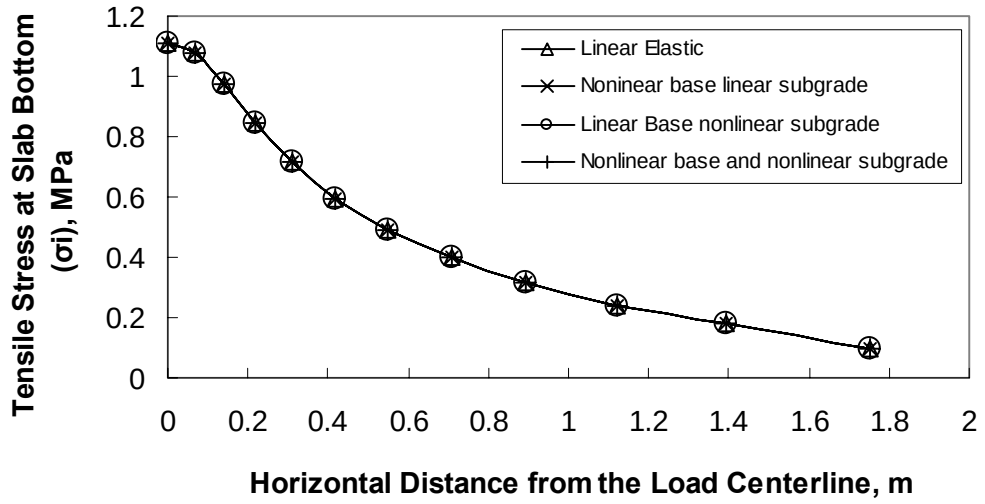

Fig. 4.15. Tensile Stress at Slab Bottom along Longitudinal Direction of Pavement for the Four Combinations of Material Characterization (Axisymmetric FE Analysis)

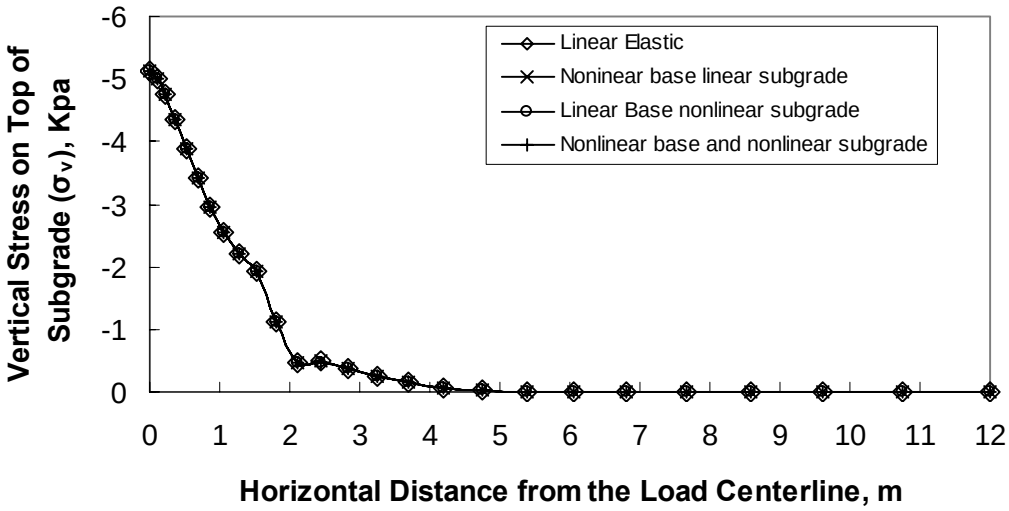

Fig. 4.16: Vertical Stress on Slab Top along Longitudinal Direction of Pavement for the Four Combinations of Material Characterization (Axisymmetric FE Analysis)

Contours of the predicted pavement responses from the axisymmeteric analysis due to traffic wheel load are shown in Fig. 4.11, 4.12, and 4.13. In Fig. 4.11, vertical deflection of the pavement system is displayed.

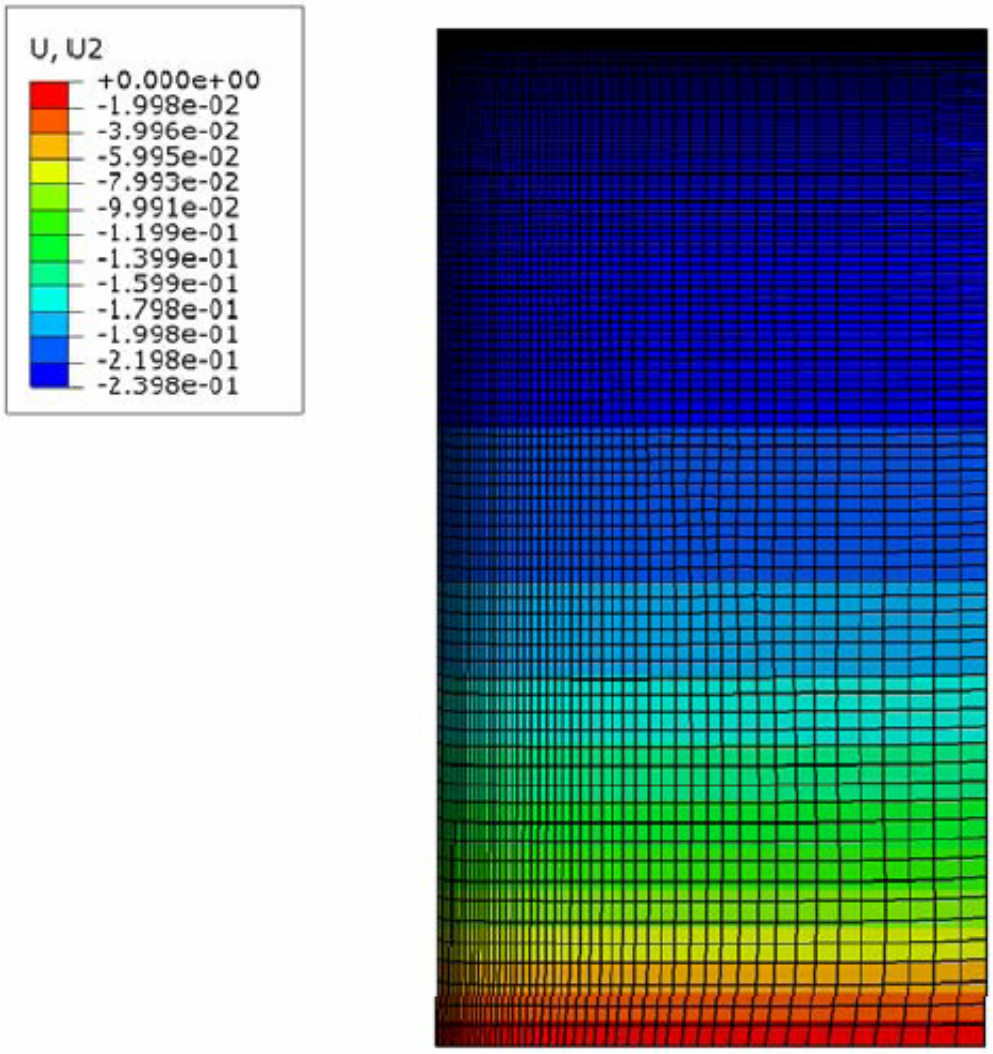

Fig. 4.11: Contours of Vertical Deflection of the Reference Model for Axisymmetric FE Analysis

Fig. 4.12 shows the maximum principal stress in the pavement system and the vertical compressive stress is shown in Fig 4.13.

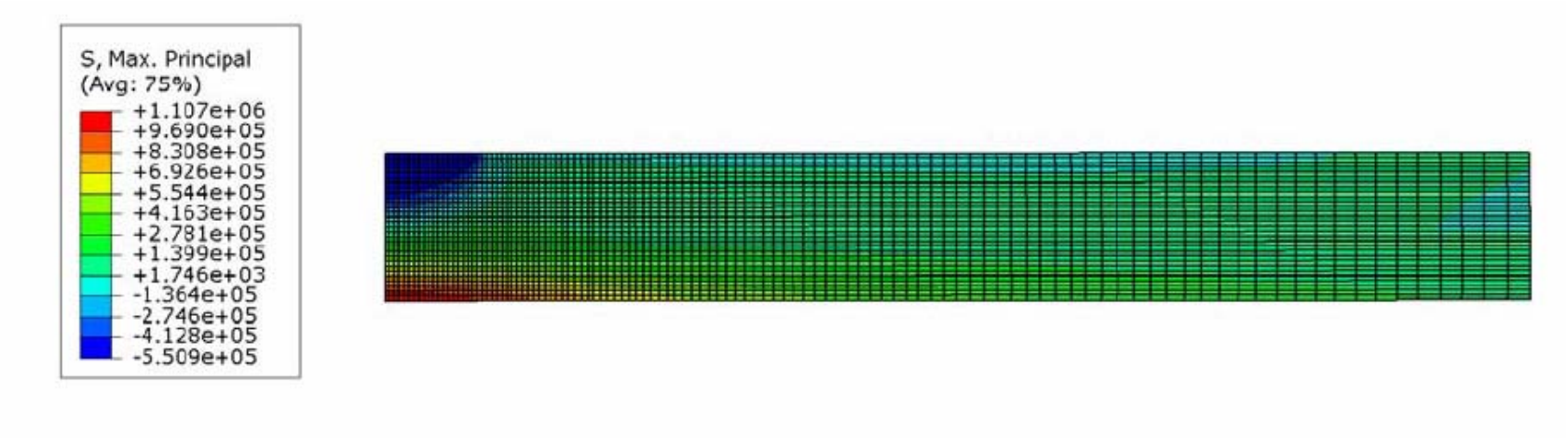

Fig. 4.12: Contours of Maximum Principal Stress of the Reference Model for Axisymmetric FE Analysis

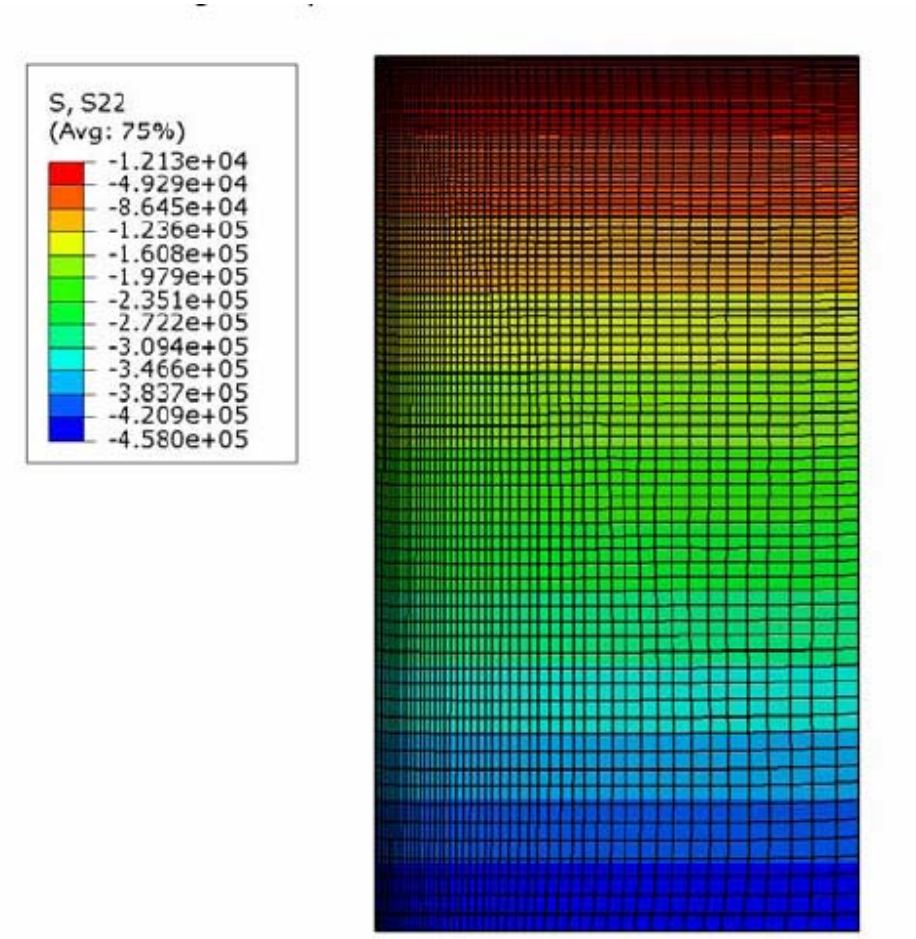

Fig. 4.13: Contours of Vertical Compressive Stress of the Reference Model for Axisymmetric FE Analysis

4.4 SELECTION OF PARAMETERS

Different parameters selected to assess their influence on the jointed plain concrete pavement responses are listed below:

1. Thickness of Concrete slab,
2. Thickness of Base Course,
3. Different Types of Base Course Material,
4. Different Types of Subgrade Soil.

In order to carry out the parametric study, the 3D reference model developed in the preceding chapter was used considering nonlinear base and subgrade. To observe the influence of a single parameter, only the value of that corresponding parameter was changed keeping the other parameters of the reference model unchanged.

4.4.1 Effect of Concrete Slab Thickness

A whole series of 3D finite element analysis were performed using the reference model to observe the effect of concrete slab thickness on the pavement responses. A reasonably wide range of concrete slab thickness was considered, starting from a considerably thin section of 100 mm (4 inch) thick to a large section of 350 mm (14 inch). For different values of slab thickness other geometrical properties of the reference model were kept constant. The effect of concrete slab thickness on the pavement responses are shown in Fig. 4.17, 4.18, and 4.19.

Fig. 4.17 shows the influence of slab thickness on the vertical deflection ($\delta_{surface)}$ of the top of concrete surface below the center of the circular loaded area. Fig. 4.17 distinctly illustrates that vertical deflection of the top concrete surface decreases significantly with the increase of slab thickness up to a thickness of 225 mm (9 inch). Above this thickness of 225 mm, the influence is reduced. This behaviour is of concrete slab is easily perceivable, since the rigidity of the concrete slab increases with an increase of its thickness.

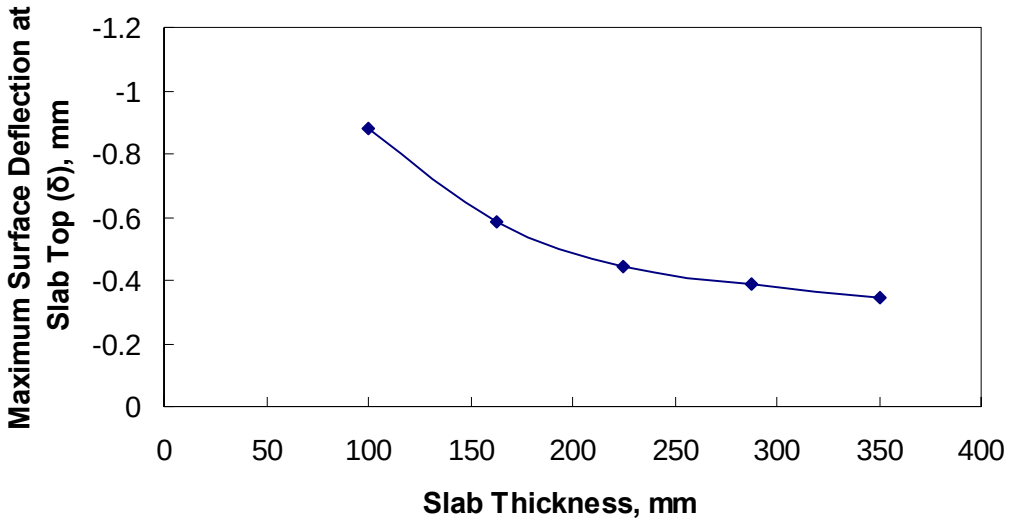

Fig. 4.17: Variation of Vertical Surface Deflection of Slab Top with Slab Thickness

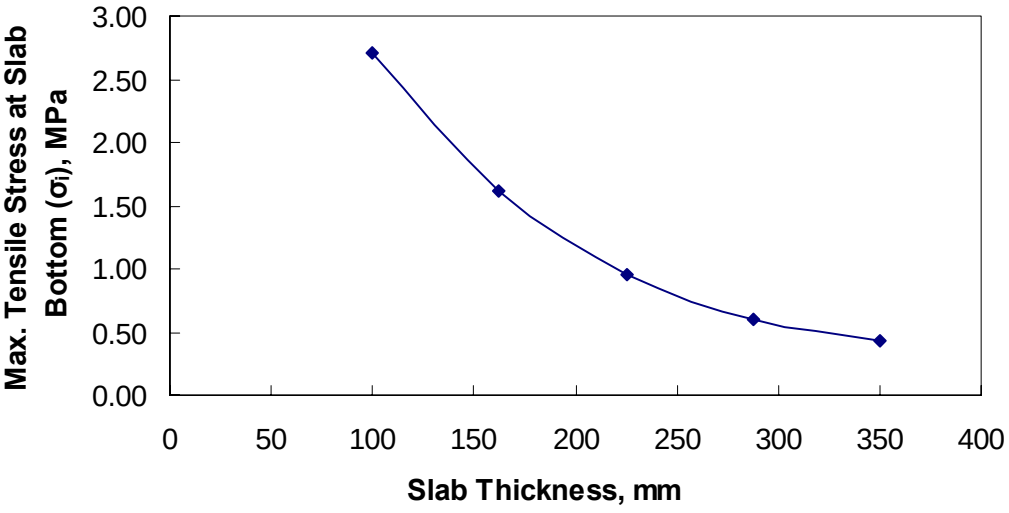

Fig. 4.18: Variation of Maximum Tensile Stress at Slab Bottom with Slab Thickness

The influence of slab thickness on the maximum tensile stress at the bottom of concrete slab (σ_i) due to circular wheel load is shown in Fig. 4.18. From Fig. 4.18, it can be easily

observed that the tensile stress developed ate the bottom surface of the concrete slab decreases significantly with a corresponding increase of slab thickness up to 225 mm (9inch) above which the effects of increasing slab thickness on maximum tensile stress on slab bottom diminishes. This variation of tensile stress at the bottom of concrete is easily predictable since with an increase in thickness, the inertia of the cross sectional area increases at a much higher rate than the increase in distance of bottom fibre of concrete slab from the neutral axis resulting in less tensile stress at the bottom fibre of the slab.

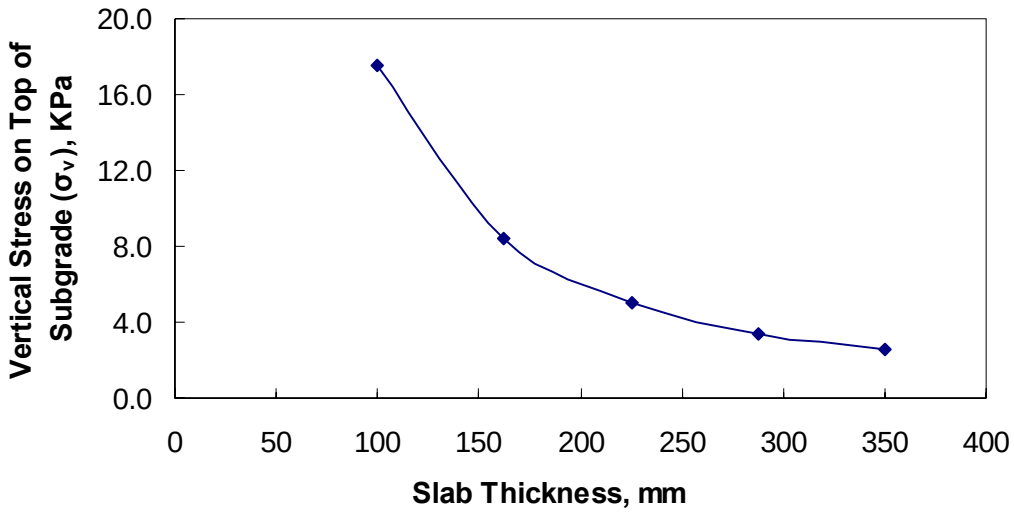

Fig. 4.19: Variation of Compressive Stress on Top of Subgrade with Slab Thickness

The influence of slab thickness on the compressive stress (σ_v) on the top of subgrade below the center of the circular loaded area is displayed in Fig. 4.19. It is obvious from Fig.4.19 that with an increase in slab thickness, the corresponding vertical compressive stress on the top of subgrade is reduced and the influence is highly significant up to a thickness of 225 mm. With an increase in slab thickness, the rigidity of the slab increase resulting in less deflection of the area under the circular loaded portion of the concrete slab which results in a more uniform stress distribution on top of the base material and hence on the top of subgrade.

4.4.2 Effect of Thickness of Base Course

Similar to the parametric study performed for the effect of slab thickness on pavement responses as described in the preceding section, a whole series of 3D finite element analysis were performed using the reference model to observe the effect of thickness of base course material on the pavement responses. A reasonably wide range of base course thickness was considered for the parametric study, starting from 150 mm (6 inch) to 600 mm (24 inch) thickness. For different values of base thickness other geometrical properties of the reference model were kept constant. The effects are shown in Fig. 4.20, 4.21, and 4.22.

The influence of base thickness on the vertical deflection ($\delta_{surface)}$ of the top of concrete surface below the center of the circular loaded area is shown in Fig. 4.20. It can be easily observed from Fig. 4.20 that the vertical deflection of the top concrete surface decreases with the increase of base thickness, but this decrease in surface deflection is very insignificant.

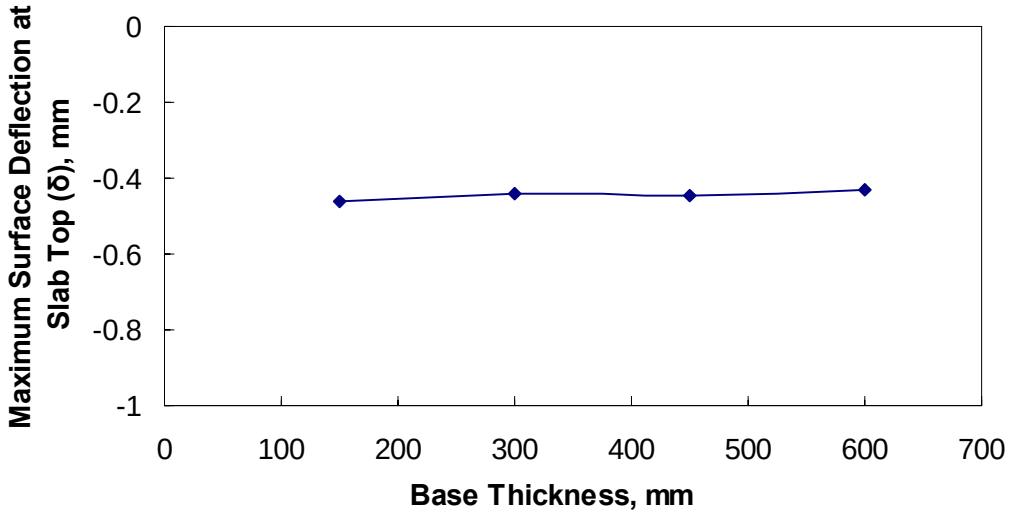

Fig. 4.20: Variation of Vertical Surface Deflection of Slab Top with Base Thickness

The influence of base thickness on the maximum tensile stress at the bottom of concrete slab (σ_i) due to circular wheel load is shown in Fig. 4.21 and shows that the tensile stress

developed at the bottom surface of the concrete slab decreases slightly with a corresponding increase of slab thickness.

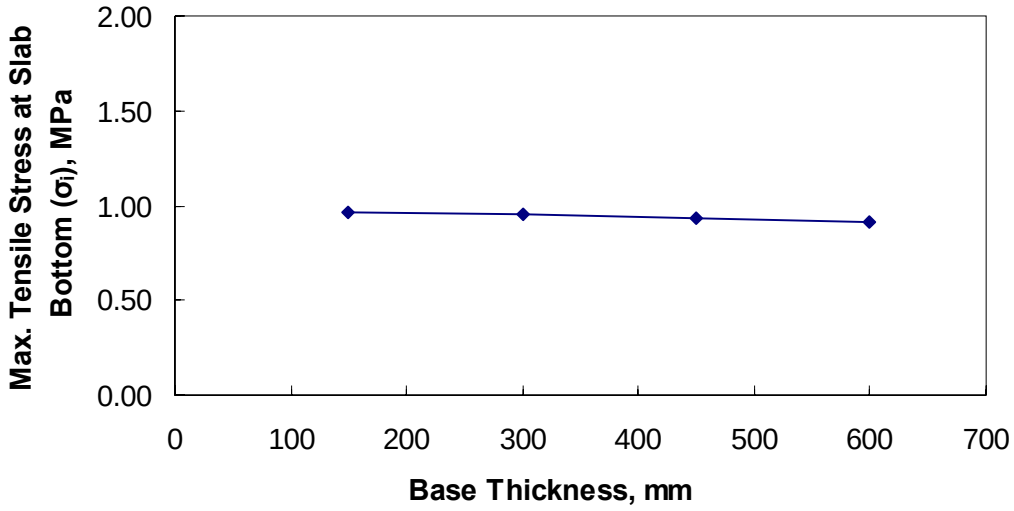

Fig. 4.21: Variation of Maximum Tensile Stress at Slab Bottom with Thickness

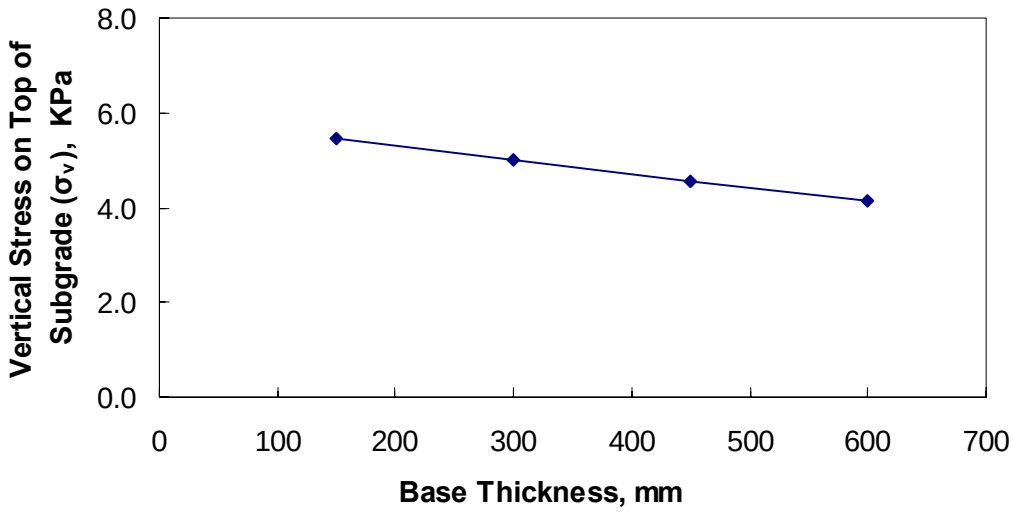

Fig. 4.22: Variation of Compressive Stress on Top of Subgrade with Base Thickness

The influence of base thickness on the compressive stress (σ_v) on the top of subgrade below the center of the circular loaded area is displayed in Fig. 4.22. It is obvious from Fig.4.22 that with an increase in slab thickness, the corresponding vertical compressive

stress on the top of subgrade is reduced. The influence of base thickness on the vertical stress at the top of subgrade below the centreline of the loaded area is insignificant compared to the reduction in vertical compressive stress resulting from changes in concrete slab thickness. But the increase in base thickness has more influence on compressive stress on subgrade top than the other two response i.e. vertical deflection of slab top surface and maximum tensile stress at slab bottom.

4.4.3 Effect of Base Course Material Properties

To observe the effect of different base course material on the pavement responses, four different base course material properties were used to predict the pavement responses utilizing the reference model developed in the previous chapter. The material properties for the four different kinds of bases were obtained from the Minnesota Road Project mentioned in the previous chapter. For this study, the four base course materials are designated by a number from 1 to 4 with base 1 being the strongest of the materials and base 4 being the weakest and base 2 and 3 in between the two.. Table 4.8 lists the designation of the four bases and their modulus of elasticity.

Table: 4.8. Base Course Material Designation and Modulous of Elasticity (*Es*)

Designation for the Present Study	**Minnesota Road Project Designation**	**Modulus of Elasticity (*Es*) (MPa)**
Base 1	cl 6 Sp	120
Base 2	cl 3 Sp	92
Base 3	cl 5 Sp	47
Base 4	cl 4 Sp	32

The influence of the different bases on the pavement responses are demonstrated in Fig. 4.23, 4.24, and 4.25. From Fig 4.23 it is evident that the use of stronger base course material results in a reduction in vertical surface deflection below the center of the circular loading area. This is obvious, since stronger materials are supposed to deflect less compared to weaker material under load. But the most significant observation that can be made from the Fig. 4.23 is that, the decrease in surface deflection is not significant enough to warrant the use of stronger base material to reduce surface deflection appreciably.

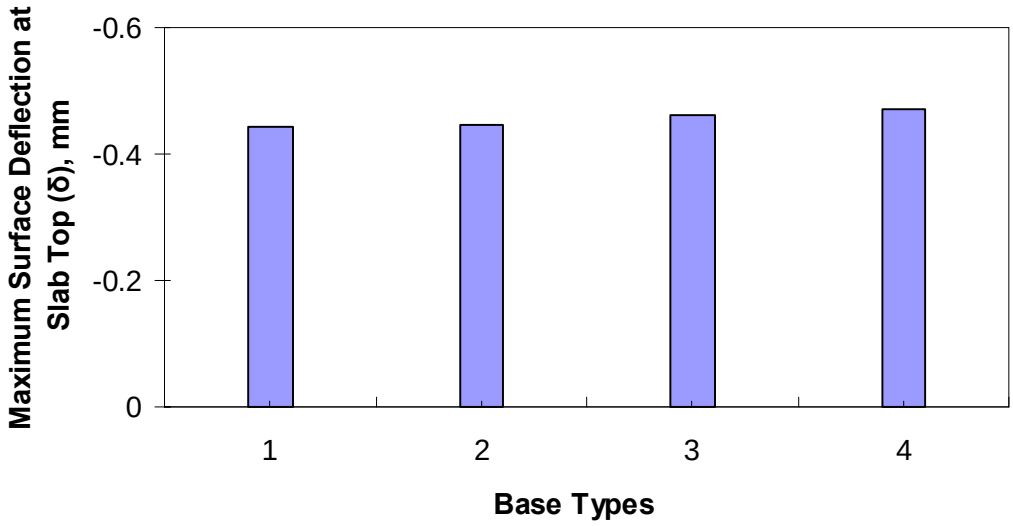

Fig. 4.23: Variation of Vertical Surface Deflection of Slab Top with Base Type

Fig. 4.24 displays the variation of maximum tensile stress at slab bottom with the change in base curse material strength. An increase in the strength of the base course material results in a consequent decrease of maximum tensile stress at the bottom surface of the concrete slab. This behaviour can be supported by the fact that increase of base strength properties result in less surface deflection near the loading area and therefore less relative deflection between the enter of loading and outer edge of the slab. But the tensile stress does not decrease significantly with a significant change in base course material properties.

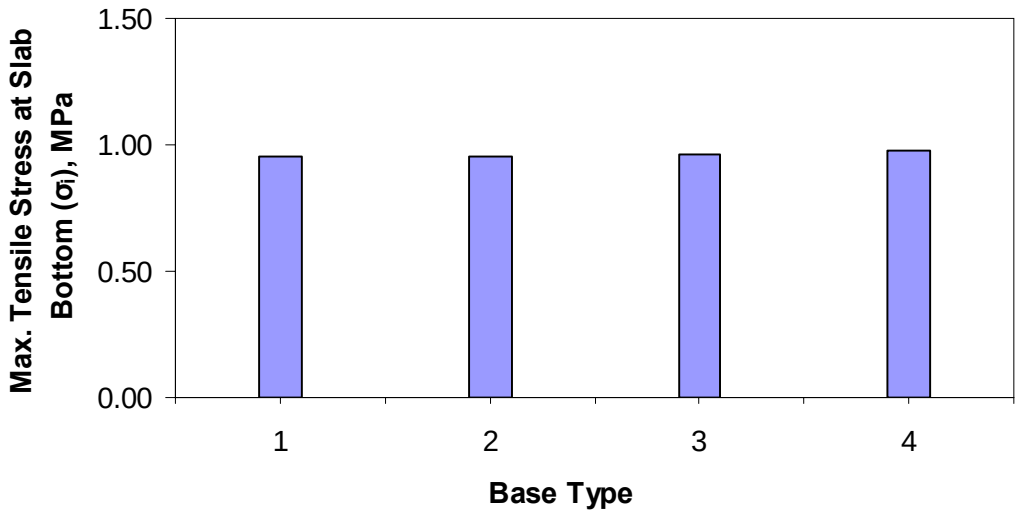

Fig. 4.24: Variation of Maximum Tensile Stress at Slab Bottom with Base Type

Fig. 4.25 shows the effect of base course material strength properties on the compressive stress developed on the surface of the subgrade due to wheel load. Close observation of the Fig.25 shows that the magnitude of the vertical stress generated on the subgrade surface increases with the use of stronger base course material. But it is also evident from the figure that the variation is insignificant relative to the change in pavement strength.

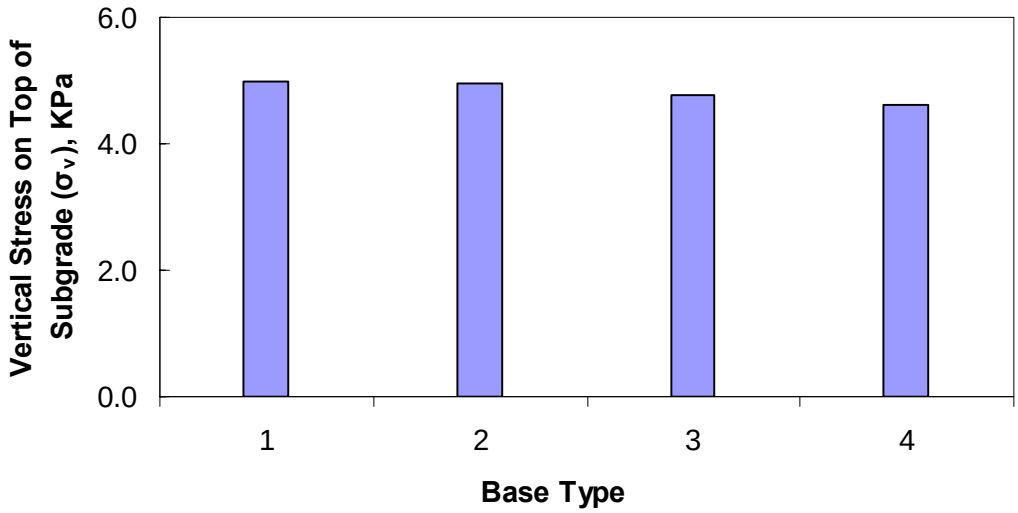

Fig. 4.25: Variation of Compressive Stress on Top of Subgrade with Base Type

4.4.4 Effect of Subgrade Soil Characteristics

In this study, a cohesive soil was used as the subgrade soil and pavement responses were predicted considering its nonlinear material characterization. To observe the effect of a different subgrade soil type, a cohesionless soil (sand) was used. The cohesionless soil was modeled using modified Drucker Prager model with hardening. The material properties used in the analysis are listed in Table 4.9.

Table: 4.9. Properties of Sandy Soil Subgrade for Drucker Prager Model (Source BRTC Test Report)

Material Property	**Specific Values**
Modulus of Elasticity , ***Es*** (MPa)	31.85
Poisson's Ratio, **υ**	0.3
Unit Weight, Kg/m^3	1920
Angle of Internal Friction of Soil (Coulomb)	36°
Angle to Yield Surface (Drucker Prager), **β**	55.62°
Material cohesion (Drucker Prager), ***d***	10 Pa
Dilation Angle of Soil, **ψ**	20°

The critical pavement responses for the two different types of subgrade are displayed in Fig. 4.26, 4.27 and 4.28. Figure 4.26 displays the vertical deflection of the top surface of the concrete slab along pavement direction. It can be observed from the figure that the vertical deflection predicted for the cohesionless soil is less compared to that of cohesive soil. This may be due to the fact that the cohesionless soil is stronger subgrade material compared to the cohesive soil.

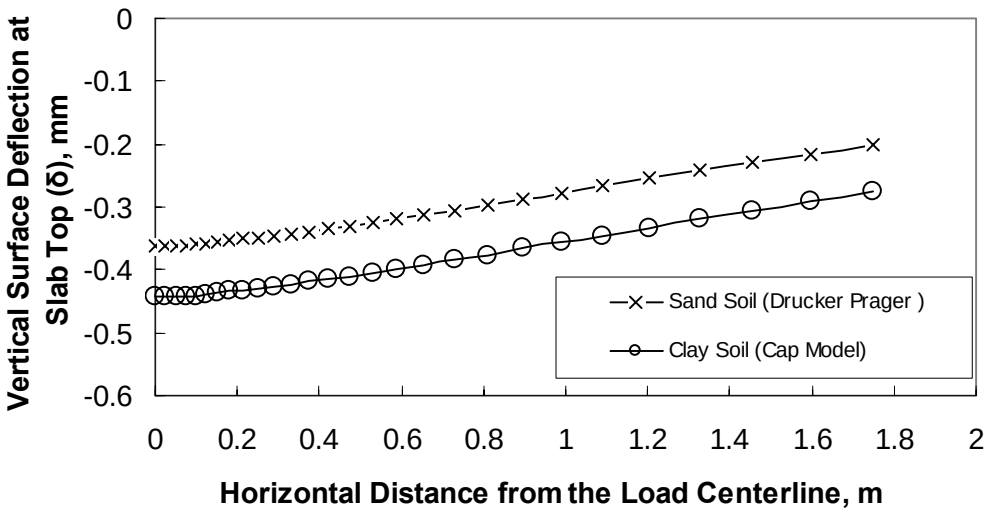

Fig. 4.26: Vertical Surface Deflection at Slab Top vs. Horizontal Distance from Load centreline for Different Subgrade Type

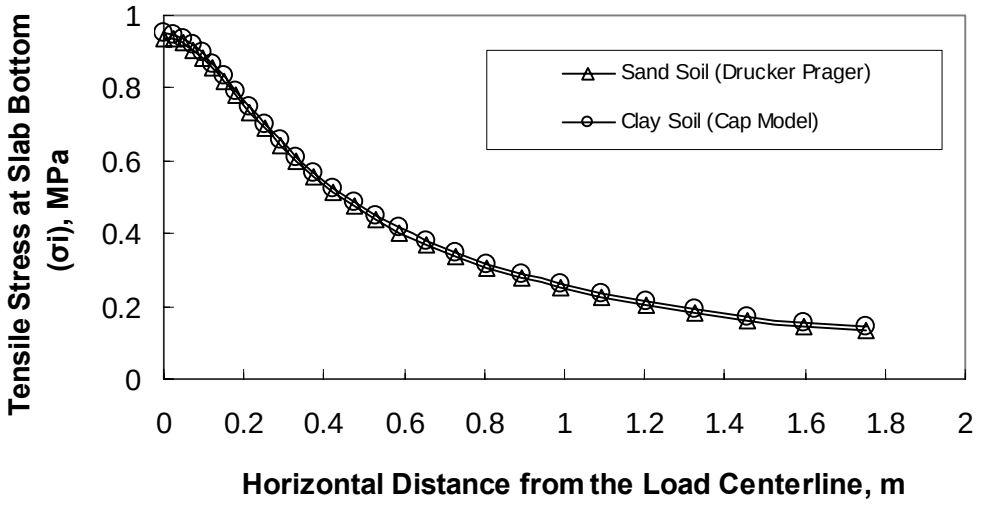

Fig. 4.27: Tensile Stress at Slab Top vs. Horizontal Distance from Load centreline for Different Subgrade Type

Figure 4.27 displays the variation of tensile stress at the bottom of the slab for the two different types of subgrade soil. Form the Fig. 4.27, it is evident that the predicted tensile stress for cohesionless soil is also slightly lower than the values of tensile stress for cohesive soil. This phenomenon can be explained by referring to the previous Fig.4.26 of vertical deflection of concrete slab where the relative deflection of the center of the slab and its corner is less resulting in lower tensile stress at bottom of the slab.

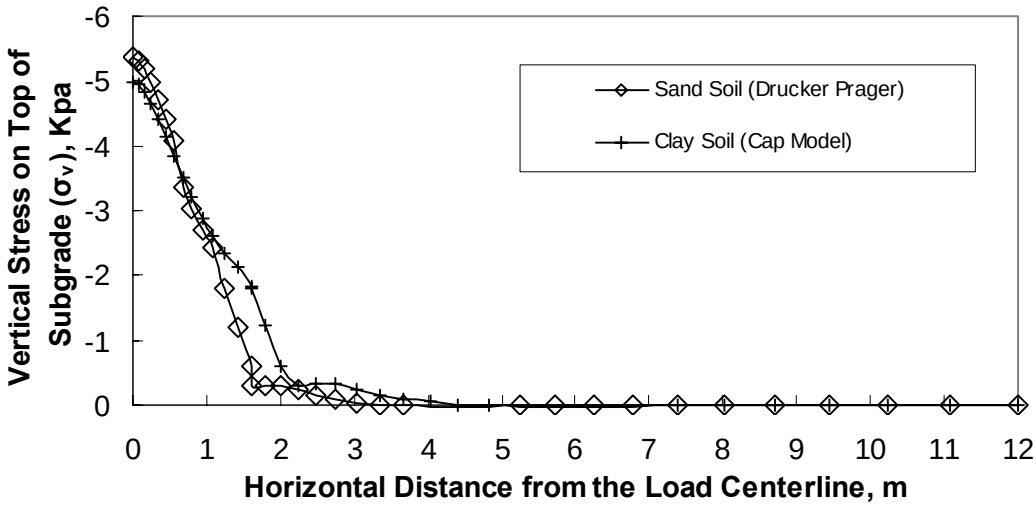

Fig. 4.28: Vertical Stress at Top of Subgrade vs. Horizontal Distance from Load centreline for Different Subgrade Type

Fig. 4.28 shows the variation of vertical compressive stress on top of subgrade for the two types of subgrade soil. The vertical compressive stress predicted at the top surface of the subgrade below the centreline of the wheel load is greater for cohesionless soil but the stress reduces more rapidly than the cohesive soil along the pavement direction. On the contrary, the vertical stress on the top surface of subgrade for cohesive soil is significantly large beyond the edge of the concrete slab up to a considerable distance. This may be due to the cohesive property of the soil.

4.5 SUMMARY

In this chapter, the results obtained for the 3D and axisymmetric FE analysis performed on the jointed plain concrete pavement are discussed in detail. The variation of pavement responses for four combinations of material characterizations along the pavement direction is plotted and the possible reasons behind the observed response patterns are presented. Nonlinear material characterization of base course material is not warranted for lower magnitude of applied wheel loads. But it may be important for higher axle loads coming from heavier vehicles. Nonlinear material characterization of subgrade soil has resulted in greater deflection of the slab top surface with less influence on tensile stress at slab bottom due to the greater stiffness of the concrete slab which acts as a plate under the applied wheel load. It also summarizes the detailed parametric study carried out for observing the behaviour of the developed FE model under different conditions. Thickness of concrete slab has displayed significantly greater influence on pavement responses than base course thickness and base course material strength. Subgrade soil type is also influential to pavement response to some degree.

Chapter 5
CONCLUSIONS AND RECOMMENDATIONS

5.1 CONCLUSIONS

Outcomes of this analytical study on the jointed plain concrete pavement (JPCP) responses due to wheel load are summarized in this chapter. Through out the study a finite element model is developed and its performance is verified with available numerical results. The study conducted in here focuses on the critical pavement responses (i.e. stresses and strains) vital for the development of pavement design procedures. Critical responses like the maximum tensile stress developed at the bottom of the concrete slab governs the allowable number of repetitions to cause fatigue cracking which is the stress ratio between flexural tensile stress and the concrete modulus of rupture. Although permanent deformations are not considered in rigid pavement design, the resilient deformation under repeated wheel loads will cause pumping of the slabs.

From this study it is clear that the critical pavement responses predicted by two dimensional axisymmetric analyses of the jointed plain concrete pavement system are in good agreement with those predicted by the three dimensional analysis results under the present idealized pavement system instead of the fact that the rigid pavement system is not a true axisymmetric problem. Considerations like load transfer across the joints may change the situation and suggests the necessity of further investigation. Different parameters, which have significant influence over the critical pavement responses, are identified and their effects are evaluated with three dimensional finite element analysis.

In brief, the following conclusion can be drawn:

1. The effects of concrete slab thickness on critical pavement responses are highly significant up to 225 mm (9inch). An increase in slab thickness results in a considerable decrease in vertical deflection of top surface. Maximum tensile stress developed at the bottom of the concrete slab and the vertical compressive

stress on the subgrade surface also decreases significantly. Above this critical thickness of 225 mm, the influence of concrete slab thickness on critical pavement responses diminishes. Based on this finding, it is recommended to take special care in designing a concrete slab below a thickness of 225 mm.

2. On the contrary, effects of base course thickness on pavement responses are found to be of little importance. The increase in thickness has little effect on reducing the critical pavement stresses and deflection. So the use of a base course material is limited in extent for drainage purpose.

3. Base course material strength properties have no considerable influence on the pavement responses of the jointed plain concrete pavement system. The use of a stronger base course material is therefore unnecessary to reduce the critical pavement responses compared to its cost.

4. The developed 3D FE model was successfully verified with available numerical results. 3D finite element analysis results for nonlinear material characterization predicts 12.4% higher surface deflection than linear elastic characterization. But the maximum tensile stress and vertical compressive stress on top of subgrade for both nonlinear and linear analysis were found to be negligible.

5. 2D axisymmetric FE analysis was carried out and the results were compared with those predicted by 3D FE analysis. The axisymmetric finite element analysis results conforms closely with the 3D FE analysis results for vertical surface deflection and compressive stress on top of subgrade with a variation of 1.3% and 2.4% respectively. But the maximum tensile stress predicted by axisymmetric FE analysis at the bottom of the concrete slab is about 14% grater than the 3D FE analysis result.

6. Nonlinear characterization of the base course material has no significant effect on the pavement responses as the stresses developed in the base course material layer

is within the elastic limit. As a result, the base course material behaves as an elastic material under the present loading and geometry conditions.

7. Nonlinear characterization of subgrade soil has considerable effect on the pavement responses especially on the deflection of the top surface. But the relative deflection of the center of the concrete slab with respect to its edge doesn't change significantly. As a result, the tensile stress developed at the bottom surface of the concrete slab doesn't change significantly and is almost negligible.

8. Subgrade soil is an important consideration in the analysis of pavement system for critical pavement responses as has been observed from the present study.

5.2 RECOMMENDATIONS FOR FUTURE STUDIES

Consistent with the objectives of the present study, the behavior of the jointed plain concrete pavement (JPCP) system has been analyzed and critical pavement responses have been predicted. Effects of the various significant pavement geometry and material strength parameters have also been studied and presented. However, there are potential scope for further works to be done in this filed, some indications of which are given below:

- For gaining confidence in the finite element analysis results, a full scale model may be tested and compared with the analysis results.

- This study has been limited in extent to jointed plain concrete pavement. Other types of concrete pavement like jointed reinforced concrete pavement (JRCP), continuously reinforced concrete pavement (CRCP), precast and prestressed concrete pavement systems may also be analyzed.

- Load transfer across joints (by aggregate interlock or dowel bars) has not been considered in the present study. This may be incorporated to study their effects on pavement responses.

- Only interior loading was considered for this study. Other loading conditions with different wheel configurations may be studied to find out their effects on pavement responses.

- Effect of water table is not included in the present study. So effect of water table can be considered for further study.

- Nonlinear soil properties like consolidation; creep etc can be incorporated in the numerical model to investigate their effects on the concrete pavement system.

REFERENCES

AASHTO, "Guide for design of Pavement Structures," American Association of State Highway and Transportation Officials, Washington, D.C., 1993.

ABAQUS User's Manual , Dassault Systemes Simulia Corp., Providence, RI, USA, 2008.

Bowles, J.E.,"Foundation Analysis and Design", 4th edition, McGraw Hill, 1988.

Brown, S. F., and Pappin, J. W., "Analysis of Pavements with Granular Bases", Transportation Research Record, 810, Transportation Research Board, Washington, D.C., pp. 17–23, 1981.

Darestani1, M. Y., Thambiratnam, D. P., Nataatmadja, A., and Baweja, D.," Structural Response of Concrete Pavements under Moving Truck Loads", Journal of Transportation Engineering, ASCE, Vol. 133, No. 12, pp. 670-676, 2007.

Delatte, N., "Concrete Pavement Design, Construction and Performance", Taylor and Francis e-Library, London and New York, 2007.

Griffiths, G., and Thom, N., "Concrete Pavement Design Guidance Notes", Taylor and Francis e-Library, London and New York, 2007.

Heinrichs, K.W., Liu, M. J., Darter, M. I., Carpenter, S. H., and Ionnides, A. M., "Rigid Pavement Analysis and Design", Report No. FHWA-RD-88-068. Federal Highway Administration, 1989.

Helwany, S., "Applied Soil Mechanics with ABAQUS Applications", Willy, John & Sons, Inc, 2007.

Hossain, M., “Rational and Economic Design of Reinforced Concrete Pavements Based on Finite Element Analysis”, Masters Thesis, Department of Civil Engineering, Bangladesh University of Engineering and Technology, 1992.

Huang, Y. H., “Pavement Analysis and Design”, Prentice-Hall, Englewood Cliffs, New Jersey, 1993.

Kim, M., Tutumluer, E., and Kwon, J., “Nonlinear Pavement Foundation Modeling for Three-Dimensional Finite-Element Analysis of Flexible Pavements”, International Journal of Geomechanics, ASCE, Vol. 9, No. 5, pp. 195-208, 2009.

Kohler, E., Kannekanti, V., and Harvey, J., “California Efforts Towards Mechanistic-Empirical Pavement Design”, International Journal of Airfield and Highway Pavement 2006, ASCE, pp. 74-85, 2006.

Kuo, C. M., and Chou, F. J., “Development of 3-D Finite Element Model for flexible Pavements”, Journal of Chinese Institute of Engineers, Vol.27, No.5, pp. 707-717, 2004.

Kuo, C. M., and Huang, C.W.,” Three-Dimensional Pavement Analysis with Nonlinear Subgrade Materials”, Journal of Materials in Civil Engineering, ASCE, Vol. 18, No., pp. 537-544, 2006.

Nazarian, S., and Boddspati, K. M., “Pavement-Falling Weight Deflection Interaction Using Dynamic Finite Element Analysis”, In Transportation Research Record 1449, TRB, National Research Council, Washington, D., C., pp.123-133, 1995.

Newcomb, D. E., and Olson, R., “Aggregate Research at Minnesota Road Research Project”,

Pavement Design Manual, Queensland Department of Main Roads Pavements, Materials & Geotechnical Division, Second Edition, Amendment 2, 2005.

Rigid Pavement Design Manual, Florida Department of Transportation, Pavement Management Office, 2009.

Rowshanzamir, M. A., “Resilient Cross-Anisotropic Behavior of Granular Base Materials under Repetitive Loading.” Ph.D. dissertation, School of Civil Engineering, Univ. of New South Wales, Kensington, Australia, 1995.

Saad, B., Mitri, H., and Poorooshasb, H., “ Three Dimensional Dynamic Analysis of Flexible Conventional Pavement Foundation’, Journal of Transportation Engineers, ASCE, Vol. 131, No. 6, pp. 460-469, 2005.

Shaikh, G. M., and Ahmed, Z., “Behavioral Study of a Rigid Pavement Section through Finite Element Analysis”, Journal of Institution of Engineers, Singapore, Vol.45, Issue2, pp. 1-18, 2005.

Thompson, M. R., and Robnett, Q. L., “Resilient Properties of Subgrade Soils.” Transportation Engineering Journal, 105(1), pp.71–89, 1979.

Tutumluer, E., “Predicting Behavior of Flexible Pavements with Granular Bases”, Ph.D. dissertation, School of Civil and Environmental Engineering, Georgia Institute of Technology, Atlanta, 1995.

Uzan, J., “Characterization of Granular Materials”, Transportation Research Record. 1022, Transportation Research Board, Washington, D.C., pp. 52–59, 1985.

Zaghloul, S.M., and White, T.D., “Use of a Three-Dimensional, Dynamic Finite Element Program for Analysis of Flexible Pavement”, In Transportation Research Record 1388, TRB, National Research Council, Washington, D., C., pp.60-69, 1993.